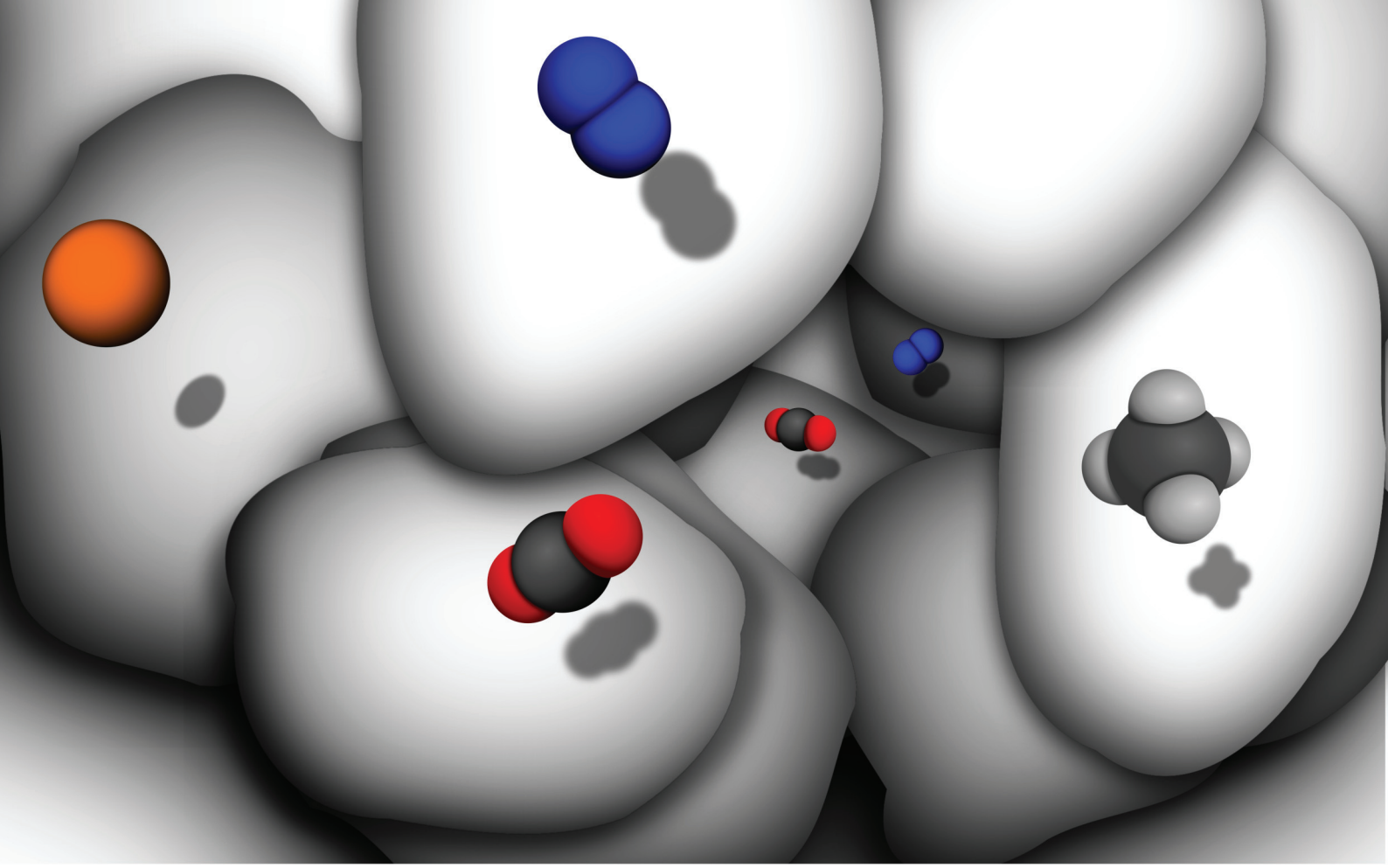

Benjamin Besser

Gas diffusion in functionalized mesoporous membranes

Gas diffusion in functionalized mesoporous membranes

Vom Fachbereich Produktionstechnik

der

UNIVERSITÄT BREMEN

zur Erlangung des Grades
Doktor-Ingenieur
genehmigte

Dissertation

von

M. Sc. Benjamin Besser

Gutachter:
Prof. Dr.-Ing. Kurosch Rezwan, Universität Bremen
Prof. Dr. Niklas Hedin, Stockholm University, Sweden

Tag der mündlichen Prüfung: 07.02.2017

Für meine Eltern.

Danksagung

Diese Dissertation entstand im Rahmen meiner Tätigkeit als wissenschaftlicher Mitarbeiter im Fachgebiet Keramische Werkstoffe und Bauteile in enger Zusammenarbeit mit dem Zentrum für Umweltforschung und nachhaltige Technologien (UFT) des Fachbereichs Produktionstechnik der Universität Bremen. Mein Dank gilt daher besonders Herrn Prof. Dr.-Ing. Kurosch Rezwan und Herrn Prof. Dr.-Ing. Jorg Thöming für das entgegengebrachte Vertrauen, die Möglichkeit der experimentellen Arbeit und die wissenschaftliche Weiterbildung. Des Weiteren danke ich Herrn Prof. Niklas Hedin für das Interesse an meiner Arbeit und die Bereitschaft, diese Arbeit als Zweitgutachter zu bewerten.

Darüber hinaus gilt mein herzlicher Dank Dr. Stephen Kroll für seine stetige Hilfsbereitschaft, sowie die unzähligen fachlichen Diskussionen und das ausgezeichnete Feedback während dieser Zeit. Ebenso von Herzen bedanken möchte ich mich bei Dr. Michael Baune und Dr. Thomas Veltzke für die herausragende Unterstützung bei wissenschaftlichen Fragestellungen oder technischen Problemen während der gesamten Kooperationszeit.

Besonders bedanken möchte ich mich außerdem für die fachliche Unterstützung bei meinem ehemaligen Komilitonen und Freund Jochen Dreyer. Ein herzlicher Dank gebührt ebenfalls meinen Kollegen und Freunden aus dem Fachgebiet, durch die ich meine Promotionszeit in schöner Erinnerung behalten werde. Insbesondere gilt mein Dank Julia Bartels für die Vielzahl an Diskussionen und für ein jederzeit offenes Ohr. Für die großartige Unterstützung im Labor möchte ich mich auch bei Tina Kühn und Christian Ellenberg bedanken.

Abschließend gilt meine tiefe Dankbarkeit meiner Familie und meiner Freundin, die mich uneingeschränkt unterstützt haben und mir jederzeit als Antrieb und Haltepunkt dienten.

Zusammenfassung

Ziel der vorliegenden Arbeit ist die grundlegende Untersuchung von Gasdiffusion in funktionalisiteren, mesoporösen Strukturen mit Porendurchmessern von ca. 20 nm. Hierzu werden defektfreie Kapillarmembranen aus Yttrium stabilisierten Zirkonoxid mittels Extrusion hergestellt. Die bei 1050 °C für 2 h gesinterten Membranen haben eine homogene Mikrostruktur und eine offene Porosität von ca. 40 % bei einer monomodalen Porengrößenverteilung, wobei der mittlere Durchmesser zwischen 23 und 26 nm liegt.
Um den Einfluss einer Oberflächenfunktionalisierung auf den Gasfluss zu untersuchen, werden funktionelle Gruppen mittels eines nasschemischern Verfahrens kovalent an die Oberfläche gebunden. Hexadecyltrimethoxysilane, ein Silan mit einer C_{16} Alkyl-Kette als funktionelle Gruppe, fungiert als Modellsilan. Nach der Funktionalisierung beträgt die Dichte der Gruppen zwischen 2 und 4 Gruppen nm^{-2}, abhängig von der Silankonzentration während der Funktionalisierung. Analysen zeigen eine verringerte offene Porositat (27 %) und etwas kleinere Porendurchmesser von ca. 20 nm, welche auf eine Monolayerbildung hinweisen.
Die Gasdiffusionseigenschaften werden bei Einzelgasmessungen im Dead-End Modus ermittelt. Die Messungen werden bei unterschiedlichen Temperaturen (0-80 °C) mit Stickstoff (N_2), Argon (Ar), Methan (CH_4) und Kohlenstoffdioxid (CO_2) durchgeführt. Nicht funktionalisierte Strukturen zeigen unabhängig von Temperatur und untersuchtem Gas ideales Knudsen-Diffusionsverhalten. Dem gegenüber zeigen funktionalisierte Strukturen um bis zu einer Größenordnung verringerte Flüsse, welches mit der Gruppendichte auf der Oberfläche korreliert. Darüber hinaus weisen die Selektivitäten eine Abweichung von der Knudsen-Theorie auf, wobei der Einfluss auf CO_2 am größten ist. Die Abweichung verstärkt sich mit zunehmender Temperatur.
Es wird angenommen, dass eine sterische Behinderung der Gasmoleküle durch die langen C_{16}-Ketten für die ermittelte Diffusionscharakteristik verantwortlich ist. Darüber hinaus wird die Hypothese aufgestellt, dass die Abweichung der Selektivitäten durch die unterschiedliche Größe der Gasmoleküle verursacht wird und das temperaturabhängige Verhalten auf die thermische Bewegung der Alkyl-Ketten zurückzuführen ist. Die hier präsentierten Ergebnisse leisten einen Beitrag zum grundsätzlichen Verständnis von Gasdiffusion in funktionalisierten Strukturen, wie etwa vorhanden in Gastrennmembranen oder Chromatographiesäulen.

Abstract

This work investigates the fundamentals of gas diffusion in functionalized mesoporous structures with pore diameters of around 20 nm. For this purpose, an extrusion process based on a yttria stabilized zirconia nanopowder is optimized to shape defect-free capillary membranes. The membranes sintered at 1050 °C for 2 h show a highly homogeneous microstructure with an open porosity of around 40 % and a monomodal pore size distribution with mean pore diameters between 23 and 26 nm.

To investigate the influence of surface functionalizations on the gas flow, functional groups are covalently bond onto the pore walls using a wet-chemical silanization process. Hexadecyltrimethoxysilane, a silane with a C_{16} alkyl-chain as functional group, is chosen as functional model silane. After successful surface functionalization, the membranes show a functional group density between 2 and 4 groups nm^{-2} depending on the silane concentration during functionalization. Structural analysis reveal decreased open porosities (27 %) and slightly smaller mean pore diameters of around 20 nm which indicate a monolayer of immobilized C_{16}-chains.

The gas diffusion properties are analyzed via single gas permeation measurements using a setup operating in dead-end mode. Measurements are performed under different temperature conditions (0-80 °C) using nitrogen (N_2), argon (Ar), methane (CH_4) and carbon dioxide (CO_2). Non-functionalized structures show ideal Knudsen diffusion behavior, independent of gas type and temperature. In contrast, the gas permeation of alkyl-functionalized structures is decreasing up to one order of magnitude with increasing alkyl-chain density on the pore walls. Furthermore, the ideal selectivities show an increased deviation from Knudsen theory, having the highest influence on CO_2. These deviations are further increased with increasing operating temperature.

It is assumed that sterical hinderance due to the long C_{16}-chains on the material surface is responsible for the determined gas flow characteristics. In addition, it is hypothesized that the deviations in ideal selectivity are caused by the difference in molecular size of the gas species and that the increased deviation with increased temperature is caused by the temperature movement of the surface functional groups. The results contribute to the fundamental understanding of gas diffusion in functionalized structures as present in many applications, ranging from gas separation membranes to gas chromatography.

Contents

Nomenclature

α	Selectivity, dimensionless
ΔH_{ads}	Heat of adsorption in $\mathrm{J\,mol^{-1}}$
δ	Membrane thickness in m
$\dot{n}$	Molar flow rate in $\mathrm{mol\ s^{-1}}$
ϵ	Porosity, dimensionless
γ	Surface tension in $\mathrm{J\,m^{-2}}$
κ	Tortuosity factor, dimensionless, $\kappa = \tau^2 = \left(\frac{l_{eff}}{l}\right)^2$
λ	Mean free path of gas molecule in m
ϕ	Contact angle
σ	Kinetic diameter of gas molecule in m
τ	Tortuosity, dimensionless, $\tau = \frac{l_{eff}}{l}$
θ	Surface coverage in $\mathrm{mol\,m^{-2}}$
A	Membrane area in $\mathrm{m^2}$
$B_{1,2}$	Constants for temperature conversions in $\mathrm{^\circ C^{-1,2}}$
b_{N2}	Y-intercept of calibration curve of $\mathrm{N_2}$ for the flow sensor in $\mathrm{mln\,min^{-1}}$
C	Constant
c	Constant
c_p	Specific heat capacity in $\mathrm{J\,kg^{-1}\,K^{-1}}$
CF	Gas conversion factor obtained from Bronkhorst in $\mathrm{kg\,s^{-1}\cdot mln^{-1}\,min}$
d	Pore diameter in m
I	Current in mA
k_B	Boltzmann constant, $k_B = 1.38 \cdot 10^{-23}\,J\,K^{-1}$
K_F	Adsorption isotherm constants according to Henry and Langmuir in $\mathrm{mol\,m^{-2}\,Pa^{-n_F}}$
$K_{H,L}$	Adsorption isotherm constants according to Henry and Langmuir in $\mathrm{mol\,m^{-2}\,Pa^{-1}}$
M	Molar mass in $\mathrm{g\ mol^{-1}}$
m	Weight in kg
m_{N2}	Slope of calibration curve of $\mathrm{N_2}$ for the flow sensor in $\mathrm{mln\,min^{-1}\,mA^{-1}}$
N_A	Avogadro constant, $N_A = 6.022 \cdot 10^{23}\,\mathrm{mol^{-1}}$

n_F Freundlich exponent, dimensionless

p Pressure in Pa

q Adsorbed amount in $\mathrm{mol\,m^{-2}}$

R Universal gas constant, $R = 8.314\,J\,mol^{-1}\,K^{-1}$

r Radius in m

s specific entropy in $\mathrm{J\,K^{-1}}$

S_0 Average surface area occupied by a nitrogen molecule in $\mathrm{nm^2}$

T Temperature in K

t Layer thickness of adsorbed gas phase in m

U Voltage in V

U_0 Nominal voltage at 0 °C, U_0=1 V

V Volume in $\mathrm{m^3}$

v Specific volume in $\mathrm{m^3\,g^{-1}}$

v_m Specific volume of a mono-layer in $\mathrm{m^3\,g^{-1}}$

Kn Knudsen number, dimensionless

APTES 3-Aminopropyltriethoxysilane

DSC Differential scanning calorimetry

DTA Differential thermal analysis

E-C Evaporation-condensation

FTIR Fourier-transform infrared spectroscopy

GB Grain boundary diffusion

IC Inorganic carbon

IR Infrared

PF Plastic flow

PVA Polyvinyl alcohol

SD Surface diffusion

TC Total carbon

TGA Thermogravimetric Analysis

TOC Total organic carbon

VD Volume diffusion

XPS X-ray photoelectron spectroscopy

YSZ Yttria-stabilized zirconia

1. Introduction and Aim of Work

1.1. General Introduction

In many technical applications, gases are propagating through porous media. Examples of such cases are solid oxide fuel cells, chromatography columns, heterogeneous catalysis or porous membranes.[1–6] For further optimization of the current materials and for new developments in these areas, it is crucial to fully understand the transport processes and interactions of gases in porous materials.

Gas transport in porous media is very complex and depends on many parameters such as temperature, pressure, gas-solid interactions, gas-gas interactions, pore size and porosity. In addition, the gas transport often occurs in pores of several length scales simultaneously, for instance from mm" sized pores between the granules of a packed bed to nm-sized pores of the primary particles. In fact, in the fields of catalysis and swing adsorption processes hierarchically structured materials with pore sizes over multiple length scales are specifically developed to overcome certain diffusion limitations and increase the process efficiency.[7–15]

Also gas separation membranes are hierarchically structured systems which are build up by multiple layers, each possessing a different pore size range.[6,16–18] The separation of gases can only be achieved in very small pores, either by molecular sieving in micropores (<2 nm) or by surface selective flow in small mesopores (<10 nm). The smaller the pore size, the higher the pressure drop and for this reason, these membranes are asymmetrically shaped to avoid high pressure drops. For this, the separative layer is coated very thin on top of a porous support, providing shape and mechanical stability. To cover the pore size gap between the support and the so called top layer, the porous support itself consists of multiple layers with gradually decreasing pore sizes.

For gases propagating through such hierarchical structures, the governing transport mechanism highly depends on the pore size. Therefore, multiple gas transport mechanisms may be present at the same time. Accordingly, the overall performance and efficiency of a hierarchical structured system is defined by the superposition of multiple gas transport mechanisms. To optimize and tune these systems, the mechanisms of gas transport on each length scale need to be known.

In general, the principle of the process is often based on the molecule interactions at the nanoscale, such as catalytic reactions or simple adsorption and desorption of gases on solid surfaces.[19] Usually, adsorption and desorption effects only show a significant impact either when the pore size is very small, or when the diffusion paths are long enough, for example, in gas separation membranes or in chromatography columns. Both aforementioned fields of research use the principle of molecule adsorption on solid surfaces aiming at an increased selective flow, based on surface diffusion in the case of gas separation membranes, and on the selective retention due to adsorption and desorption in the case of chromatography columns.[2,6] To increase the separation efficiency, surface functionalizations are often applied on the solid surface to alter the surface chemistry and tune the adsorptive properties.

Despite the differences in pore size between chromatography columns and gas separation membranes, chemical surface functionalizations with similar functional groups are applied in both fields of research. Especially in the case of chromatography columns, a large variety of column types with different stationary phases and various polarities are available, depending on the application.[2] Still, apolar surface functionalizations based on C_{18} alkyl-silanes are frequently applied in chromatography columns, mostly in high-performance liquid chromatography.[20–25] In addition, they also show great potential for gas-solid chromatography applications.[26] Similar surface functionalizations using alkyl-silanes featuring different spacer lengths are applied to gas separation membranes for the separation of aggressive gases and longer hydrocarbons.[27–35] Other types of membrane surface functionalizations include fluorinated-[34–37] or amino-groups, in most cases aiming at the separation of carbon dioxide.[38–41]

Surface functionalizations are often prepared by wet-chemical approaches using silanes.[22–26,28–41] These functionalizations are usually applied af-

ter shaping and heat treatment of the porous structure, as a post-processing step. Consequently, when functionalizing, for example, an asymmetric membrane with this technique, the whole hierarchical structured membrane, including top layer, intermediate layers and supporting structure, is functionalized. The effects of surface functionalizations has been intensively investigated on asymmetric structures and in small mesopores[27–41] but little is known about the influence of surface functional groups on the gas flow in pores larger than 10 nm, in which surface diffusion usually is neglected.

1.2. Aim of Work

"How does a surface functionalization influences the gas transport in large mesopores?"
The question is very broad and the answers can be versatile, or maybe contradictory, depending on the type of functional group or the exact pore size. This study aims to contribute some of the possible answers to this fundamental question. Of course, the work presented here is more focused on a specific aspect in this field of research. The focus within this work lies on the experimental investigation of the gas transport in mesopores of around 20 nm and the impact of an C_{16}-alkyl chain functionalization on the gas diffusion through such pores. For this, certain goals must be reached:

The first challenge is to prepare a defect-free homogeneous structure with a controlled and uniform pore size distribution in the upper mesoporous region (10-50 nm), serving as a model structure. To achieve this, an extrusion process shall be used to shape tubular ceramic capillaries whose final pore structure is formed by the inter particular space between the primary particles after partial sintering.
The second challenge is focused on a reproducible immobilization of hexadecyltrimethoxysilane (HDTMS) molecules on the pore walls of the membrane to form a stable C_{16}-alkyl chain functionalization. A wet-chemical functionalization process shall be applied for this purpose. It is crucial to investigate the influence of the functional layer on the pore size, ensuring comparability of the non-functionalized and C_{16}-functionalized structures in terms of the dominating transport mechanism. Furthermore, a suitable method for quantification of the surface functionalization needs to be applied to verify the functionalization process.
The third challenge is related to the integration of the capillary membranes into a single gas permeation setup which operates in dead-end mode to perform highly reproducible measurements. For this, the gas permeation setup needs to be adapted and optimized and a testing procedure needs to be developed to ensure reproducibility.

Finally, to contribute answers to the general question stated above, the influence of the C_{16}-alkyl chain functionalization on the gas flow of argon (Ar) and nitrogen (N_2), as well as carbon dioxide (CO_2) and methane (CH_4) shall be investigated (see chapter 4). Furthermore, important parameters for the gas-solid interactions such as the temperature (see chapter 5) and the functional layer density (see chapter 6) shall be analyzed to achieve a more comprehensive understanding of the interactions between the gas molecules and the functional layer.

References

[1] Weidong He, Weiqiang Lv, and James H. Dickerson. *Gas Transport in Solid Oxide Fuel Cells*. SpringerBriefs in Energy. Springer International Publishing, 2014, pp. 9–17. DOI: 10.1007/978-3-319-09737-4_2.

[2] V.G. Berezkin and J. de Zeeuw. *Capillary Gas Adsorption Chromatography*. Hüthig Heidelberg, 1996.

[3] Thomas Veltzke, Lars Kiewidt, and Jorg Thöming. "Multicomponent gas diffusion in nonuniform tubes". In: *AIChE J.* 61.4 (2015), pp. 1404–1412. DOI: 10.1002/aic.14711.

[4] R.B. Bird, W.E. Stewart, and E.N. Lightfoot. *Transport Phenomena*. Wiley International edition. Wiley, 2007.

[5] Andreas Seidel-Morgenstern. *Membrane Reactors*. Ed. by Andreas Seidel-Morgenstern. Wiley-VCH, 2010.

[6] Ahmad F Ismail, Kailash C Khulbe, and Takeshi Matsuura. *Gas Separation Membranes - Polymeric and Inorganic*. Springer International Publishing, 2015. DOI: 10.1007/978-3-319-01095-3.

[7] Stefan Gheorghiu and Marc-Olivier Coppens. "Optimal bimodal pore networks for heterogeneous catalysis". In: *AIChE J* 50.4 (2004), pp. 812–820. DOI: 10.1002/aic.10076.

[8] Marc-Olivier Coppens. "A nature-inspired approach to reactor and catalysis engineering". In: *Curr. Opin. Chem. Eng.* 1.3 (Aug. 2012), pp. 281–289. DOI: 10.1016/j.coche.2012.03.002.

[9] Gang Wang and Marc-Olivier Coppens. "Calculation of the Optimal Macropore Size in Nanoporous Catalysts and Its Application to DeNOx Catalysis". In: *Ind. Eng. Chem. Res.* 47.11 (2008), pp. 3847–3855. DOI: 10.1021/ie071550+.

[10] Gang Wang and Marc-Olivier Coppens. "Rational design of hierarchically structured porous catalysts for autothermal reforming of methane". In: *Chem. Eng. Sci.* 65.7 (Apr. 2010), pp. 2344–2351.

[11] Benjamin Besser et al. "Hierarchical Porous Zeolite Structures for Pressure Swing Adsorption Applications". In: *ACS Appl. Mater. Interfaces* 8.5 (Feb. 2016), pp. 3277–3286. DOI: 10.1021/acsami.5b11120.

[12] Arto Ojuva et al. "Laminated Adsorbents with Very Rapid CO2 Uptake by Freeze-Casting of Zeolites". In: *ACS Appl. Mater. Interfaces* 5.7 (Apr. 2013), pp. 2669–2676. DOI: 10.1021/am400122r.

[13] Fateme Rezaei and Paul A. Webley. "Optimal design of engineered gas adsorbents - Pore-scale level". In: *Chem. Eng. Sci.* 69.1 (Feb. 2012), pp. 270–278.

[14] Farid Akhtar et al. "Structuring adsorbents and catalysts by processing of porous powders". In: *J. Eur. Ceram. Soc.* 34.7 (July 2014), pp. 1643–1666.

[15] T Ohji and M Fukushima. "Macro-porous ceramics - processing and properties". In: *Int. Mater. Rev.* 57.2 (2012), pp. 115–131. DOI: 10.1179/1743280411Y.0000000006.

[16] H. Verweij. "Ceramic membranes - Morphology and transport". In: *J. Mater. Sci.* 38.23 (2003), pp. 4677–4695. DOI: 10.1023/A:1027410616041.

[17] A. J. Burggraaf and L. Cot. *Fundamentals of Inorganic Membrane Science and Technology*. Elsevier, Amsterdam, 1996.

[18] Marcel Mulder. *Basic Principles of Membrane Technology*. Kluwer Academic Publishers, 1996.

[19] Arthur W. Adamson and Alice P. Gast. *Physical Chemistry of Surfaces*. 6th. JOHN WILEY & SONS, INCORPORATED, 1997.

[20] J.K. Haken. "Polysiloxane stationary phases in gas chromatography". In: *J. Chromatogr. A* 141.3 (1977), pp. 247–288. DOI: http://dx.doi.org/10.1016/S0021-9673(00)93536-2.

[21] Marianna Kele and Georges Guiochon. "Repeatability and reproducibility of retention data and band profiles on reversed-phase liquid chromatography columns: IV. Results obtained with Luna {C18} (2) columns". In: *J. Chromatogr. A* 869.1–2 (2000), pp. 181–209. DOI: http://dx.doi.org/10.1016/S0021-9673(99)01092-4.

[22] F Großmann et al. "Impact of the post-treatment conditions of parent silica on the silanization of n-octadecyl bonded silica packings in reversed-phase high-performance liquid chromatography". In: *J. Chromatogr. A* 910.2 (2001), pp. 223–236. DOI: http://dx.doi.org/10.1016/S0021-9673(00)01194-8.

[23] C.du Fresne von Hohenesche, V Ehwald, and K.K Unger. "Development of standard operation procedures for the manufacture of n-octadecyl bonded silicas as packing material in certified reference columns for reversed-phase liquid chromatography". In: *J. Chromatogr. A* 1025.2 (2004), pp. 177–187. DOI: http://dx.doi.org/10.1016/j.chroma.2003.10.091.

[24] Maria T. Matyska and Joseph J. Pesek. "Comparison of silanization/hydrosilation and organosilanization modification procedures on etched capillaries for electrokinetic chromatography". In: *J. Chromatogr. A* 1079.1–2 (2005). Separation Science: Past, Present and FutureA Tribute to Csaba Horváth, pp. 366–371. DOI: http://dx.doi.org/10.1016/j.chroma.2005.03.010.

[25] E. Mery et al. "A silicon microfluidic chip integrating an ordered micropillar array separation column and a nano-electrospray emitter for LC/MS analysis of peptides". In: *Sens. Actuators, B* 134.2 (2008), pp. 438–

446. DOI: http://dx.doi.org/10.1016/j.snb.2008.05.037.

[26] Dong Wang et al. "Highly Stable Surface Functionalization of Microgas Chromatography Columns Using Layer-by-Layer Self-Assembly of Silica Nanoparticles". In: *Anal. Chem.* 85.17 (Sept. 2013), pp. 8135–8141. DOI: 10.1021/ac401080u.

[27] Scott Higgins, William DeSisto, and Douglas Ruthven. "Diffusive transport through mesoporous silica membranes". In: *Microporous Mesoporous Mater.* 117.1-2 (Jan. 2009), pp. 268–277. DOI: 10.1016/j.micromeso.2008.06.030.

[28] Asad Javaid et al. "Solubility-based gas separation with oligomer-modified inorganic membranes". In: *J. Membr. Sci.* 187.1-2 (June 2001), pp. 141–150.

[29] K Kuraoka, Y Chujo, and T Yazawa. "Hydrocarbon separation via porous glass membranes surface-modified using organosilane compounds". In: *J. Membr. Sci.* 182.1-2 (Feb. 2001), pp. 139–149. DOI: 10.1016/S0376-7388(00)00559-7.

[30] Christian Leger, Helio De L. Lira, and Russell Paterson. "Preparation and properties of surface modified ceramic membranes. Part III. Gas permeation of 5 nm alumina membranes modified by trichlorooctadecylsilane". In: *J. Membr. Sci.* 120.2 (Nov. 1996), pp. 187–195.

[31] Arne Lindbråthen and May-Britt Hägg. "Glass membranes for purification of aggressive gases - Part II. Adsorption measurements and diffusion coefficient estimations". In: *J. Membr. Sci.* 259.1-2 (Aug. 2005), pp. 154–160.

[32] Arne Lindbråthen and May-Britt Hägg. "Glass membranes for purification of aggressive gases - Part I. Permeability and stability". In: *J. Membr. Sci.* 259.1–2 (2005), pp. 145–153. DOI: http://dx.doi.org/10.1016/j.memsci.2005.03.056.

[33] Rajinder P. Singh, J. Douglas Way, and Steven F. Dec. "Silane modified inorganic membranes - Effects of silane surface structure". In: *J. Membr. Sci.* 259.1-2 (Aug. 2005), pp. 34–46. DOI: 10.1016/j.memsci.2005.03.004.

[34] Arne Lindbråthen and May-Britt Hägg. "Membrane separation of chlorine gas". In: *Chem. Eng. Process.* 48.1 (Jan. 2009), pp. 1–16.

[35] Geoffrey D. Bothun, Katif Peay, and Shamsuddin Ilias. "Role of tail chemistry on liquid and gas transport through organosilane-modified mesoporous ceramic membranes". In: *J. Membr. Sci.* 301.1-2 (Sept. 2007), pp. 162–170.

[36] C Picard et al. "Grafting of ceramic membranes by fluorinated silanes: hydrophobic features". In: *Sep. Purif. Technol.* 25.1-3 (Oct. 2001), pp. 65–69.

[37] N. Abidi et al. "Surface modification of mesoporous membranes by fluoro-silane coupling reagent for CO2 separation". In: *J. Membr. Sci.* 270.1-2 (Feb. 2006), pp. 101–107. DOI: 10.1016/j.memsci.2005.06.054.

[38] Yuzuru Sakamoto et al. "Preparation and CO_2 separation properties of amine-modified mesoporous silica membranes". In: *Microporous Mesoporous Mater.* 101.1-2 (Apr. 2007), pp. 303–311. DOI: 10.1016/j.micromeso.2006.11.007.

[39] Mayur Ostwal et al. "3-Aminopropyltriethoxysilane functionalized inorganic membranes for high temperature CO_2/N_2 separation". In: *J. Membr. Sci.* 369 (Nov. 2011), pp. 139–147. DOI: 10.1016/j.memsci.2010.11.053.

[40] Daniel Stoltenberg and Andreas Seidel-Morgenstern. "An attempt to alter the gas separation of mesoporous glass membranes by amine modification". In: *Microporous Mesoporous Mater.* 154 (May 2012), pp. 148–152. DOI: 10.1016/j.micromeso.2011.11.013.

[41] B. A. McCool and W. J. DeSisto. "Amino-Functionalized Silica Membranes for Enhanced Carbon Dioxide Permeation". In: *Adv. Funct. Mater.* 15.10 (Oct. 2005), pp. 1635–1640.

2. Scientific Background

2.1. Gas Transport in Porous Media

2.1.1. Governing Transport Mechanism and Knudsen Number

Gas propagation through a porous solid is a complex process which includes the interaction between gas molecules and the pore wall as well as interactions between the gas molecules themselves. Which interaction and consequently which transport process dominates depends on gaseous rarefaction. To determine this rarefaction state, the mean free path of the gas molecules λ is usually compared to a characteristic length d. This dimensionless value is commonly known as the Knudsen number:[1]

$$Kn = \frac{\lambda}{d}. \tag{2.1}$$

The mean free path λ is defined by temperature T, pressure p and molecular diameter of the gas molecules σ as well as the Boltzmann constant $k_B = 1.38 \cdot 10^{-23}\, kg\, m^2\, s^{-2}\, K^{-1}$:

$$\lambda = \frac{k_B T}{\sqrt{2}\pi\sigma^2 p}. \tag{2.2}$$

The characteristic length is a representative physical length scale for the geometrical dimensions of the considered system and is chosen according to the specific application. This could for example be the airfoil length of an airplane or the diameter of a pipe. In the specific case of porous solids, usually the mean pore diameter is used as the characteristic length. In general, the Knudsen number (eq. 2.1) links the average distance between collisions of gas molecules with the spacial dimension of their surrounding environment, which allows general statements about the molecule-wall interactions, i.e. the state of rarefaction of the gas. For example, if the Knudsen number is very small ($Kn << 1$) the average length between the collision of two molecules is considerably smaller than the pore diameter. Consequently, the probability of a gas molecule to collide with the pore wall becomes very small and molecule-molecule interactions dominate the gas flow behavior. If the Knudsen number is very high ($Kn > 10$), the probability of a gas molecule to interact with another one of its species becomes very small and the gas-wall interactions dominate the gas transport.[1–3] Of course, the predominating transport mechanism depends on the gas molecule-wall interactions and the rarefied state of the gas. When only a single gas moves through the structure, interactions between different gas species* - such as free molecular diffusion - can be neglected.[8] Therefore, three governing transport mechanisms can be identified in porous media as schematically illustrated in Fig. 2.1, namely viscous flow ($Kn << 1$), Knudsen diffusion ($1 < Kn < 10$) and surface diffusion ($Kn > 10$).[2,9]

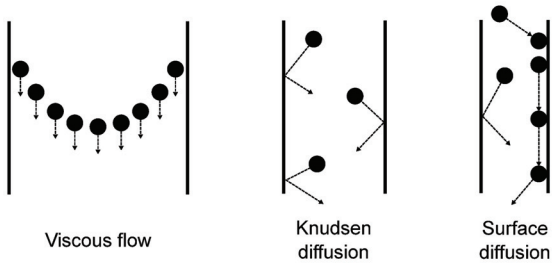

Figure 2.1.: Transport mechanisms in porous media for single gases.

The pore sizes of porous solids can be very different ranging from several micrometers to nanometers. Fig. 2.2 shows the Knudsen number depending on the pore diameter at a pressure of 80 kPa (800 mbar) at temperatures of 0, 20 and 80 °C for molecular diameters between 330 and 380 pm covering CO_2 (330 pm), Ar (340 pm), N_2 (364 pm) and CH_4 (380 pm). The parameters for the calculation are chosen according to the experimental conditions of the measurements performed within this work (see chapter 4-6). The results show, that the Knudsen number is always smaller than 1 as long as the mean pore diameter is larger than 73 nm ($Kn < 1 \,\forall\, d > 73\,\text{nm}$) and it is larger than 10 when the pore diameter is smaller than 7.3 nm ($Kn > 10 \,\forall\, d < 7.3\,\text{nm}$).

*For descriptions and theoretical modeling of multi component diffusion in porous media it is referred to the books from Krishna and coworkers[4,5] who give an in-depth overview, for example introducing the Maxwell-Stefan approach[6,7]

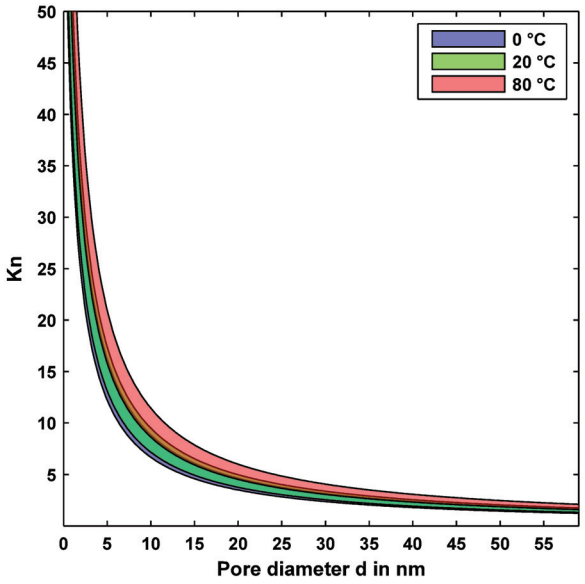

Figure 2.2.: Knudsen number depending on the pore size for gases with kinetic diameters between 330 and 380 pm at temperatures of 0, 20 and 80 °C

.

2.1.2. Viscous Flow

Viscous flow is driven by a pressure gradient and occurs when the intermolecular collisions dominate the gas transport ($Kn << 1$), for example in pores larger than 73 nm. It describes a laminar flow of the gas phase where the fluid flow can be described using continuum quantities such as viscosity.[9,10] To describe the laminar flow of a compressible fluid, the Hagen-Poiseuille law with a pressure dependent viscosity can be used according to equation 2.3.[3,8,11]

$$\frac{\dot{n}}{A} = \frac{\epsilon d_{pore}^2}{32\nu\kappa RT}\frac{p_m \Delta p}{\delta} \tag{2.3}$$

Here, the molar flow $\dot{n}$ through a porous membrane of surface area A is proportional to the mean pressure and the pressure difference $p_m \Delta p$ leading to a quadratic dependency between pressure and molar flow. The relation is further characterized by the temperature T and the universal gas constant R as well as parameters describing the porous structure such as porosity ϵ, mean pore size d_{pore} and the tortuosity factor κ. It is pointed out that the definition of tortuosity is often confused with the tortuosity factor having the relation $\kappa = \tau^2$.[12]

2.1.3. Knudsen Diffusion

Viscous flow gradually disappears at higher Knudsen numbers (e.g. smaller pore sizes) moving towards the so called Knudsen region ($Kn > 1$), which is the case for structures with mean pore diameters smaller than 73 nm according to the aforementioned example. Here, the gas molecule-wall interaction increases and collisions with the pore walls are more likely than collisions with other gas molecules. In this case, the exchange in momentum primarily occurs with the pore walls and the molecules move independently from each other according to their average kinetic energy per molecule, which is related to temperature and molecular mass.[3,9,13] This transport mechanism was first discovered by Martin C. H. Knudsen who showed that rarefied gases propagate through tubes proportional to the applied pressure difference and inversely proportional to their molecular mass M.[14] The so called Knudsen diffusion can be defined for a gas propagating through a porous material according to equation 2.4.[11]

$$\frac{\dot{n}}{A} = \frac{4\epsilon d_{Pore}}{3\kappa\sqrt{2\pi RTM}}\frac{\Delta p}{\delta} \tag{2.4}$$

In contrast to viscous flow, Knudsen diffusion has a linear relation between pressure and gas flow and it depends on the molecular mass of the gas species. That means, assuming identical conditions of temperature and pressure, a heavier gas (e.g. CO_2) diffuses slower through a porous structure than a lighter gas (e.g. N_2). Consequently, the gas flow of two different gas species i and j through the same structure will differ depending on their molecular mass leading to a weak selectivity α as presented in equation 2.5.[11,15]

$$\alpha_{Kn,ij} = \frac{\dot{n}_i}{\dot{n}_j} = \sqrt{\frac{M_j}{M_i}} \tag{2.5}$$

The term selectivity, also known as separation factor, is defined as the ratio of the gas flow of two gases i and j. Selectivities calculated from the Knudsen theory are referred to as Knudsen selectivities (for selectivities obtained from measurement results see section 3.3.5). It is pointed out that according to Knudsen the molar flow of a gas is inversely proportional to the square root of its molar mass, leading to reversed indexes of i and j on the right hand side of equation 2.5. In general, this work follows the notation of $M_i < M_j$ resulting in Knudsen selectivities larger than unity ($\alpha_{Kn,ij} > 1$).

2.1.4. Surface Diffusion

When the pore size is sufficiently small and the Knudsen number very high ($Kn > 10$), Knudsen diffusion can be accompanied by surface diffusion. This mechanism is characterized by preferential adsorption and diffusion - i.e. hopping of molecules along specific adsorption sites - of a gas species along the pore walls of the porous material.[16,17] Surface diffusion increases the gas flow of the adsorbed gas species and reduces the effective pore diameter at the same time which increases the selectivity.[2,3] The driving force for surface diffusion is a concentration gradient of the adsorbed species which is often related to the pressure for gas-solid systems. The total amount of adsorbed molecules strongly depends on temperature as well as the interaction between the adsorbate and the solid surface. Consequently, surface diffusion is only present for adsorbing gas species at low temperatures. A comprehensive review of surface diffusion in porous media is given by Medveď and Černý.[18] According to the aforementioned example, the Knudsen number exceeds 10 for pore diameters of 7.3-12.5 nm, depending on temperature and gas type which is consistent with observations in the literature.[19–21]

2.2. Mesoporous Ceramic Structures

2.2.1. The Need for Uniform Structures

In section 2.1 different transport mechanisms for gases propagating through porous structures are introduced. It is pointed out that, assuming similar thermodynamic conditions, the governing gas transport mechanism strongly depends on the pore size of the material. Mesoporous membranes are usually prepared by deposition techniques, mainly slip-casting or dip-coating (see also section 2.2.2), where different layers are formed on top of a porous support, resulting in asymmetric structures consisting of different pore sizes. Inorganic membranes are the most prominent examples of such asymmetric structures and they usually consist of a macroporous support (>50 nm, usually 1-10 μm), one or two mesoporous intermediate layers (10-50 nm) and a micro- or mesoporous top layer (< 10 nm),[2,22] as exemplary shown in Fig. 2.3. For a gas propagating through such an asymmetric structure, the Knudsen number changes depending on the pore size of each layer. This often leads to Knudsen numbers varying over several orders of magnitude, from $Kn_{1\,\mu m} < 0.13$ in the macroporous support to $Kn_{50...10\,nm} > 1.5$ in the mesoporous supporting structure and $Kn_{10\,nm} > 7.3$ in the top layer, assuming the gas species and thermodynamic conditions from the example in section 2.1. Accordingly, multiple gas transport mechanisms occur simultaneously and the total gas flow through such a hierarchical structure will be a superposition of the gas transport kinetics of each layer. Therefore, it will be difficult to allocate single gas transport characteristics, for example when only interested in the influence of a specific surface functional group on the gas flow behavior. For this reason, asymmetric structures are not favorable for studies aiming to investigate the fundamentals of gas diffusion. Uniform pore networks present a more suitable platform for this purpose, providing a more simple system with a homogeneous gas transport.

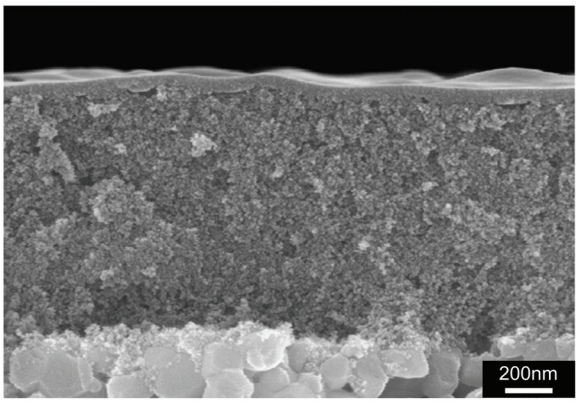

Figure 2.3.: SEM picture of a yttria (8 mol%) stabilized zirconia multi-layer membrane prepared by sol-gel dip-coating, adapted with permission from van Gestel et al.[23]

2.2.2. Processing Strategies

A number of different techniques are available to prepare non-metallic, inorganic structures with pores in the mesopore region. The method of choice depends on the desired material as well as the pore size and structure.[2] The preparation techniques include partial sintering, molten salt inclusion, phase separation and leaching, dynamic deposition, anodic oxidation, pyrolysis, spin or dip-coating, thin film deposition and more.[3,24] Comprehensive reviews about the different processing techniques are given by Burggraaf and Cot[25] as well as Mulder.[26] Many of the aforementioned

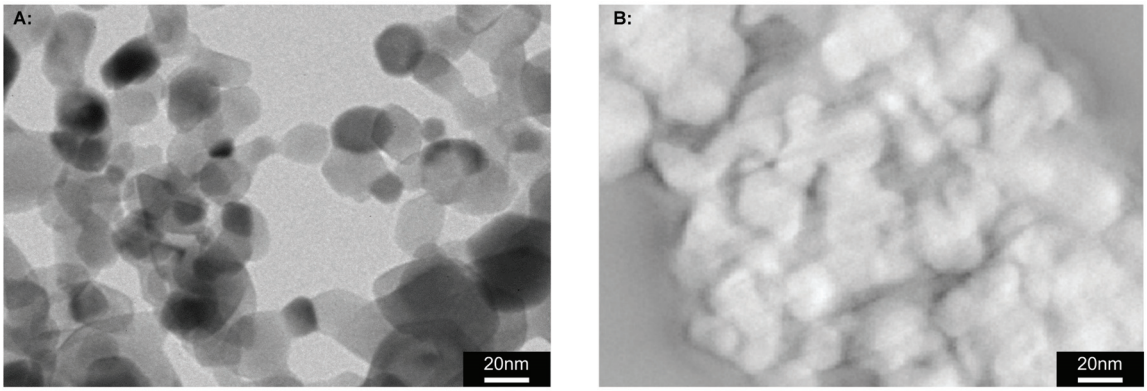

Figure 2.4.: Transmission electron microscope (TEM) image of the yttria-stabilized zirconia (YSZ) nanopowder used in this work (A). TEM tomography reconstruction of a broken piece of the sintered body from extruded YSZ nanopowder (B).

techniques are used to prepare asymmetric membranes, where the structure possessing the desired pore size is deposited as a top layer onto a porous support. The reason for this can be addressed to the requirements of most applications, where low pressure drops and high fluxes are aimed. The smaller the pore sizes of the structure, the higher the pressure drop. For this reason it is advantageous when a porous structure containing small pores is deposited as a thin layer onto a porous support with bigger pore sizes in order to reduce the pressure drop.[27] Furthermore, some of the fabrication techniques require a substrate, for example coating or thin film deposition.[25,28,29]
This work focuses on the preparation of symmetric structures for the fundamental investigation of gas diffusion. To prepare homogeneous membranes with a uniform mesopore distribution, only a few techniques are available. The most prominent examples are phase separation and leaching, as well as partial sintering of a particle network.

Phase Separation and Leaching One strategy to prepare porous ceramics with a uniform microstructure throughout the sample is phase separation and leaching. This technique is used to prepare a wide range of porous glasses with mean pore sizes in the range between 0.3 and 1000 nm.[30] The principle is based on the miscibility gap in the alkali borosilicate phase diagram where the glass coexists for certain glass compositions simultaneously in two phases. A heat treatment between 500 and 580 °C initiates this so called phase separation. The two obtained glass phases are an alkali-rich borate phase and an almost pure silica phase. In contrast to the silica phase, the alkali-rich borate phase is soluble in hot mineral acids, water or alcohols which is used to leach it out in a second step to obtain the porous glass. After the leaching process, the structure consists almost entirely of silica. The structural properties of the final material are defined by the initial glass composition, the heat treatment (temperature and time) as well as the leaching conditions.[26]

Particle Network and Sintering Another strategy for the preparation of porous ceramic structures is the formation of a network of uniform particles in combination with partial sintering. Here, the pore network is build up by the inter particular pore volume in between the ceramic particles, whose pore size is mainly determined by the particle size (pore size $\approx \frac{1}{3}$particle size).[27] For this reason, normally only macropores in between 0.1 and 10 μm can be achieved because ceramic nanopowders with primary particle sizes below 150 nm are rare, expensive and usually difficult to handle in conventional processing techniques.
There are different ways to form bodies from ceramic powder, such as various pressing techniques, slip or tape casting, extrusion and injection moulding. Each process has its advantageous and disadvantageous, but for this work an extrusion process is used.[†] This forming process consists of pressing a homogeneous plastic suspension of ceramic particles through a die to produce long shapes with uniform cross section. It is possible to fabricate numerous different shapes, for example rods, mono- or multichannel tubes and honeycomb structures, by changing the geometry of the die. In particular, tubes with very small di-

[†]For more general information about ceramic powder processing techniques see the books from Salmang and Scholze[31] (German) or Burggraaf and Cot[25] (English)

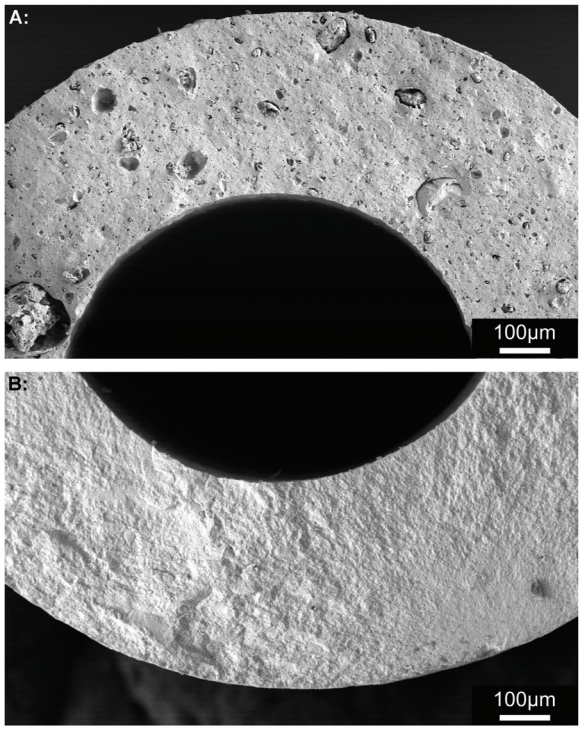

Figure 2.5.: Scanning electron microscopy images of fracture surfaces from sintered capillaries prepared without (A) and with dissolved PVA (B).

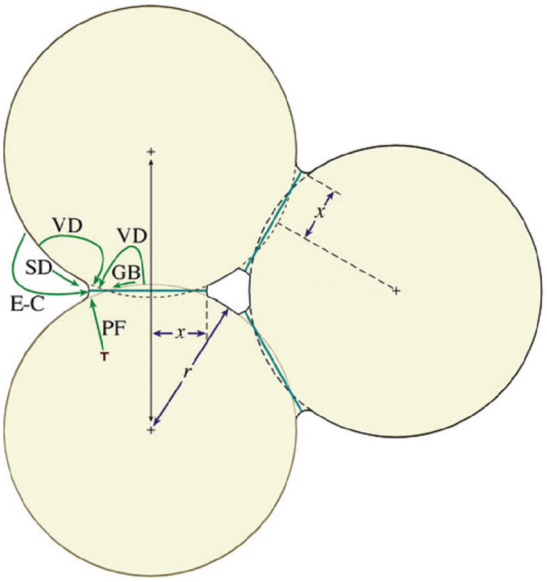

Figure 2.6.: Two-dimensional projection of the sintering of three spheres showing the developement of a pore. The indicated material transport mechanisms are surface diffusion (SD), evaporation-condensation (E-C), grain boundary diffusion (GB), volume diffusion (VD) and plastic flow (PF). Adapted with permission from Carter and Norton.[37]

ameters, such as capillaries, are of interest due to their potential for high packing densities in applications which results in a high surface to volume ratio.[32] Besides the raw ceramic powder, an extrusion process requires the use of additives, such as binders, surfactants or plasticizer, to achieve the necessary suspension properties. Examples for binders in aqueous systems are cellulose derivatives, polyvinyl alcohol (PVA) or polyethylene glycols with a high molecular weight whereas glycols with a low molar weight are used as plasticizer.[33] In this particular case, mesoporous structures with mean pore diameters of around 20 nm are prepared by extrusion based on an extremely fine yttria (3 mol%) stabilized zirconia nanopowder (YSZ, VP Zirkonoxid 3-YSZ, Lot. 3157061469, Evonic Industries, Germany) with a primary particle size of 55 nm[34] (30 nm according to manufacturer). Fig. 2.4A shows a transmission electron spectroscopy image of the YSZ nanopowder before processing. For extrusion, the powder is dispersed with 3-aminopropyltriethoxysilane (APTES) in water to form a stable solution (see also zeta-potential measurements in Fig. A1 in the appendix) and PVA is used as binder. To obtain uniform structures, it is necessary to dissolve the PVA in water[‡] to avoid defects and holes due to binder aggregates, as shown in Fig. 2.5. After extrusion and partially sintering, a porous particle network is obtained as indicated by a TEM tomography reconstruction in Fig. 2.4B. SEM micrographs show a highly homogeneous structure throughout the whole capillary membrane (see Fig. 4.3 in chapter 4). In addition, due to the dissolved PVA, the bending strength of the capillaries increased significantly, indicating a more homogeneous structure without large defects (see Fig. A2 in the appendix).

Partial sintering of powder compacts is the most frequently used approach to fabricate porous ceramic structures.[35] In general, sintering is the process of transforming a powder into a solid body at high temperatures without melting.[36] The main driving force for this is the reduction of the Gibbs free energy of the particle system, mostly by reducing surface and grain boundary area. Conventional sintering processes for ceramic bodies are characterized by, and divided into, three stages. The sintering process begins with particle reori-

[‡]For a 25 wt.% PVA-water solution, 90 g of PVA is dissolved in 270 ml double deionized water containing 3.7 M tris(hydroxymethyl)aminomethane and 5.6 M sodium chloride with a pH of 9.5 while carefully heating the solution using a microwave oven.

entation and neck formation in the first stage, which can be explained with an idealized spherical particle model, as shown in Fig. 2.6. Different mechanisms can contribute to the material formation, such as surface diffusion (SD), evaporation-condensation (E-C), grain boundary diffusion (GB), volume diffusion (VD) and plastic flow (PF). However, the most dominant mechanism in the initial state is surface diffusion.[37] The second (intermediate) state is predominantly driven by lattice and grain boundary diffusion. The sintering necks start to grow further and the porosity of the structure decreases significantly. The final (third) stage is characterized by grain growth with volume diffusion as main diffusive mechanism. Here, pore elimination takes place and the porosity asymptotically approaches its minimum value. For the preparation of porous structures, usually high porosities are desired. Therefore, the material is only partially sintered by terminating the heat treatment before reaching the full density, preferably within the first stage, when sintering necks have already been formed and the porosity is still high.[35]

In this particular case, Kroll et al. investigated the influence of the heat treatment conditions on pore size, porosity as well as mechanical stability of capillaries prepared using the aforementioned YSZ nanopowder.[38] They conclude, that for ceramic bodies consisting of this powder type, a heat treatment for 2 h at a maximum temperature of 1050 °C offers a narrow pore size distribution with a high open porosity in combination with a suitable mechanical strength of the capillaries.

2.2.3. Surface Chemistry of Sintered Solid Oxides

In mesoporous materials, the gas-solid interactions dominate and Knudsen diffusion is the governing transport mechanism (see section 2.1). Therefore, knowledge of the surface chemistry of the native solid oxide material is important, in particular, when a surface functionalization is desired. The native material used in this work is partially stabilized zirconia using a small amount of yttria (3 mol%), see also energy dispersive X-ray measurements in Fig. A3 and X-ray photoelectron spectroscopy measurements in Fig. A4 in the appendix. For this composition, the structure partially consists of a metastable tetragonal phase, as well as a cubic phase,[33] with little amount of monoclinic zirconia as shown by X-ray diffraction measurements (see Fig.A5 in the appendix). Fig. 2.7 shows the crystal structure of ZrO_2 in the cubic phase as a representative geometrical composition. Of course, the true YSZ material is not a single crystal. Each particle, and therefore also the final porous structure, consists of randomly oriented grains with different crystal orientations. The atoms on the outer surface are able to form hydroxyl groups in the presence of water.[39,40] According to Nawrocki et al., a zirconia surface (and in general each oxidic surface) will "tend to bind any available molecule so as to satisfy its unsaturated coordination."[41] They also show that a zirconia surface will always contain chemisorbed species such as water (hydroxyl groups) or CO_2 (carbonate groups), unless the sample is heat treated at very high temperatures (>300-550 °C).[42] This implies that each oxidic surface handled under normal conditions is inevitable covered with a chemisorbed layer of molecules, forming different kinds of functional surface groups. The amount of hydroxyl groups per surface area can be estimated theoretically from crystallographic data as well as experimentally. Here, values measured for zirconia show approximately 13-14 (OH) groups nm^{-2}, which is in good agreement with the theoretical estimate of 15 (OH) groups nm^{-2}.[41,43–45] In this particular case, X-ray photo-electron spectroscopy measurements show the presence of hydroxyl surface groups and indicate a small presence of carbonate groups (see Fig. A4).

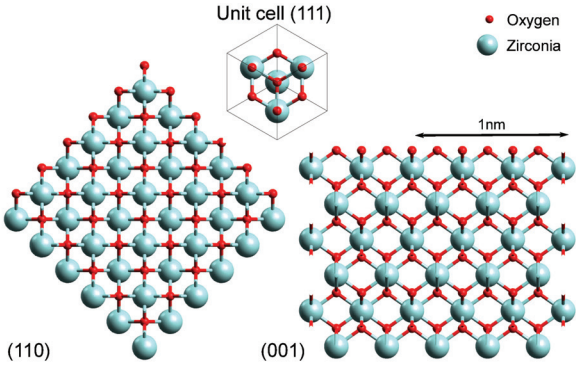

Figure 2.7.: Crystal structure of cubic ZrO_2 visualized with Avogadro (version 1.1.1).

2.3. Tailoring Surface Functionalities

2.3.1. Surface Activation

Most strategies to tailor the surface functionality of metal oxides use surface hydroxyl groups as binding partners for the functional molecules. For this reason, it is desirable to increase the density of OH-groups on the solid surface prior to the functionalization step. To fulfill this goal, different techniques are available ranging from physical to chemical treatments.

Oxygen Plasma Treatment One way to generate hydroxyl groups on ceramic surfaces is oxygen plasma. In a plasma, the gas atoms are excited to higher energy states and ionized by introducing a large amount of energy. A common way of generating a low temperature plasma is applying an electric current on a low gas pressure. Comprehensive reviews about plasma processes are given by Tendero et al.[46] and Bárdos and Baránková.[47] In general, the reactive ions, electrons and radicals, as well as the emitted photons (mostly ultra-violett) in the oxygen plasma interact with a ceramic surface when it is exposed to this environment. This leads to the oxidation of carbons on the surface of the material, as well as generating polar oxygen and hydroxyl groups.[48] However, the oxygen plasma technique does not penetrate very deep into porous structures which leads to anisotropic surface activations.[49]

Hydrothermal Treatment Another way to activate the surface of solid oxides is hydrothermal treatment. This has been demonstrated for different ceramic surfaces such as alumina, silica and mullite,[50–52] as well as for zirconia.[53] In this process, the oxidic surface is usually exposed to water or water vapor under high pressures and temperatures, for example in an autoclave. Kroll et al. compared the hydroxylation efficiencies of different surface activation techniques on microtubes, consisting of a yttria stabilized nanopowder comparable to the one used in this work (yttria (3 mol%) stabilized zirconia). They found that a hydrothermal treatment does not significantly increase the concentration of hydroxyl groups on the surface in contrast to a wet-chemical treatment using acid or base.[38]

Wet-Chemical Treatment Wet-chemical hydroxylation is another way to directly create hydroxyl groups on a solid oxide surface. The OH-groups are generated either by strong acid or base solutions. The degree of hydroxylation of the surfaces depends not only on concentration, but also on incubation time and temperature. Common basic treatments include, for example, sodium hydroxide (NaOH) solutions with a high concentration (usually 1 M NaOH), operating at temperatures of around 100 °C for 24 h,[54,55] or working with concentrated ammonia at elevated temperatures (70 °C).[56] For an acidic hydroxylation, different acids are used ranging from phosphoric (H_3PO_4) or hydrochloric acid (HCl) to piranha solution, a 3:1 mixture of sulfuric acid (H_2SO_4) and hydrogen peroxide (H_2O_2), mostly operating at elevated temperatures.[57]
Nawrocki et al.[42] stated that a basic hydroxylation yields a higher amount of additional surface hydroxyl groups on monoclinic zirconia than an acidic treatment. In contrast, Lohbauer et al.,[57] as well as Kroll et al.,[38] reported independently from each other, that an acidic hydroxylation leads to a higher surface activation for partially stabilized zirconia (3 mol% of yttria), as used in this work. In summary, Lohbauer et al. investigated the treatment with 15 M NaOH, 5 M H_3PO_4 and a mixture of oxalic acid ($H_2C_20_4$) and HCl at temperatures of 95 °C for a rather long time of 4 d, compared to Piranha solution at room temperature (also 4 d). They recorded the highest values for surface hydroxyl groups for samples treated with Piranha solution. The same conclusion is drawn by Kroll et al., who compared the surface activation by Piranha solution at room temperature and 95 °C (30 min), 15 M NaOH at 95 °C and a hydrothermal treatment. Here, the highest values of surface hydroxyl groups are also obtained with Piranha solution, without a noticeable difference between a treatment at room temperature and a treatment at 95 °C. For this reason, the surface hydroxylation is carried out at room temperature using Piranha solution for 30 min in this study.

2.3.2. Surface Functionalization

There are many ways to alter the surface functionality of ceramic materials, ranging from the electrostatic adsorption of molecules due to difference in charge, to simultaneous functional layer generation by chemical vapor deposition of silanes.[58] However, the physical adsorption strength is

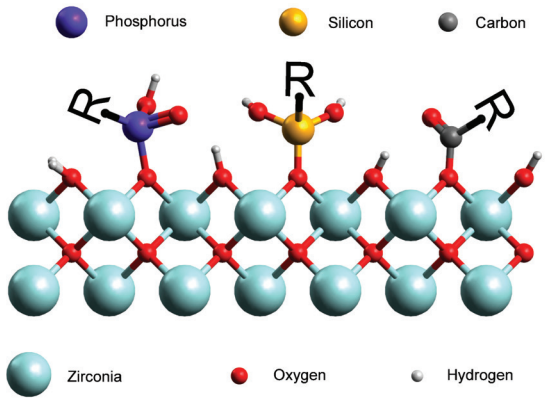

Figure 2.8.: Schematic illustration of the wet-chemical functionalizations using phosphates, silanes and carboxylates on metal oxide surfaces visualized with Avogadro (version 1.1.1).

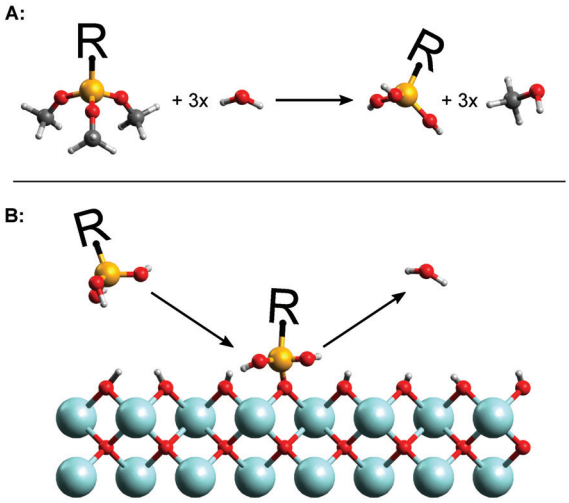

Figure 2.9.: Hydrolysis reaction of a methyl-silane molecule (A) and a schematical condensation reaction of an hydrolyzed silane molecule with a hydroxylated ZrO_2 surface (B) visualized with Avogadro (version 1.1.1).

rather weak compared to a covalent bonding which is therefore desired in most cases. Different bonding molecules such as phosphates, silanes and carboxylates are used to covalently bind specific functional groups onto the surface, as schematically shown in Fig. 2.8.[59,60] These surface functionalizations are mostly carried out using wet-chemical treatments, where the functional molecules react with surface hydroxyl groups to form covalent bonds. For this reason, a surface hydroxylation is often carried out prior to the functionalization step to increase the amount of hydroxyl groups on the solid surface as described in section 2.3.1.

Silanization The most common approach to functionalize an oxidic surface is wet-chemical treatment using silane molecules, also called silanization.[61] The reason for the popularity of this method is the wide range of different available silane molecules, in combination with the straightforward process, which does not require expensive equipment or distinct conditions. The variety of functional groups attached to the silane molecules is large, including amino-groups,[62] sulfonate-groups,[63] alkyl-[64,65] or fluorinated groups,[66,67] all available with different spacer length.[§] In a silane molecule, the silicon atom is bonded to one or more functional groups, as well as to groups which can be hydrolyzed such as alcohols[62,69] or chlorine containing groups.[65,67] Fig. 2.9A shows an exemplary hydrolysis step for a silane molecule with three methanol-groups and one functional group. With water as reaction partner, the silane molecule is hydrolyzed while forming methanol as a byproduct. If this silane molecule comes into contact with a surface containing hydroxyl groups, it can bond covalently to the surface by forming a water molecule in a condensation reaction (Fig. 2.9B).

This hydrolysis-condensation reaction is performed using a variety of solvents, for example water[69] or organic solvents such as ethanol,[70] toluene,[65] chloroform[66] or acetone.[49] Apparently, the choice of solvent used for silanization is highly heterogeneous throughout the literature and the same can be found for handling the water content. Where some take extremely care of a water-free environment,[64,65] others perform the silanization using water as a solvent[63,69] or specifically add a small amount of water as a catalyst for the condensation reaction.[49] The argument for working in a dry environment is the possibility of multi-layer formation and cross-linking, especially when working with silanes showing polar functional groups. Of course, this probability will be significantly smaller for silanes showing apolar functional groups, such as alkyl-chains, as used in this work. Besides that, the apolar silanes are often not soluble in water, but it can be shown that a certain amount of water present enhances the hydrolysis-condensation reaction which leads to a higher surface coverage (see thermo gravimetric analysis in Fig. A6 in the appendix). For this reason, a mixture containing 95 % acetone and 5 % water (v:v) is chosen as solvent in this work.

[§]For more detailed information regarding silanes see Hermanson.[68]

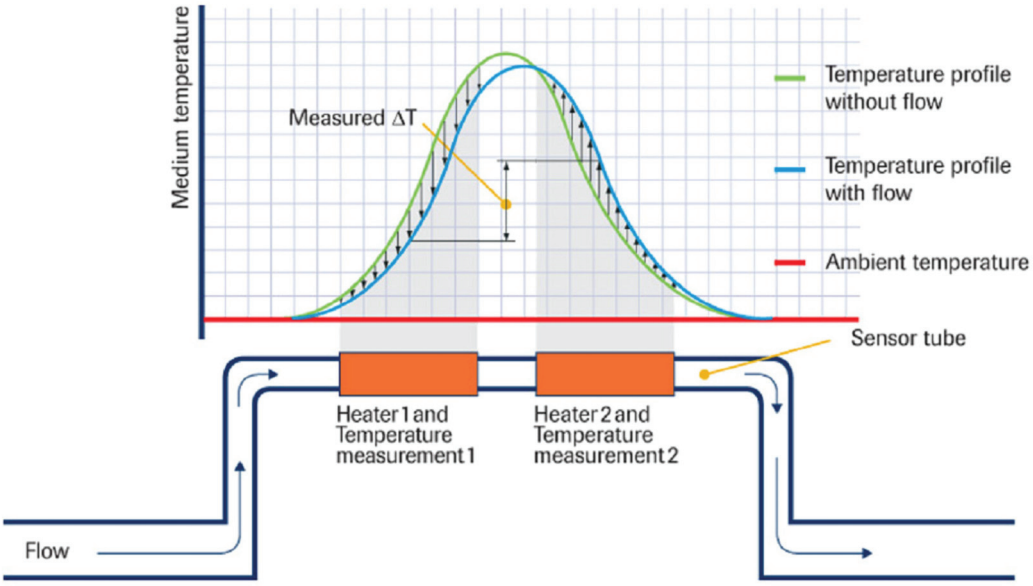

Figure 2.10.: Functional scheme of thermal mass flow sensor (F-110C)[73]

The silanization reaction is mainly influenced by three parameters: Silane concentration, reaction temperature and time. Incubation times used for functionalization range from 60 min[63] to 24 h[69] while using different silane concentrations mostly ranging from 0.01[49] to 0.2 M.[69] In general, the reaction is performed at elevated temperatures above 65 °C, usually boiling under reflux for several hours. Experiments show that the reproducibility significantly increases with increasing incubation time (data not shown). For this reason, the silanization procedure in this work is carried out boiling under reflux (80 °C) for 16 h, using a silane concentration of 0.2 M.

2.4. Measurement of gas permeation

To investigate transport mechanisms in porous media and the influence of surface functionalizations, many techniques are available to experimentally determine gas flows in porous structures. Some of which are for example gas chromatography and steady state or transient diffusion cells, just to name a few[¶].[10] Especially the measurement of steady-state flux in permeation cells is a suitable method for this purpose, because it is simple to carry out and the flux is measured directly.[71]
The measurement principle is fairly easy and closely related to the original permeation measurements of Darcy in the nineteenth century.[10] A constant pressure drop Δp is applied on the sample and the gas flow $\dot{n}$ (or $\dot{m}$) across the membrane is measured, representing the key parameters in the equations 2.3-2.5. The gas flow itself can be measured using different techniques and the sensor types can be broadly separated into non-thermal and thermal flow sensors.[72] Non-thermal flow sensors, using for example drag force, pressure or the Coriolis principle, suffer from a range of disadvantages related to the gas density or the temperature. For this reason, thermal flow sensors are often preferred and are also used here.
The measurement setup was originally developed by Thomas Veltzke[74,75] and was further optimized within this study (see also section 3.3). It is based on the dead-end measurement principle and the gas flow is measured in steady state condition by a thermal flow sensor (F-110C, Bronckhorst, Germany). The measurement principle is schematically shown in Fig. 2.10. The gas flows through the sensor tube and its heating elements, inducing a temperature profile. The temperature of the gas i is measured at two points and the temperature difference is directly proportional to the mass or molar flow through the sensor. It can be calculated according to equation 2.6, with C being a constant and $c_{p,i}$ the specific heat capacity of gas i.

$$\Delta T = C \cdot c_{p,i} \cdot \dot{m}_i = C \cdot c_{p,i} \cdot \dot{n}_i \cdot M_i \qquad (2.6)$$

This so called calorimetric measurement principle has a low uncertainty in comparison to other tech-

[¶]For a comprehensive review about the different measurement techniques for example the Wicke-Kallenbach method it is referred to Park et al.[71]

niques and is not vulnerable against varying temperature and ambient conditions.[75] In turn, these sensors have a restricted measurement range and the lower limit of this range is comparably high. Nevertheless, the measurement range is easily adjusted by an appropriate size of membrane area, which can simply be controlled by the length of the used capillary shaped membranes.

References

[1] Weidong He, Weiqiang Lv, and James H. Dickerson. *Gas Transport in Solid Oxide Fuel Cells*. SpringerBriefs in Energy. Springer International Publishing, 2014, pp. 9–17. DOI: 10.1007/978-3-319-09737-4_2.

[2] Ahmad F Ismail, Kailash C Khulbe, and Takeshi Matsuura. *Gas Separation Membranes - Polymeric and Inorganic*. Springer International Publishing, 2015. DOI: 10.1007/978-3-319-01095-3.

[3] Pratibha Pandey and R.S. Chauhan. "Membranes for gas separation". In: *Prog. Polym. Sci.* 26.6 (Aug. 2001), pp. 853–893.

[4] R. Krishna and R. Taylor. *Multicomponent Mass Transfer*. Wiley, 1993.

[5] J.A. Krishna R.and Wesselingh. *Mass Transfer in Multicomponent Mixtures*. Delft Academic Press, 2000.

[6] J. Clerk Maxwell. "On the dynamical theory of gases". In: *Philos. Trans. R. Soc. Lond.* 157 (1867), pp. 49–88.

[7] Josef Stefan. "Über das Gleichgewicht und Bewegung, insbesondere die Diffusion von Gemischen". In: *Sitzungsberichte der Akademie der Wissenschaften mathematisch-naturwissenschaftliche Klasse* 63.2 (1871), pp. 63–124.

[8] E. Nagy. *Basic Equations of the Mass Transport through a Membrane Layer*. Elsevier, 2012.

[9] Andreas Seidel-Morgenstern. *Membrane Reactors*. Ed. by Andreas Seidel-Morgenstern. Wiley-VCH, 2010.

[10] Jeong-Gil Choi, D. D. Do, and H. D. Do. "Surface Diffusion of Adsorbed Molecules in Porous Media - Monolayer, Multilayer, and Capillary Condensation Regimes". In: *Ind. Eng. Chem. Res.* 40.19 (2001), pp. 4005–4031. DOI: 10.1021/ie010195z.

[11] T. Melin and R. Rautenbach. *Membranverfahren*. Vol. 3. Springer Berlin Heidelberg, 2007.

[12] N. Epstein. "On tortuosity and the toruosity factor in flow and diffusion through porous media". In: *Chem. Eng. Sci.* 44.3 (1989), pp. 777–779.

[13] Harold Grad. "On the kinetic theory of rarefied gases". In: *Commun. Pure Appl. Math.* 2.4 (1949), pp. 331–407. DOI: 10.1002/cpa.3160020403.

[14] Martin Knudsen. "The law of the molecular flow and viscosity of gases moving through tubes". In: *Ann. Phys. (Leipzig)* 28 (1909), pp. 75–130.

[15] S. Higgins et al. "Covalent Attachment of Monochlorosilanes to Mesoporous Silica Membranes using Supercritical Fluid Deposition". In: *Sep. Sci. Technol.* 43.16 (Nov. 2008), pp. 4113–4128. DOI: 10.1080/01496390802414692.

[16] A. Marković et al. "Gas permeation through porous glass membranes - Part I. Mesoporous glasses–Effect of pore diameter and surface properties". In: *J. Membr. Sci.* 336.1–2 (2009), pp. 17–31. DOI: 10.1016/j.memsci.2009.02.031.

[17] William J Koros and Rajiv Mahajan. "Pushing the limits on possibilities for large scale gas separation - which strategies?" In: *J. Membr. Sci.* 175.2 (Aug. 2000), pp. 181–196. DOI: 10.1016/S0376-7388(00)00418-X.

[18] Igor Medveď and Robert Černý. "Surface diffusion in porous media: A critical review". In: *Microporous Mesoporous Mater.* 142.2-3 (2011), pp. 405–422. DOI: 10.1016/j.micromeso.2011.01.015.

[19] A. D. Wiheeb et al. "Identification of Molecular Transport Mechanisms in Micro-Porous Hydrotalcite-Silica Membrane". In: *Transp. Porous Media* 104.1 (May 2014), pp. 133–144. DOI: 10.1007/s11242-014-0324-5.

[20] R. Krishna and J.M. van Baten. "An investigation of the characteristics of Maxwell-Stefan diffusivities of binary mixtures in silica nanopores". In: *Chem. Eng. Sci.* 64.5 (Mar. 2009), pp. 870–882. DOI: 10.1016/j.ces.2008.10.045.

[21] Simón E. Albo, Linda J. Broadbelt, and Randall Q. Snurr. "Multiscale modeling of transport and residence times in nanostructured membranes". In: *American Institute of Chemical Engineers* 52.11 (2006), pp. 3679–3687. DOI: 10.1002/aic.10998.

[22] H. Verweij. "Ceramic membranes - Morphology and transport". In: *J. Mater. Sci.* 38.23 (2003), pp. 4677–4695. DOI: 10.1023/A:1027410616041.

[23] Tim Van Gestel et al. "Potentialities of microporous membranes for H2/CO2 separation in future fossil fuel power plants: Evaluation of SiO2, ZrO2, Y2O3–ZrO2 and TiO2–ZrO2 sol–gel membranes". In: *J. Membr. Sci.* 359.1–2 (2010). Membranes and {CO2} Separation, pp. 64–79. DOI: 10.1016/j.memsci.2010.04.002.

[24] Ramesh R. Bhave. *Inorganc Membranes - Synthesis, Characteristics and Applications*. Van Nostrand Reinhold, New York, 1991.

[25] A. J. Burggraaf and L. Cot. *Fundamentals of Inorganic Membrane Science and Technology*. Elsevier, Amsterdam, 1996.

[26] Marcel Mulder. *Basic Principles of Membrane Technology*. Kluwer Academic Publishers, 1996.

[27] K. Ohlrogge and K. Ebert. *Membranen*. WILEY-VCH Verlag GmbH & Co KGaA, Weinheim, 2006.

[28] C. J. Brinker et al. "Fundamentals of sol-gel dip coating". In: *Thin Solid Films* 2001 (1991), pp. 97–108.

[29] Thomas P. Niesen and Mark R. De Guire. "Review: Deposition of Ceramic Thin Films at Low Temperatures from Aqueous Solutions". In: *J. Electroceram.* 6.3 (2001), pp. 169–207. DOI: 10.1023/A:1011496429540.

[30] D. Enke, F. Janowski, and W. Schwieger. "Porous glasses in the 21st century - a short review". In: *Microporous Mesoporous Mater.* 60.1–3 (2003), pp. 19–30. DOI: 10.1016/S1387-1811(03)00329-9.

[31] Hermann Salmang and Horst Scholze. *Keramik*. Ed. by Rainer Telle. 7th ed. Springer Berlin Heidelberg New York, 2007.

[32] Stephen Kroll et al. "High virus retention mediated by zirconia microtubes with tailored porosity". In: *J. Eur. Ceram. Soc.* 32.16 (Dec. 2012), pp. 4111–4120. DOI: 10.1016/j.jeurceramsoc.2012.07.026.

[33] Philippe Boch and Jean-Claude Niepce. *Ceramic Materials: Processes, Properties and Applications*. Wiley, 2010.

[34] Julia Werner et al. "Production of ceramic membranes with different pore sizes for virus retention". In: *J. Water Process Eng.* 4 (Dec. 2014), pp. 201–211. DOI: 10.1016/j.jwpe.2014.10.007.

[35] T Ohji and M Fukushima. "Macro-porous ceramics - processing and properties". In: *Int. Mater. Rev.* 57.2 (2012), pp. 115–131. DOI: 10.1179/1743280411Y.0000000006.

[36] M.N. Rahaman. *Ceramic Processing and Sintering*. Marcel Dekker, Inc., 2003.

[37] C. Barry Carter and M. Grant Norton. *Ceramic Materials Science and Engineering*. Springer, 2013.

[38] Stephen Kroll et al. "Highly efficient enzyme-functionalized porous zirconia microtubes for bacteria filtration". In: *Environ. Sci. Technol.* 46.16 (July 2012), pp. 8739–8747. DOI: 10.1021/es3006496.

[39] M.A. Blesa et al. "The interaction of metal oxide surfaces with complexing agents dissolved in water". In: *Coord. Chem. Rev.* 196.1 (2000), pp. 31–63. DOI: 10.1016/S0010-8545(99)00005-3.

[40] Susan E. Redfern, Robin W. Grimes, and Rees D. Rawlings. "The hydroxylation of t-ZrO2 surfaces". In: *J. Mater. Chem.* 11 (2 2001), pp. 449–455. DOI: 10.1039/B007789P.

[41] J. Nawrocki et al. "Chemistry of zirconia and its use in chromatography". In: *J Chromatogr A* 657.2 (Dec. 1993), pp. 229–282.

[42] J. Nawrocki et al. "A TGA investigation of hydrated monoclinic zirconia". English. In: *Anal. Chim. Acta* 327.3 (July 1996), pp. 261–266. DOI: 10.1016/0003-2670(96)00110-9.

[43] J. Randon et al. “Sulfate adsorption on zirconium dioxide”. In: *Langmuir* 7.11 (1991), pp. 2654–2658. DOI: 10.1021/la00059a043.

[44] J. Randon et al. “Study of ZrO_2 Membrane - Aqueous Solutions Interface”. In: *Key Eng. Mater.* 61-62 (1992), pp. 495–498. DOI: 10.4028/www.scientific.net/kem.61-62.495.

[45] Hideaki Kita et al. “Measurement of acid-base properties on metal oxide surfaces in aqueous solution”. In: *J. Chem. Soc., Faraday Trans. 1* 77 (10 1981), pp. 2451–2463. DOI: 10.1039/F19817702451.

[46] Claire Tendero et al. “Atmospheric pressure plasmas - A review”. In: *Spectrochim. Acta, Part B* 61.1 (2006), pp. 2–30. DOI: http://dx.doi.org/10.1016/j.sab.2005.10.003.

[47] L. Bárdos and H. Baránková. “Cold atmospheric plasma - Sources, processes, and applications”. In: *Thin Solid Films* 518.23 (2010), pp. 6705–6713. DOI: http://dx.doi.org/10.1016/j.tsf.2010.07.044.

[48] Akio Noro et al. “Influence of surface topography and surface physicochemistry on wettability of zirconia (tetragonal zirconia polycrystal)”. In: *J. Biomed. Mater. Res. Part B* 101B.2 (2013), pp. 355–363. DOI: 10.1002/jbm.b.32846.

[49] Stephen Kroll et al. “Colored ceramic foams with tailored pore size and surface functionalization used as spawning plates for fish breeding”. In: *Ceram. Int.* 40.10 (Dec. 2014), pp. 15763–15773. DOI: 10.1016/j.ceramint.2014.07.100.

[50] Ludmilla Derr et al. “Assessment of the Proteolytic Activity of alpha-Al2O3-Chymotrypsin Immobilized on Colloidal Particles by Matrix-Assisted Laser Desorption Ionization Time-of-Flight Mass Spectrometry”. In: *Anal. Lett.* 48.3 (2015), pp. 424–441. DOI: 10.1080/00032719.2014.951449.

[51] Nadine Eils et al. “High-Temperature Hydroxylation and Surface Corrosion of 2/1-Mullite Single Crystals in Water Vapor Environments”. In: *J. Am. Ceram. Soc.* 89.9 (2006), pp. 2887–2894. DOI: 10.1111/j.1551-2916.2006.01170.x.

[52] Claus H. Rüscher, Shiro Shimada, and Hartmut Schneider. “High-Temperature Hydroxylation of Mullite”. In: *J. Am. Ceram. Soc.* 85.6 (2002), pp. 1616–1618. DOI: 10.1111/j.1151-2916.2002.tb00322.x.

[53] E. M. Moser et al. “Surface analytical study of hydrothermally treated zirconia ceramics”. In: *Fresenius. J. Anal. Chem.* 346.1 (1993), pp. 255–260. DOI: 10.1007/BF00321426.

[54] Frederik Böke, Karolina Schickle, and Horst Fischer. “Biological Activation of Inert Ceramics - Recent Advances Using Tailored Self-Assembled Monolayers on Implant Ceramic Surfaces”. In: *Materials* 7.6 (2014), pp. 4473–4492. DOI: 10.3390/ma7064473.

[55] Horst Fischer et al. “Bioactivation of inert alumina ceramics by hydroxylation”. In: *Biomaterials* 26.31 (2005), pp. 6151–6157. DOI: http://dx.doi.org/10.1016/j.biomaterials.2005.04.038.

[56] Alexandra Ancelmo Piscitelli Mansur et al. “Chemical functionalization of ceramic tile surfaces by silane coupling agents - polymer modified mortar adhesion mechanism implications”. en. In: *Mater. Res.* 11 (Sept. 2008), pp. 293–302. DOI: 10.1590/S1516-14392008000300011.

[57] Ulrich Lohbauer et al. “Hydroxylation of dental zirconia surfaces - Characterization and bonding potential”. In: *J. Biomed. Mater. Res. Part B* 87B.2 (2008), pp. 461–467. DOI: 10.1002/jbm.b.31126.

[58] Shunsuke Suzuki et al. “Development of inorganic-organic hybrid membranes for carbon dioxide/methane separation”. In: *J. Membr. Sci.* 471 (Dec. 2014), pp. 402–411.

[59] Remi Boissezon et al. “Organophosphonates as anchoring agents onto metal oxide-based materials - synthesis and applications”. In: *RSC Adv.* 4 (67 2014), pp. 35690–35707. DOI: 10.1039/C4RA05414H.

[60] Marie-Alexandra Neouze and Ulrich Schubert. “Surface Modification and Functionalization of Metal and Metal Oxide Nanoparticles by Organic Ligands”. In: *Monatsh. Chem.* 139.3 (2008), pp. 183–195. DOI: 10.1007/s00706-007-0775-2.

[61] Laura Treccani et al. “Functionalized ceramics for biomedical, biotechnological and environmental applications”. In: *Acta Biomater.* 9.7 (July 2013), pp. 7115–7150. DOI: 10.1016/j.actbio.2013.03.036.

[62] Mayur Ostwal et al. “3-Aminopropyltriethoxysilane functionalized inorganic membranes for high temperature CO_2/N_2 separation”. In: *J. Membr. Sci.* 369 (Nov. 2011), pp. 139–147. DOI: 10.1016/j.memsci.2010.11.053.

[63] F. Meder et al. “Protein adsorption on colloidal alumina particles functionalized with amino, carboxyl, sulfonate and phosphate groups”. In: *Acta Biomater.* 8.3 (2012), pp. 1221–1229. DOI: 10.1016/j.actbio.2011.09.014.

[64] K Kuraoka, Y Chujo, and T Yazawa. “Hydrocarbon separation via porous glass membranes surface-modified using organosilane compounds”. In: *J. Membr. Sci.* 182.1-2 (Feb. 2001), pp. 139–149. DOI: 10.1016/S0376-7388(00)00559-7.

[65] Asad Javaid et al. “Solubility-based gas separation with oligomer-modified inorganic membranes”. In: *J. Membr. Sci.* 187.1-2 (June 2001), pp. 141–150.

[66] N. Abidi et al. “Surface modification of mesoporous membranes by fluoro-silane coupling reagent for CO2 separation”. In: *J. Membr. Sci.* 270.1-2 (Feb. 2006), pp. 101–107. DOI: 10.1016/j.memsci.2005.06.054.

[67] Geoffrey D. Bothun, Katif Peay, and Shamsuddin Ilias. “Role of tail chemistry on liquid and gas transport through organosilane-modified mesoporous ceramic membranes”. In: *J. Membr. Sci.* 301.1-2 (Sept. 2007), pp. 162–170.

[68] Greg T. Hermanson. “Chapter 13 - Silane Coupling Agents”. In: *Bioconjugate Techniques (Third edition)*. Ed. by Greg T. Hermanson. Boston: Academic Press, 2013, pp. 535–548.

[69] Julia Bartels et al. “Amino-functionalized ceramic capillary membranes for controlled virus retention”. In: *Environ. Sci. Technol.* 50.4 (Jan. 2016), pp. 1973–1981. DOI: 10.1021/acs.est.5b05124.

[70] Nengwen Gao et al. “Improving the filtration performance of ZrO2 membrane in nonpolar organic solvents by surface hydrophobic modification”. In: *J. Membr. Sci.* 375.1-2 (2011), pp. 276–283. DOI: http://dx.doi.org/10.1016/j.memsci.2011.03.056.

[71] In-Soo Park, Duong D. Do, and Alirio E. Rodrigues. “Measurement of the Effective Diffusivity in Porous Media by the Diffusion Cell Method”. In: *Catal. Rev. - Sci. Eng.* 38.2 (1996), pp. 189–247. DOI: 10.1080/01614949608006458.

[72] Jonathan T. W. Kuo, Lawrence Yu, and Ellis Meng. “Micromachined Thermal Flow Sensors - A Review”. In: *Micromachines* 3.3 (2012), p. 550. DOI: 10.3390/mi3030550.

[73] *Datasheet F-110C - Mass Flow Meter for Gases.* Bronkhorst. Nijverheidsstraat 1a, NL-7261 AK Ruurlo, Netherlands.

[74] Thomas Veltzke, Michael Baune, and Jorg Thöming. “The contribution of diffusion to gas microflow - An experimental study”. In: *Phys. Fluids* 24.8 (2012), pages. DOI: 10.1063/1.4745004.

[75] T. Veltzke. “On gaseous microflows under isothermal conditions”. Dissertation. University of Bremen, 2013.

3. Characterization Methods

3.1. Structural Characterization

3.1.1. Helium Pycnometry

Helium pycnometry is used to determine the true density of the material. The true (or real) density is defined as the mass divided by the occupied volume according to equation 3.1.[1]

$$\delta = \frac{m}{V_{sample}} \tag{3.1}$$

The measurement principle of pycnometry is based on fluid displacement by the solid material.[2] In order to determine the volume occupied by the solid phase, two measurement chambers with well defined and known volumina are needed, one as sample chamber (V_1) and one serving as reference V_2. After evacuating both volumes, a defined gas pressure (p_1) is set in the sample chamber. Helium is being used as gas in most cases because of its inertness and its small size enabling penetration in very small pores.[3] The sample chamber is connected with the reference volume and, after pressure balance, the equilibrium pressure is determined (p_2). The sample volume can be calculated according to equation 3.2:

$$V_{sample} = V_1 - V_2 \cdot \frac{p_2}{p_1 - p_2}. \tag{3.2}$$

The measurements are performed on a Pycnomatic ATC (Thermo electron corporation, Italy) at 20 °C with a temperature stability of ±0.01 °C. The devices accuracy as well as reproducibility on sample volume is <0.01 %.[3]

3.1.2. Nitrogen Adsorption/Desorption

Besides gas adsorption can be performed using various gases, including argon and krypton,[4] nitrogen is the recommended and most commonly used adsorptive for determining the specific surface area and the mesopore size distribution.[2] Nitrogen adsorption and desorption is a measurement technique, where gaseous nitrogen is adsorbed on a solid surface at very low temperatures (-196 °C). It is possible to determine the gas adsorption with two different principles, gravimetrically and volumetrically. In this case, only measurement systems based on the volumetric method are used and should be focused. For this, the solid material is cooled to a constant temperature, usually to -196 °C in a liquid nitrogen bath, while reducing the pressure. Precise doses of nitrogen gas are consecutively introduced into the measurement chamber and the equilibrium pressure is recorded for each dose.[5] The nitrogen molecules partially adsorb on the surface of the solid material. In the equilibrium state, the amount of adsorbed molecules is proportional to the gas pressure. Therefore, the obtained isotherms represent the adsorbed amount of nitrogen depending on the gas pressure.[6] The results are usually presented in adsorbed volume of nitrogen at standard temperature and pressure (0 °C and 101.3 kPa), depending on the relative pressure $\frac{p}{p_0}$, with p_0 being the vapor pressure of nitrogen at -196 °C (p_0=101.3 kPa). Depending on the type of material, the adsorption isotherms can have different shapes. In the recommendations from the International Union of Pure and Applied Chemistry[7] (IUPAC), the physisorption isotherms are grouped into six different types.*, as schematically shown in Fig. 3.1
Reversible type I isotherms are obtained from microporous solids with relatively small external surfaces, such as some activated carbons or molecular sieve zeolites. Reversible Type II isotherms are typical for non-porous or macroporous solids, representing an unrestricted mono-layer–multi-layer formation. The point B, the beginning of the middle and almost linear section in these isotherms, usually corresponds to the completion of the mono-layer coverage, before the multi-layer formation is about to begin. A very uncommon, special case (e.g. nitrogen on polyethylene) is represented by type III isotherms. Here, no point B and therefore no mono-layer formation can be identified as the adsorbent-adsorbate interactions are relatively weak. Type IV isotherms are given by mesoporous materials and it is determined by capillary condensation of the nitrogen molecules within the porous structure after mono-layer formation, leading to the characteristic hysteresis.

*Thommes et al.[4] recently proposed an extension of the isotherm as well as hysteresis classification, which is, however, not related to the isotherm types obtained in this work.

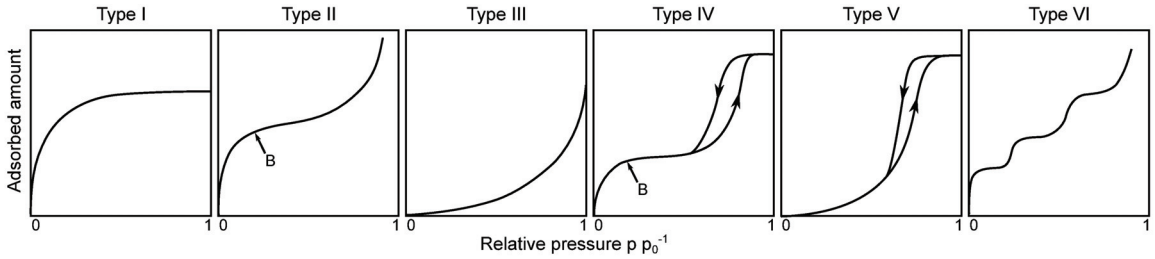

Figure 3.1.: Classification of physisorption isotherms according to IUPAC.[7]

The YSZ capillary membranes prepared in this work show this exact type of isotherms with the characteristic hysteresis. The type V isotherms are very similar to the type III and also represent a special case, which is not further discussed here. Finally, type VI isotherms are representatives of a layer-by-layer adsorption on a highly uniform, nonporous surface such as argon or krypton adsorption on some carbon blacks.[4,7]

In this work, nitrogen adsorption measurements at liquid nitrogen temperature (-196 °C) are performed using a BELSORP-mini II (Bel Japan Inc., Japan) and a BELSORP-max (Bel Japan Inc., Japan). For both measurement systems, standard sample cells with about 1.8 cm^3 of volume are used, operating in high accuracy mode with two ports. The full adsorption is carried out until a set point for the relative pressure $\frac{p}{p_0}$ of 0.99 and the minimum set pressure for desorption is 0.3. This results in around 40 distinctive adsorption and ∼25 desorption points with the chosen easy mode. For measurements only used for BET analysis, just the adsorption is carried out up to a relative pressure of 0.6. The first measurement point is set below 140 Pa, usually around 60 Pa. The BELSORP-mini II pressure sensors have a resolution of 4 Pa and an accuracy of ±0.25 %. This device is suitable for analysis of materials with a specific surface area of >0.01 m^2g^{-1} and pore diameters in the range of 0.35 to 200 nm, where the pore volume resolution is about 0.025 µL.[8] The BELSORP-max is showing similar resolutions and accuracies and is used in the same mode.[9] To desorb moisture, all samples are degassed prior to measurement for at least 3 h at 120 °C and reduced pressure (≤2 Pa), followed by cooling to RT under argon atmosphere for at least 30 min.

Specific Surface Area and BET-Method To determine the specific surface area from an obtained nitrogen adsorption isotherm, the BET-method can be applied. It is named after Stephen Brunauer, Paul Hugh Emmett and Edward Teller who first published this theory in 1938.[10] With this model, they described a multi-layer adsorption of gas molecules on solid surfaces, based on the kinetic model of adsorption proposed by Irvine Langmuir in 1916. According to Langmuir, the surface of a solid is represented by an array of equivalent adsorption sites and he postulated a thermodynamic equilibrium, where the rate of gas molecules condensing on the solid surface is equal to the rate of gas desorbing.[11] To apply the concept of mono-layer adsorption, described by the Langmuir theory, to multi-layer adsorption, a number of assumptions have been introduced. Firstly, it is assumed that the gas molecules physically adsorb on the solid surface in an infinite number of layers and that the Langmuir theory is applicable for each layer; the second and higher layers are all equivalent to the liquid state. Secondly, there is no interaction between the layers, as well as between the adsorbed molecules within each layer, and that each adsorption site is independent of its neighbors.[5] Following these assumptions, Brunauer, Emmett and Teller described the adsorbed volume of gas depending on the pressure, for constant temperature, with the following equation:[10]

$$v = \frac{v_m C p}{(p_0 - p)[1 + (C-1)\frac{p}{p_0}]}. \tag{3.3}$$

where v is the specific adsorbed volume and v_m the specific volume of a mono-layer. C is a constant which can be associated with the heat of adsorption. This equation can be rewritten to

$$\frac{p}{v(p_0 - p)} = \frac{1}{v_m C} + \frac{C-1}{v_m C}\frac{p}{p_0}. \tag{3.4}$$

Equation 3.4 has a very convenient form since the pressure and the adsorbed volume is known from the adsorption isotherm. Therefore, when $\frac{p}{v(p_0-p)}$ is plotted against $\frac{p}{p_0}$ it should give a straight line whose intercept is $\frac{1}{v_m C}$ and its slope is $\frac{C-1}{v_m C}$.[10]

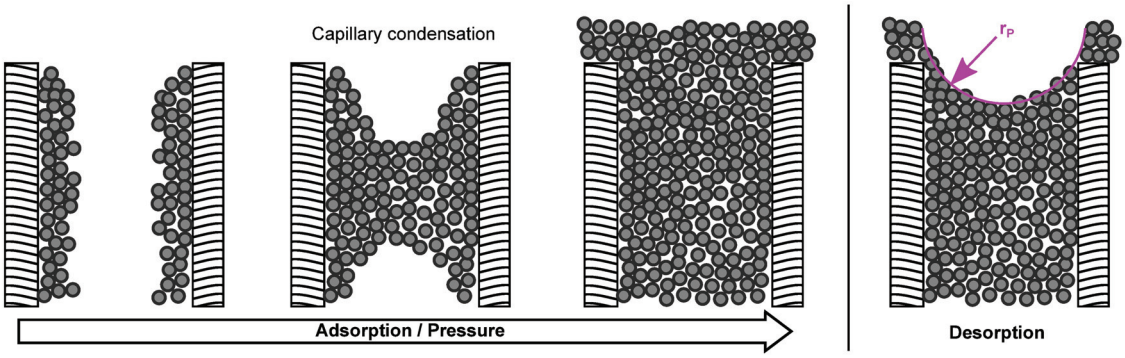

Figure 3.2.: Schematical illustration of the capillary condensation mechanism of nitrogen in mesopores.

The constant C, as well as the specific volume of one mono-layer v_m, can then be obtained by linear regression. Knowing the volume of the adsorbed mono-layer, the specific surface area can be determined by correlating it with the average area occupied by each nitrogen molecule on the surface (S_0=0.162 nm[26,8]), as well as the density (ρ_{N2}) and molecular mass (M_{N2}) of nitrogen in combination with the Avogadro constant (N_A):

$$a_{spec} = v_m \cdot \frac{\rho_{N2}}{M_{N2}} \cdot N_A \cdot S_0. \qquad (3.5)$$

Of course, the applicability of the BET-equations† are limited to a part of the nitrogen isotherm and the best fits are obtained in between 0.05 and 0.35 ($\frac{p}{p_0}$), depending on the material type.[5,6] In this work, all fits are obtained between 0.05 and 0.3.

Pore size distribution and BJH-Method In general, physisorption of non-reactive gases on stable, non-porous surfaces are completely reversible and therefore the corresponding adsorption and desorption branches are identical.[12] In contrast, physisorption isotherms of many porous materials are not reversible over particular ranges of relative pressure,[13] as already indicated in Fig. 3.1 for type IV isotherms which are characterized by a hysteresis loop. This hysteresis loop is associated with capillary condensation as schematically indicated in Fig. 3.2 and occurs if the pore sizes are small enough, for example in mesopores.[13]
Depending on the pore geometry, the shape of the hysteresis may vary. Fig. 3.3 shows the four different types (H1-H4) of hysteresis classified by IUPAC.[7] Type H1 hysteresis is often associated with narrow pore size distributions of relatively uniform (cylindrical-like) pores, as found for the YSZ

†For more comprehensive reviews on the BET-theory it is referred to the books of Lowell et al.[1] and Gregg and Sing.[12]

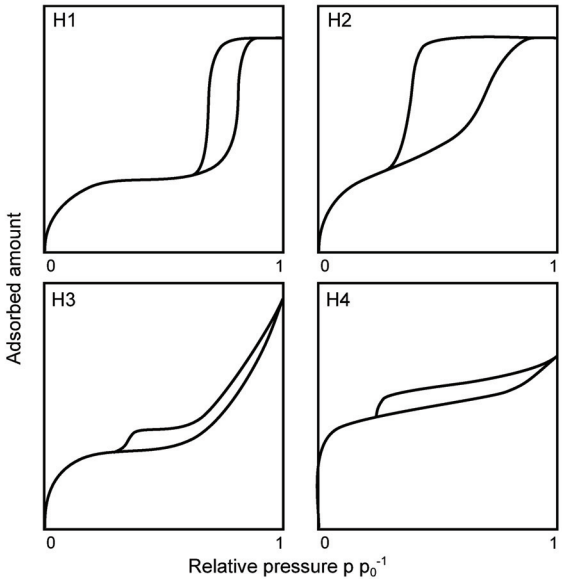

Figure 3.3.: The four types of hysteresis loops according to IUPAC.[13]

capillaries used in this work. Type H2 hysteresis represents a more complex pore structure where for example pore blocking is important. Isotherms showing a H3 hysteresis do not possess a limiting adsorption at high relative pressures and are usually caused by the existence of non-rigid aggregates of slit-shaped pores. Finally, H4 hysteresis loops are usually observed for complex materials containing micropores as well as mesopores.[14]
Assuming capillary condensation, it is well known, that the equilibrium vapor pressure above a curved liquid surface depends on the mean radius of the curvature of its meniscus r_k. This is described by the Kelvin equation which is often expressed in the approximate form as[13]

$$ln(\frac{p}{p_0}) = \frac{-2\gamma M}{\rho RT}\frac{1}{r_k}. \qquad (3.6)$$

Here, γ represents the surface tension and r_k the Kelvin radius. When equation 3.6 is applied to the case of vapor sorption in porous materials, the meniscus curvature is controlled by the pore size and shape. The variety of different pore sizes and shapes is large, consequently, there are many different procedures for the calculation of pore size distributions from the type IV isotherms. Many of these methods are based on the above assumed case and make use of a modified Kelvin equation. For this work, it should be focused on the modified Kelvin equation as 1951 proposed by Elliott P. Barret, Leslie G. Joyner and Paul P. Halenda[15] (BJH).‡

The BJH-method is based on the assumption of cylindrical pores and has been applied successfully to a wide range of porous materials. In the case of capillary condensation, the pore walls are already covered with an adsorbed film, having the thickness t which depends on the relative pressure.[12] That means, that the capillary condensation does not directly occur on the pore wall but rather on the adsorbed layer. Consequently, when applying the Kelvin model, the core size rather than the pore size is determined by r_k. In the (most simple) case of cylindrical pores, as assumed by the BJH-method, the meniscus has a radial symmetry and the contact angle between the meniscus and the adsorbed layer can be considered as zero.[13] Then, the pore radius r_P is

$$r_P = r_k + t. \tag{3.7}$$

In order to account for the thickness of the adsorbed multi-layer, the BJH-method combines the Kelvin equation with a standard isotherm, the so called t-curve.[4] This method is often used for the characterization of mesoporous materials and it is also recommended as an analysis method by IUPAC.[2] Nevertheless, several uncertainties need to be accounted for. Especially the contact angle as well as the pore morphology assumptions are critical when it comes to very small mesopores. It can be shown, that for pores with diameters <10 nm the pore size will be underestimated by 20-30 %. Here, the extrapolation of t from standard t-curves fails precision, because enhanced surface forces and curvature are not properly accounted for.[4] Being aware of the limitations of this model, it is assumed to be applicable with little uncertainties in this case, due to type IV adsorption isotherms which show a clear H1 hysteresis and pore diameters >10 nm.

‡A more detailed description of the analysis of type IV isotherms is for example given by Gregg and Sing.[12]

3.1.3. Mercury Intrusion Porosimetry

Mercury (Hg) intrusion porosimetry is a measurement technique to analyze the pore size distribution of a porous material over a wide range of pore sizes.[12] The method is widely applied to different kinds of materials and is also recommended by IUPAC for the determination of the volumetric distribution of pore sizes.[2] Hg porosimetry was originally developed to enable the determination of pore sizes in the macroporous ranges, where classical gas adsorption methods break down (see section 3.1.2). Mercury has a mean contact angle of around 140 ° on ceramic materials and is considered a non-wetting liquid.[6] Therefore, mercury cannot be spontaneously absorbed by the pores of a solid material itself because of the high surface tension of the mercury – an external pressure is required to force this liquid into a porous material. Of course, the extent of pressure which needs to be applied depends on pore size and certain properties of the liquid, such as surface tension γ or contact angle ϕ. In 1921, Edward Washburn extensively investigated the field of capillary forces and capillary flow[16] and he was the first to describe the relation of pore size and pressure for an intrusion of mercury into a capillary pore.[17] In fact, the analysis of mercury intrusion porosimetry measurements today is based on this relation, later known as Washburn equation:

$$r_P = -\frac{2\gamma\cos(\phi)}{\Delta p}. \tag{3.8}$$

The assumption made when equation 3.8 is applied on mercury intrusion data, is a cylindrical shape of the pore. Furthermore, it is assumed that the pores are invaded by mercury in decreasing order of the size. The sequential filling of pores is primarily dictated by their mode of interconnection and the assumption may be invalid for networks with a small interconnectivity. However, the network of YSZ particles used in this work is assumed to be highly interconnected and that the pores are infiltrated sequentially.[2]

Other potential drawbacks of this measurement technique are the control of temperature, which will have a high influence on the pressure within the liquid filled measurement cell. Furthermore, the compressibility of mercury, the distortion of the measurement cell at high pressures, as well as

the probability that the sample will be deformed elastically or damaged irreversibly need to be considered.[§2]

In this case, equation 3.8 is also used for the analysis of the Hg intrusion porosimetry measurements assuming cylindrical pores where ϕ_{Hg}=141.3 ° and γ_{Hg}=0.48 J m^{-2} are used for contact angle and surface tension, respectively.[18] The properties of mercury vary with temperature, therefore the room is air conditioned and the temperature is kept constant at 20 °C. The measurements are performed on a Mercury Porosimeter Pascal 140 and 440 (POROTEC GmbH, Germany) in the pressure range of 0.1 to 400 kPa with an accuracy of <0.25 %. A CD3P dilatometer with a measurement range of 0.1 to 500 mm^3 and a resolution of 0.1 mm^3 is used to measure the pore volume which leads to a measuring range of pore diameter of 3.8 nm to 116 μm. All measurements are carried out according to DIN 66133.[19] Empty measurements are performed and used as blank correction to address the compressibility of mercury, as well as the elastic distortion of the cell and other components. Sample damaging did not take place and can be excluded, especially after increasing the mechanical stability of the capillaries due to adjustments in the processing route (see section 2.2.2 and Fig. A2 in the appendix). Nevertheless, the contact angle of mercury is assumed to be constant with a value of about 140 °, but it can vary depending on the material surface and whether the mercury is penetrating or withdrawing. It can be shown that uncertainties of up to 20 % can be reckoned comparing different materials.[12] This will have a significant impact on calculations of the pore size and therefore the pore size distribution. From practical experience, the pore size distributions have little deviations in peak position of relative pore volume and all measurements are highly reproducible. However, a systematical error may be present due to the assumption of ϕ. Results obtained from nitrogen adsorption and Hg porosimetry measurements show slightly different results regarding the mean pore diameter. This deviation could also be derived from the different approaches used by the two measurement techniques. For further discussion of this topic see chapter 5.

[§]For further information regarding Hg intrusion porosimetry, Lowell et al.[1] present a very detailed description of the process, as well as the theoretical background.

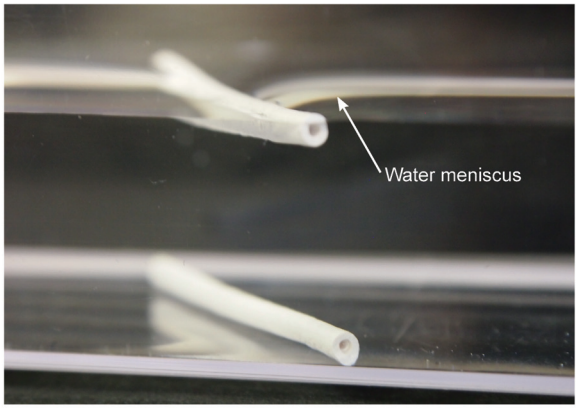

Figure 3.4.: Image of a non-functionalized and a C_{16}-functionalized capillary (floating).

3.2. Surface Characterization

Especially when the surface of a solid material is functionalized with the means of altering the surface chemistry, surface characterization techniques are required to analyze the result of the functionalization process. Different techniques are available to characterize the solid surface chemistry. They range from simple analysis, such as contact angle measurements and light microscopy, to X-ray photoelectron spectroscopy (XPS) and Fourier-transform infrared spectroscopy (FTIR). Unfortunately, easy measurement techniques such as contact angle measurements are not suitable for this purpose. They cannot be applied straightforward to porous materials and they cannot be performed on capillaries. The preparation of flat-sheet membranes, for example using uniaxial pressing, leads to porous structures with a different pore size distribution than membranes prepared by extrusion, rendering them incomparable (see Fig. A7 in the appendix). Without doubt, a qualitative demonstration using the contact angle effects is still possible, because the surface functionalization used in this work (C_{16}-alkyl chains) turns the surface highly hydrophobic, causing functionalized capillaries to float on water, however, non-functionalized samples sink to the bottom (see Fig. 3.4). However, in this particular case, a quantification of the functional groups is desired, allowing conclusions about the amount of functional groups per surface area unit. It is possible to obtain values for surface coverage and layer thickness from XPS data, but a large number of assumptions need to be made. Besides that, XPS measurements are rather complicated and not suitable for a large number of samples. Therefore, two indirect measurements, namely thermogravimet-

ric analysis (TGA) and the determination of the total organic content (TOC), are used to determine the amount of functional molecules per surface area. Both techniques determine the amount of carbon within the sample due to burn out at elevated temperatures. The amount of functional groups ($\mathrm{mol\,m^{-2}}$) is determined using the mass loss obtained by TGA and the specific surface area according to equation 3.9

$$c_{C16} = \frac{m_{TGA} \cdot M_{C16,degr}}{a_{spec}} \tag{3.9}$$

by assuming the degradable molecular mass of one functional group ($M_{C16,degr}$ in $\mathrm{g\,mol^{-1}}$) and assuming that each functional group is attached to the membrane surface.

3.2.1. Thermogravimetric Analysis (TGA)

Heating a sample of material is supposed to be one of the easiest ways to yield useful information about the nature of the material.[20] "Thermal analysis is the study of the relationship between a sample property and its temperature as the sample is heated or cooled in a controlled manner".[21] According to the IUPAC recommendation, thermogravimetric analysis is a measurement technique which monitors the change in sample weight depending on the temperature. This technique is often combined with differential thermal analysis (DTA) or differential scanning calorimetry (DSC), to determine the temperature difference or the heat flow rate of the sample compared to an inert reference, respectively.[20] For this, usually two crucibles are placed on a balance within a furnace, one containing sample material, one used as a reference. Both crucibles are subjected to a controlled temperature program. During the measurement, the furnace temperature, the change in sample weight and the temperature difference between sample and reference are measured. When relating the relative weight change of the sample to the temperature the resulting dependency is commonly referred to as TGA. DTA and DSC methods are based on the temperature difference between sample and reference. Differential temperature analysis directly relates the measured temperature difference to the absolute temperature of the furnace. In contrast, a DSC measurement system is calibrated to an original measured temperature difference and allows the recalculation to a heat flux. Here, the design of the instrument must be in a way which allows a calibration. In summary, both techniques are based on the same measurement parameter, the differential temperature, DTA presents qualitative results where DSC gives rise to quantitative analysis. More comprehensive information about thermal analysis and the different measurement techniques can be obtained from the books edited by Brown[22,23] or Haines.[20]

In this work, two different measurement systems are used, a TGA/DSC1 Star System (Mettler Toledo, Germany, see chapter 4) and a STA503 (Bähr-Thermoanalyse GmbH, Germany, see chapter 6). The first system was used for TGA and DSC results presented in section 4.3.2. This instrument has a relative temperature resolution of $0.001\,^{\circ}\mathrm{C}$ with an accuracy of $\pm 0.25\,^{\circ}\mathrm{C}$ while having a weight resolution of $1\,\mu\mathrm{g}$.[24] The measurements are performed in pure oxygen with a flow of $30\,\mathrm{mL\,min^{-1}}$. All other measurements, for example as presented in chapter 6 or in Fig. A6 in the appendix, are performed using the STA503. This system determines the relative weight loss and the differential temperature (not DSC) and has a temperature resolution of $0.01\,^{\circ}\mathrm{C}$ with an accuracy of $\pm 0.1\,^{\circ}\mathrm{C}$, the weight resolution is $1\,\mu\mathrm{g}$.[25]

According to Coats and Redfern, the main factors affecting a TGA measurements are the sample, the crucible, the heating rate and the atmosphere.[26] In order to provide similar results, similar crucible geometries with comparable amounts of sample are used for both measurement systems. Before each set of measurements, a blank measurement is performed on an empty crucible which is used as a reference in each case. The temperature profile used on both systems is identical, using $10\,^{\circ}\mathrm{C\,min^{-1}}$ as a constant heating rate up to $900\,^{\circ}\mathrm{C}$. This heating rate is also used by Sima-Ella and Mays[27] to study the oxidation reactivity of carbonaceous materials. Unfortunately, measurements on the STA503 cannot be performed under oxygen atmosphere. In order to provide enough oxygen for the reaction and to compare the results on both measurement devices, the measurements are performed in air with an increased flow rate of $10\,\mathrm{L\,min^{-1}}$.

3.2.2. Total Organic Carbon Content (TOC)

TGA measurements only provide the weight change of a sample depending on the temperature and statements about the nature of the degrading molecules are difficult to make. In order to

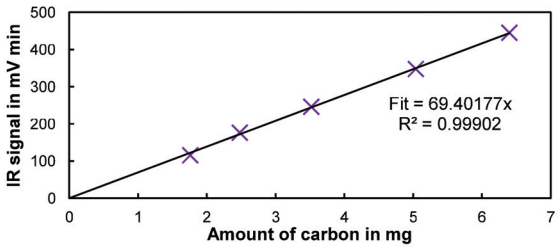

Figure 3.5.: Glucose calibration of the IR detector for TC measurements.

verify the results obtained from TGA and analyze the nature of the degrading molecules, the amount of total organic carbon (TOC) within the samples is determined. The TOC content is determined by a two step analysis also known as TC-IC. The total carbon (TC) content and the inorganic carbon (IC) content are measured separately, and the TOC is calculated by the subtraction of IC from TC. The basic approach to determine TC is similar to the TGA measurements, the sample is exposed to a high temperature in an oxygen environment but in contrast to TGA measurements, the amount of formed CO_2 is analyzed. To determine the IC, the sample material is acidified in order to convert the IC to CO_2 which is then measured in the same way. In this case, a SSM-5000A solid sample module (Shimadzu, Japan) in combination with an infrared (IR) detector (TOC-V, Shimadzu, Japan) is used to determine TC and IC. The device has a measurement range of 0.1-30 mg (TC) and 0.1-20 mg (IC) with a reproducibility of $\pm 1\,\%$.[28] Prior to TC measurements, the system is calibrated with glucose, the calibration curve is shown in Fig. 3.5. For IC measurements the system is calibrated with sodium carbonate (data not shown).

3.2.3. CO_2-Adsorption and Isosteric Heat of Adsorption

When the pressure exceeds zero there will always be gas molecules adsorbed on solid surfaces and the adsorbed amount will be in equilibrium with the amount in the gas phase. This is not only the case for liquid nitrogen temperatures, as described in section 3.1.2, but also for higher temperatures, for example between 0 and 80 °C, as investigated in this study using CO_2. The extent of adsorbed amount depends on temperature, pressure, gas type and solid surface and adsorption isotherms with different shapes are possible. Fig 3.6 shows three exemplary and frequently used models which

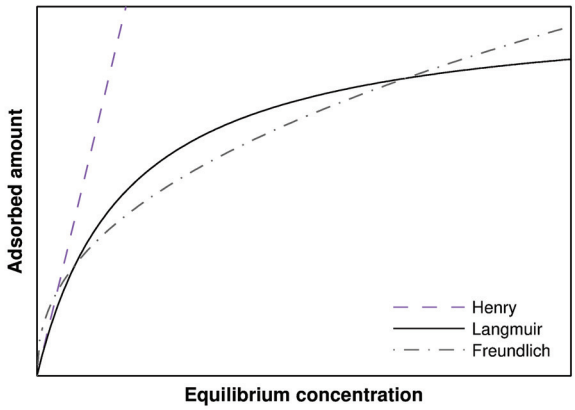

Figure 3.6.: Schematic drawing of adsorption isotherms according to Henry, Langmuir and Freundlich.

can be applied to adsorption isotherms.[¶] A Henry type isotherm is the most simple, linear relation between the equilibrium pressure p and the adsorbed amount q with the Henry constant K_H:

$$q = K_H \cdot p. \tag{3.10}$$

Despite this simple approach of a linear relation, equation 3.10 often describes the adsorption isotherms sufficiently enough for low surface coverages. Another approach was suggested by Irving Langmuir as already mentioned earlier. He describes the adsorption of a mono-layer of gas molecules on a solid surface as follows:[11]

$$\frac{q}{q_0} = \frac{K_L \cdot p}{1 + K_L \cdot p}. \tag{3.11}$$

Here K_L represents the sorption equilibrium constant according to Langmuir and q_0 the quantity of a complete mono-layer. This sorption isotherm is widely applied on a variety of experimental data, but it is limited to where the adsorption approaches a distinct saturation value of a mono-layer.[30] In the case of non-ideal and/or multi-layer sorption, other models can be applied such as the Freundlich isotherm which can be expressed as:[29]

$$q = K_F \cdot p^{\frac{1}{n_F}}. \tag{3.12}$$

In addition to the Freundlich coefficient K_F, equation 3.12 incorporates a second parameter, n_F, the so called Freundlich exponent. This model describes adsorption on heterogeneous surfaces, where the uptake of adsorbate decreases with increasing amount of adsorbed species. In contrast

[¶] For more comprehensive information and further adsorption models it is referred to the literature, for example the book of Adamson and Gast.[29]

to Langmuir, it does not show a limiting or saturation value. Furthermore, the Henry isotherm does not apply at low concentrations.[29]

Whenever a gas molecule adsorbs on a surface, heat is released, generally deriving from the loss of molecular motion associated with the change from a 3-dimensional gas phase to a 2-dimensional adsorbed phase.[1] The heat of adsorption provides an information about the chemical affinity of the adsorbate towards the adsorbent, being larger for a stronger bond. At a distinct pressure and temperature, in an equilibrium state, the adsorbed "liquid" layer and the gas phase possess the same chemical potential. This applies to the full phase transition line, also known as coexistence curve in a p-T diagram. Applying the fundamental laws of thermodynamics by the definitions of internal energy, enthalpy and Gibbs free energy, the slope of the tangent to the coexistence curve can be expressed by the means of pressure (p), temperature (T), specific volume (v) and specific entropy (s):[31,32]

$$\frac{dp}{dT} = \frac{\Delta S}{\Delta V}. \tag{3.13}$$

Equation 3.13 is known as the Clapeyron equation and it is valid for all phase transitions. When considering the phase transition between an adsorbed phase ("liquid") and a gas phase, where the specific volume of the gas phase is significantly larger than the adsorbed phase, approximations lead to the Clausius-Clapeyron equation:[33]

$$\ln(p) = -\frac{\Delta H_{ads}}{R}\frac{1}{T} + C. \tag{3.14}$$

In this case ΔH_{ads} is the heat of adsorption and C is a constant. In practice, equation 3.14 is applied to a set of data by plotting $\ln(p)$ against $\frac{1}{T}$ for a constant surface coverage θ=const. and linear regression is used to obtain the isosteric heat of adsorption ΔH_{ads}.

To determine the influence of a C_{16} surface functionalization on the gas adsorption behavior, CO_2 adsorption measurements are performed at different temperatures in order to obtain the isosteric heat of adsorption. The measurements are performed with a BELSORP-max (Bel Japan Inc., Japan) operating in high accuracy mode using two ports and standard sample cells with about 1.8 cm^3 of volume. For resolution and accuracy of the measurements see section 3.1.2. Before each measurement, the samples are degassed for at least 3 h at 120 °C and reduced pressure (≤2 Pa) followed by cooling to RT under argon atmosphere.

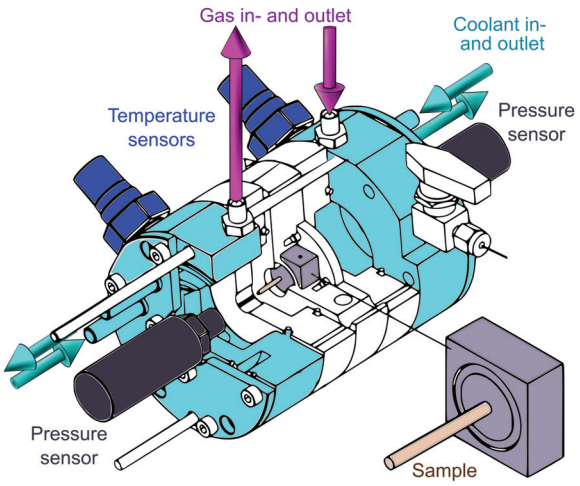

Figure 3.7.: Schematical drawing of the permeation cell

Due to the small amount of adsorbed quantity, a comparably large amount of sample is used (∼0.6 g). In contrast to nitrogen adsorption measurements (see section 3.1.2), the adsorption is carried out in detailed mode at 22 specific pressure set points, namely 10^{-7}, 10^{-6}, 10^{-5}, 10^{-4}, 10^{-3}, 10^{-2}, 10^{-1}, 1, 2.5, 5, 10, 20, 30, 40, 50, 60, 70, 80, 90, 100 and 105 kPa with a pressure tolerance of 0.1 %.

3.3. Gas Permeation Measurements

3.3.1. Gas Permeation Setup

Gas propagation through porous structures and membranes can be determined in different ways. In this case, a steady-state permeation cell is used to directly measure the flux for an applied pressure difference with a calorimetric flow sensor (see also section 2.4). The measurement system was originally developed by Thomas Veltzke[34] and it is further adapted and optimized within this work. Here, single gases are forced through the porous YSZ capillaries into a dead-end tank, the volume of which is large compared to the volume of the system. The permeation cell itself is schematically shown in Fig. 3.7, a more detailed drawing of the complete measurement system is given in Fig. A8 in the appendix. The permeation setup consists of two compartments each build up by two stainless steel blocks, one of which can be actively cooled due to a circular channel, incorporating the coolant (indicated in cyan blue in Fig. 3.7). In between these two compartments, the

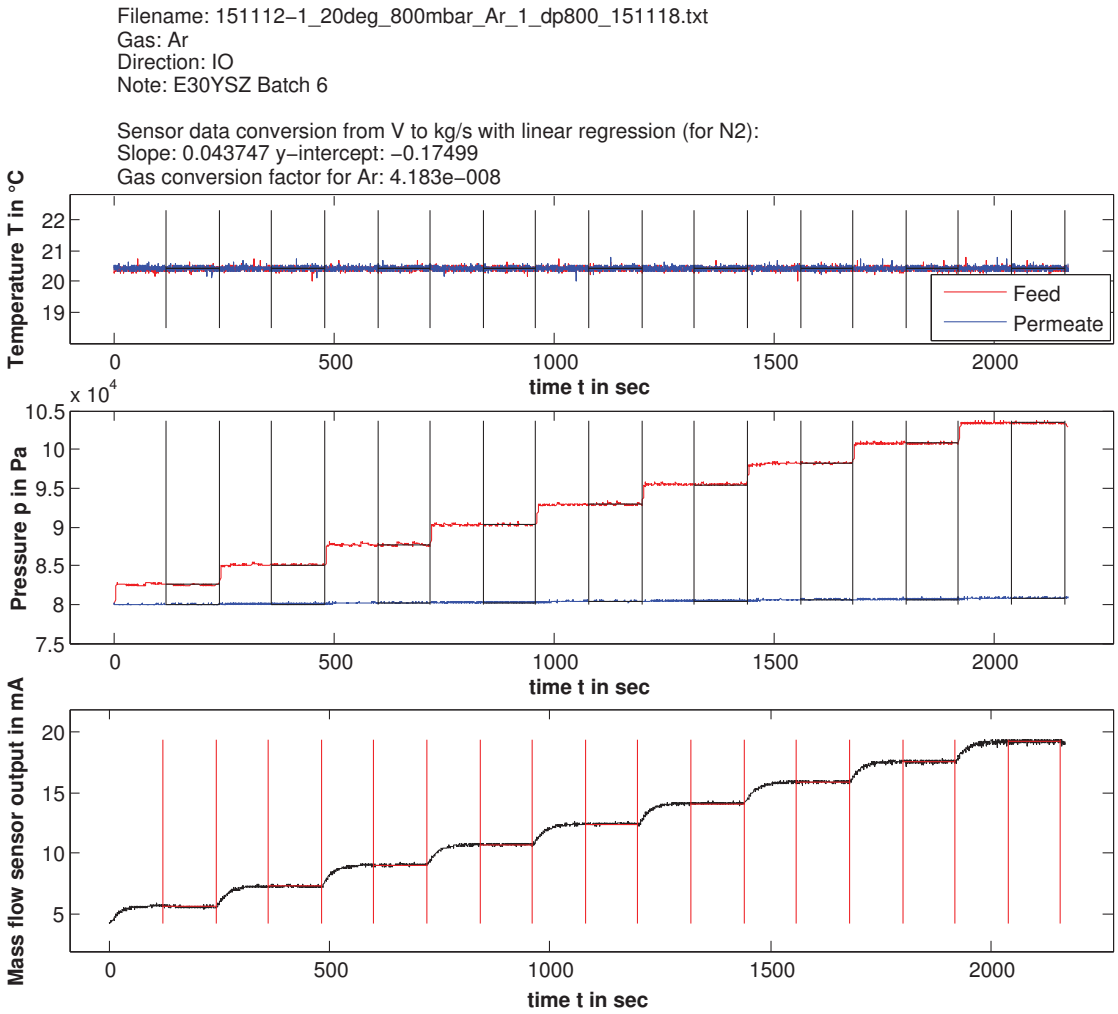

Figure 3.8.: Raw data of a single measurement with argon on a non-functionalized membrane at 20 °C

YSZ capillaries are mounted. For this, the sample holder (square aluminum block, light gray) is held in place by a metal or plastic piece as the two compartments are pressed together by screws to form a sealed permeation cell (also see Fig. 4.2A and Fig. 5.1 in chapter 4 and 5, respectively). Both compartments are equipped with temperature (blue) and pressure sensors (dark gray), as well as a gas inlet and a gas outlet (magenta). The flow controller as well as the flow sensor are located outside of the permeation cell (also see Fig. 5.1 in chapter 5). In contrast to the originally developed system, the setup was redesigned to be completely isolated from the environment to ensure purity of the gas and to avoid the influence of moisture. The connections to different gas supplies are permanent. Each part of the system can be separately shut off from the rest and directly connected to a vacuum pump for evacuation. Only when mounting a new sample, a part of the measurement cell is exposed to the environment.

3.3.2. Measurement Procedure and Data Acquisition

To determine the gas flow under steady state conditions, nine different pressure drops are applied in a continuous test procedure, as shown in Fig. 3.8. The analogue signals of the temperature, pressure and mass flow sensors are converted into digital signals using a A/D converter and the frequency of acquisition is chosen to 6 Hz.[34] LabVIEW[‖] is used for data processing and the following relations are applied to convert the created voltage signals into physical quantities:[34]

$$T = -\frac{B_1}{2B_2} + \sqrt{\frac{B_1^2}{4B_2^2} - \frac{U_0 - U}{B_2 U_0}} \qquad (3.15)$$

with $B_1 = 3.9083 \cdot 10^{-3}\,°C^{-1}$ and $B_2 = -5.775 \cdot 10^{-7}\,°C^{-2}$. U_0 is the nominal voltage at 0 °C which is calculated given the nominal resistance at this

[‖]National Instruments LabVIEW, version 8.5

Table 3.1.: Conversion factor obtained from FLUIDAT and molar mass for different gas types as used in this work

Gas i	Conversion factor CF in $\mathrm{kg\,s^{-1}\cdot mln^{-1}\,min}$	Molar mass M in $\mathrm{g\,mol^{-1}}$
Ar	$4.183{\cdot}10^{-08}$	39.948
N_2	$2.084{\cdot}10^{-08}$	28.014
CO_2	$2.444{\cdot}10^{-08}$	44.009
CH_4	$9.110{\cdot}10^{-09}$	16.043

temperature (1000 Ω) as well as the applied current (1 mA from a highly constant source[34]).

$$p = 16019.78\,Pa\,V^{-1}\cdot U. \tag{3.16}$$

Fig. 3.8 exemplary shows the raw data of a measurement of Ar at 20 °C performed on a non-functionalized YSZ capillary. The pressure differences are set individually for each sample according to the sample properties and the measurement range of the pressure sensors (0.1-160 kPa ±0.04 %) and the mass flow sensor ($3.0\text{-}150.9{\cdot}10^{-10}$ kg/s ±0.8 %) – see also sensor specifications in table 5.1 in chapter 5. The pressure is controlled by a mass flow controller operating in a simple boolean mode (either open or closed), depending on the pressure difference and its set-value.[34] Each pressure step holds for 240 s. The current signal generated by the flow sensor (in mA) is converted into a molar flow rate (in $\mathrm{mol\,s^{-1}}$) during post-processing with MATLAB** using the following relation:

$$\dot{n}_i = (I\cdot m_{N2} + b_{N2})\cdot CF_i\cdot\frac{1000}{M_i}. \tag{3.17}$$

Here, m_{N2} and b_{N2} are the slope and the intercept of the calibration curve for N_2 from the sensor certificate issued by Bronkhorst for this mass flow sensor which is converting the mA signal into a flow of $\mathrm{mln\,min^{-1}}$. Furthermore, CF_i is the conversion factor to recalculate $\mathrm{mln\,min^{-1}}$ into $\mathrm{kg\,s^{-1}}$ of gas i. The specific values used in this work are obtained using the FLUIDAT software†† and are presented in table 3.1 alongside the molar mass of the used gases. For post-processing, the first 120 s of measurement data for each pressure step are ignored, to ensure steady-state conditions. Afterwards, all signals are averaged over 120 s as indicated with bars in Fig. 3.8.

**The MathWorks, Inc., MATLAB version R2011b

††Bronkhorst High-Tech B.V. FLUIDAT, online tool at www.fluidat.com

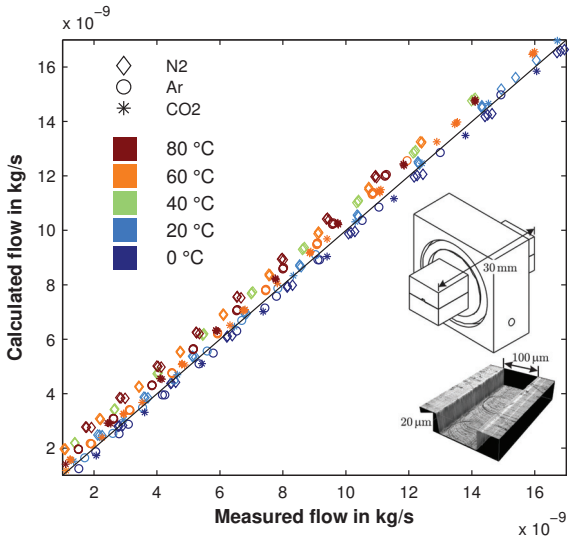

Figure 3.9.: Mass flow calculated according to Poiseuille's law plotted against the measured mass flow through a uniform microchannel with rectangular cross section. Microchannel drawing and picture adapted with permission from.[34]

3.3.3. Validation of the Setup

To validate the test setup for different gas types operating under various temperature conditions, measurements are performed on a uniform microchannel with rectangular cross section, as shown in Fig. 3.9. The aluminum microchannel is fabricated by micro-milling‡‡ and has a height of 20 µm, a width of 100 µm and a length of around 30 mm. Measurements are performed for all used gas types within this work and the results are compared with calculations by the means of Poiseuille's law. In addition, Sutherland's law is used to model the relationship between the dynamic viscosity and the temperature of the gas. Fig. 3.9 shows the obtained results for Ar, N_2 and CO_2 at temperatures ranging from 0-80 °C. In general, the measured flow rate is in good agreement with the calculated mass flow for all temperatures and gas types. Nevertheless, the values drift slightly with temperature. The reason for this temperature drift can be caused by the thermal expansion of the aluminum microchannel. Another possible explanation is a drift of the pressure sensors with temperature. However, this drift is only present for measurements performed on the microchannel and it is not present for measurements performed on ceramic capillaries as shown in Fig 5.5 and Fig. 5.6 in chapter 5. Even if the

‡‡Manufactured by Laboratory for Precision Machining (LFM), University of Bremen[34]

absolute values of the pressure sensors drift with temperature, this will only have an effect for systems dominated by viscous flow (see equation 2.3). When Knudsen diffusion is dominating, the flow rate depends only on the relative pressure difference (see equation 2.4), not on absolute pressure. Both pressure sensors will have the same drift which will not affect the relative pressure and, in turn, will not have an effect on samples dominated by Knudsen diffusion. It cannot be stated whether a thermal expansion of the microchannel or a temperature drift of the pressure sensors cause this behavior. In any case, this will not have an effect on measurements performed on the mesoporous material used in this work.

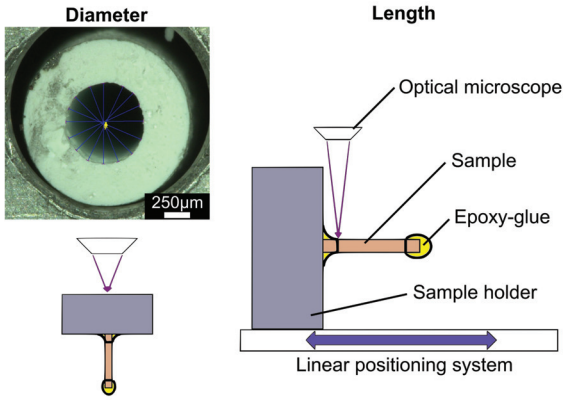

Figure 3.10.: Measurement of sample geometry: Inner and outer diameter and membrane length.

3.3.4. Sample Preparation and Pretreatment

To integrate the YSZ capillary membranes into the gas permeation cell, the samples are glued into a sample holder using a two-component epoxy glue (UHU Plus endfest 300, UHU GmbH & Co. KG, Germany). This glue is specifically chosen, because it does not absorb or interact with the used gas species. Silicon based glues, for example, absorb CO_2, influencing the measurement results. The sample holder consists of an aluminum block with gaskets on both sides and a through hole. The sample is placed in the hole and is sealed with glue. After a drying step overnight, the tip of the sample is sealed with glue and the sample is placed upside down for another drying process. Please note: The drying process needs to be carried out between 20 and 25 °C. Even though a higher temperature will lead to an increased mechanical strength of the glue, its viscosity decreases significantly when temperatures exceed 25 °C, may causing unsuccessful sealing or excessive contamination of the membrane surface.
To determine the geometrical sample dimensions, such as the active membrane surface area, the sample is analyzed using optical microscopes as schematically shown in Fig. 3.10. The inner and outer diameter of the sample is obtained from the bottom by placing the sample upside down under a digital microscope (VHX-600DSO, Keyence, Japan). The inner and the outer diameter is then measured in eight different directions and the mean value and standard deviations are calculated. The membrane length is measured by placing the sample holder sideways on a micrometer table (Plμ 2300, Sensofar technology, Spain) and the distance between both glue points is measured from four sides to calculate mean value and standard deviation.
Before mounting the samples in the permeation cell, they are heated for 3 h at 120 °C to desorb moisture and ensure equivalent conditions. Within this time, the temperature of the measurement system is controlled to reach its set-point. The samples are integrated into the setup directly from the furnace while being hot and the permeation cell is immediately sealed (∼1 min). Directly after sealing the setup, the whole system is evacuated to around 0.3 kPa and refilled again with the test gas to 160 kPa three times. After reaching steady state conditions for the temperature, a gas leak test is performed on the whole system. For this, the pressure is increased to 160 kPa and the steady-state condition is observed for at least 4 min to ensure a constant system pressure which is not decreasing over time. Then, the sample is flushed with the used test gas for 1 min with a pressure difference of around 160 kPa. Finally, a test measurement is performed to set the range for the maximum and minimum pressure difference before starting the measurement. Apart from the gas leak test, this procedure, including system evacuation and refilling, sample flushing and test measurement, is repeated when changing the test gas type.

3.3.5. Gas Permeability and Ideal Selectivity

The raw data (.txt files) obtained from the measurements are analyzed using MATLAB. As already indicated in Fig. 3.8, the pressure, temperature and mass flow are averaged for each step. Fig. 3.11 exemplary shows the molar flow rate plotted against the pressure difference for a non-

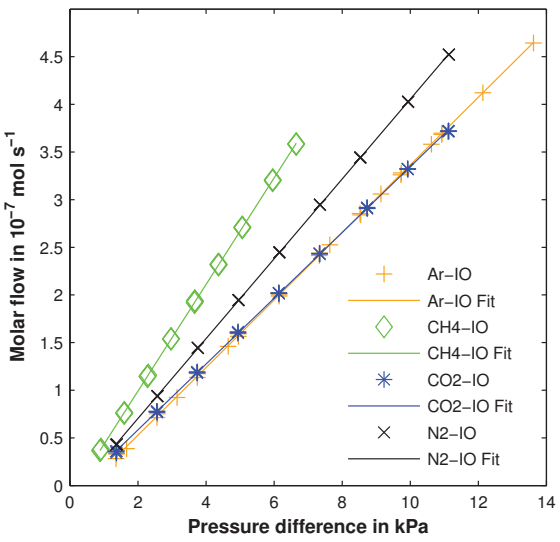

Figure 3.11.: Results from three consecutive gas permeation measurements per gas type performed on a non-functionalized sample at 20 °C.

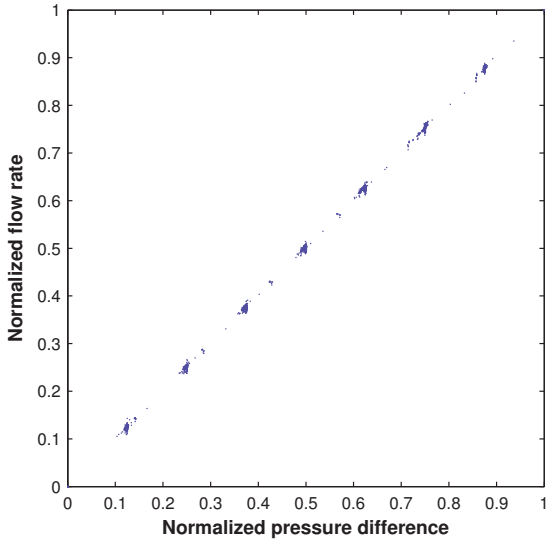

Figure 3.12.: Normalized flow rate plotted against normalized pressure difference for all measurements presented in this work (see chapter 4- 5) including measurements for Ar, N_2, CO_2 and CH_4 at temperatures ranging from 0 to 80 °C. 424 single measurements in total

functionalized sample. The results are obtained from three consecutive measurements per gas type and the mean values for molar flow and pressure difference are plotted separately for each measurement. During all measurements, the temperature is highly constant at 20.18 ±0.07 °C.
In this work, the measurement results are analyzed by the means of Knudsen flow and ideal selectivity. To analyze the gas flow, the gas permeation data ($\dot{n}$, Δp, T) is combined with the open porosity (ϵ) and the pore diameter (d_{Pore}) obtained from nitrogen adsorption/desorption measurements or Hg intrusion porosimetry. Furthermore, the membrane area (A) and thickness (δ) are obtained from optical microscopy. Then the Knudsen flow of gas i according to equation 2.4 in section 2.1 can be rewritten to:

$$\frac{3\delta\dot{n}_i\sqrt{2\pi RTM_i}}{4A\epsilon d_{Pore}}\frac{1}{p_{i,max}} = \frac{1}{\tau^2}\frac{\Delta p_i}{p_{i,max}}. \qquad (3.18)$$

R and M_i are known values and the only unknown factor is τ. Therefore, the left hand side of equation 3.18 is plotted against $\frac{\Delta p_i}{p_{i,max}}$ leading to linear plots with the slope of $\frac{1}{\tau^2}$. The left hand side of the equation is calculated and given in mean value and standard deviation. The standard deviation includes the errors for temperature, membrane thickness, membrane area, pore diameter and porosity, based on the propagation of uncertainty.
The selectivity is defined as the ratio of the permeabilities of two components (gases) penetrating through a membrane. When the gas flow is determined under "ideal" conditions using single gases, the selectivities are called ideal selectivities. In this case, the ideal selectivities are obtained by linear regression of the molar flow $\dot{n}$ of a gases i and j depending on the pressure difference:

$$\alpha_{i,j} = \frac{(\partial\dot{n}/\partial p)_i}{(\partial\dot{n}/\partial p)_j}. \qquad (3.19)$$

A linear square fit is used to perform the linear regression. The ideal selectivities are calculated in mean value and standard deviation. The standard deviation includes the errors estimated by the confidence interval of the linear regression of three individual measurements per gas type based on the propagation of uncertainty. The coefficient of determination for each linear regression is R^2 >0.9997, for all measurements presented within this work. In practice, the linear regression is always performed in a set of three individual measurements. Here, the coefficient of determination is R^2 >0.9992. In general, all measurements presented in this thesis are highly linear and follow the Knudsen law, as shown in Fig. 3.12. Fig. 3.12 summarizes the results of all measurements performed within this work by normalizing the molar flow, as well as the relative pressure to give values between 0 and 1. When fitting an quadratic function onto every single measurement plotted in Fig. 3.12, the results show linear coefficients

of around 1 while the mean curvature (quadratic coefficient, associated with viscous flow) is 0.0147 while always being smaller than 0.0413. This underlines the high reproducibility of the performed measurements and the linearity of the data which suggests that only Knudsen diffusion is present without any contribution from viscous flow (see also section 2.1).

References

[1] S. Lowell et al. *Characterization of Porous Solids and Powders: Surface Area, Pore Size and Density*. Ed. by Brian Scarlett. Springer Netherlands, 2004. DOI: 10.1007/978-1-4020-2303-3.

[2] J. Rouquerol et al. "Recommendations for the characterization of porous solids". In: *Pure Appl. Chem.* 66.8 (1994), pp. 1739–1758. DOI: 10.1351/pac199466081739.

[3] *Pycnomatic ATC (Automatic Temperatre Control) Instruction Manual*. Thermo Electron S.p.A. Strada Rivoltana, 20090 Rodano-Milan, Italy, Apr. 2004.

[4] Matthias Thommes et al. "Physisorption of gases, with special reference to the evaluation of surface area and pore size distribution (IUPAC Technical Report)". In: *Pure Appl Chem* 87.9-10 (July 2015), pp. 1051–1069. DOI: 10.1515/pac-2014-1117.

[5] Kenneth Sing. "The use of nitrogen adsorption for the characterisation of porous materials". In: *Colloids Surf., A* 187-188 (Aug. 2001), pp. 3–9.

[6] Hermann Salmang and Horst Scholze. *Keramik*. Ed. by Rainer Telle. 7th ed. Springer Berlin Heidelberg New York, 2007.

[7] K. S. W. Sing et al. "Reporting physisorption data for gas/solid systems with special reference to the determination of surface area and porosity". In: *Pure Appl Chem* 57.4 (1985), pp. 603–619.

[8] *Technical specification BELSORP series, BELSORP-mini*. BEL Japan, Inc. 1-Chome, Haradanaka, Toyonaka-City, Osaka, Japan, 2009.

[9] *Technical specification BELSORP series, BELSORP-max*. BEL Japan, Inc. 1-Chome, Haradanaka, Toyonaka-City, Osaka, Japan, 2004.

[10] Stephen Brunauer, P. H. Emmett, and Edward Teller. "Adsorption of Gases in Multimolecular Layers". In: *J. Am. Chem. Soc.* 60.2 (Feb. 1938), pp. 309–319. DOI: 10.1021/ja01269a023.

[11] Irving Langmuir. "THE CONSTITUTION AND FUNDAMENTAL PROPERTIES OF SOLIDS AND LIQUIDS. PART I. SOLIDS." In: *J. Am. Chem. Soc.* 38.11 (1916), pp. 2221–2295. DOI: 10.1021/ja02268a002.

[12] S. J. Gregg and K. S. W. Sing. *Adsorption, Surface Area and Porosity*. 1982.

[13] Kenneth S.W. Sing and Ruth T. Williams. "Physisorption Hysteresis Loops and the Characterization of Nanoporous Materials". In: *Adsorpt. Sci. Technol.* 22.10 (2004), pp. 773–782. DOI: 10.1260/0263617053499032.

[14] M. Thommes. "Physical Adsorption Characterization of Nanoporous Materials". In: *Chem. Ing. Tech.* 82.7 (June 2010), pp. 1059–1073. DOI: 10.1002/cite.201000064.

[15] Elliott P. Barrett, Leslie G. Joyner, and Paul P. Halenda. "The Determination of Pore Volume and Area Distributions in Porous Substances. I. Computations from Nitrogen Isotherms". In: *J. Am. Chem. Soc.* 73.1 (Jan. 1951), pp. 373–380. DOI: 10.1021/ja01145a126.

[16] Edward W. Washburn. "The Dynamics of Capillary Flow". In: *Phys. Rev.* 17 (3 Mar. 1921), pp. 273–283. DOI: 10.1103/PhysRev.17.273.

[17] Edward W Washburn. "Note on a Method of Determining the Distribution of Pore Sizes in a Porous Material". In: *Proc. Natl. Acad. Sci. U.S.A.* 7.4 (Apr. 1921), pp. 115–116.

[18] *Instruction Manual Porosimeter PASCAL 140/440*. Fisons Instruments. Strada Rivoltana, 20090 Rodano-Milan, Italy, 1994.

[19] *DIN 66133 - Bestimmung der Porenvolumenverteilung und der spezifischen Oberfläche von Feststoffen durch Quecksilberintrusion*. Deutsche Institut für Normung e. V. (German Institute for Standardization), June 1993.

[20] Peter G Laye et al. *Principles of Thermal Analysis and Calorimetry*. Ed. by Peter Haines. RSC Paperbacks. The Royal Society of Chemistry, 2002, pp. X001–X004. DOI: 10.1039/9781847551764.

[21] Trevor Lever et al. "ICTAC nomenclature of thermal analysis (IUPAC Recommendations 2014)". In: *Pure Appl. Chem.* 86.4 (2014), pp. 545–553. DOI: 10.1515/pac-2012-060.

[22] Michael Ewart Brown. *Introduction to Thermal Analysis*. Ed. by Michael Ewart Brown. Hot Topics in Thermal Analysis and Calorimetry. Springer Netherlands, 2001. DOI: 10.1007/0-306-48404-8.

[23] Aline Auroux et al. *Handbook of Thermal Analysis and Calorimetry*. Ed. by Michael E. Brown and Patrick K. Gallagher. Vol. 5. Elsevier, 2008.

[24] *Technical specification TGA/DSC 1 Star System*. Mettler-Toledo AG, Analytical. CH-8603 Schwerzenbach, Switzerland, 2007.

[25] *Technical specification STA503*. Bähr-Thermoanalyse GmbH. Altendorfstraße 12, 32609 Hüllhorst, Germany, 2005.

[26] A. W. Coats and J. P. Redfern. "Thermogravimetric analysis. A review". In: *Analyst* 88 (1053 1963), pp. 906–924. DOI: 10.1039/AN9638800906.

[27] E. Sima-Ella and J. T. Mays. "Analysis of the oxidation reactivity of carbonaceous materials using thermogravimetric analysis". In: *J. Therm. Anal. Calorim.* 80.1 (2005), pp. 109–113. DOI: 10.1007/s10973-005-0621-x.

[28] *Technical specification SSM-5000A*. Shimadzu Corporation. Japan, 2014.

[29] Arthur W. Adamson and Alice P. Gast. *Physical Chemistry of Surfaces*. 6th. JOHN WILEY & SONS, INCORPORATED, 1997.

[30] Xue-song Wang and Yong Qin. "Equilibrium sorption isotherms for of Cu2+ on rice bran". In: *Process Biochem.* 40.2 (2005), pp. 677–680. DOI: http://dx.doi.org/10.1016/j.procbio.2004.01.043.

[31] Hans Dieter Baehr and Stephan Kabelac. *Thermodynamik*. 13th ed. Springer, 2006.

[32] Heinz Herwig, Christian Kautz, and Andreas Moschallski. *Technische Thermodynamik*. 2nd ed. Springer, 2016. DOI: 10.1007/978-3-658-11888-4.

[33] Oliver L. I. Brown. "The Clausius-Clapeyron equation". In: *J. Chem. Educ.* 28.8 (Aug. 1951), p. 428. DOI: 10.1021/ed028p428.

[34] T. Veltzke. "On gaseous microflows under isothermal conditions". Dissertation. University of Bremen, 2013.

4. The Deviation of Ideal Selectivities in C_{16}-Functionalized Mesoporous Structures

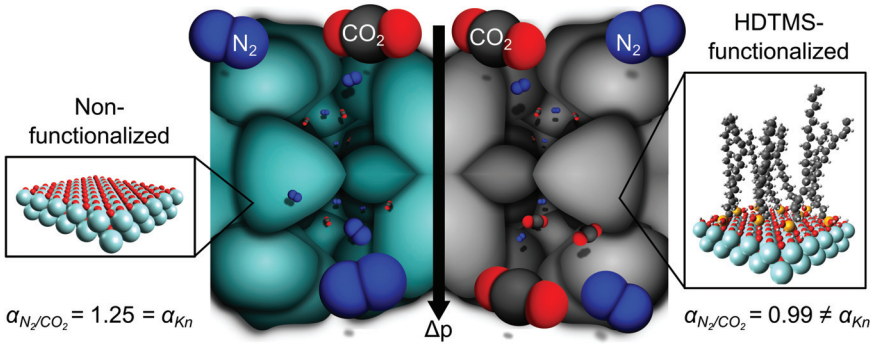

Adapted from:

A comparative experimental study on the deviation of the ideal selectivity in HDTMS- functionalized and untreated ceramic structures with pores in the upper mesoporous range

Published in:

Microporous and Mesoporous Materials, Volume 217, 15 November 2015, Pages 253–261
Received 17.02.2015, Revised 20.05.2015, Accepted 25.06.2015, Available online 06.07.2015
DOI: 10.1016/j.micromeso.2015.06.042

Authors:

Benjamin Besser[a], Thomas Veltzke[b], Jochen A.H. Dreyer[c], Julia Bartels[a], Michael Baune[b], Stephen Kroll[a,d,*], Jorg Thöming[b,d] and Kurosch Rezwan[a,d]

[a] Advanced Ceramics, University of Bremen, Am Biologischen Garten 2, 28359 Bremen, Germany
[b] Center for Environmental Research and Sustainable Technology, University of Bremen, Leobener Strasse 1, 28359 Bremen, Germany
[c] School of Energy and Environment, City University of Hong Kong, 11 Science Park West Avenue, Shatin, Hong Kong, Hongkong (SAR)
[d] Centre for Materials and Processes (MAPEX), University of Bremen, Am Fallturm 1, 28359 Bremen, Germany
[*] Corresponding author. Phone: +49 421 218 64933, E-Mail: Stephen.Kroll@Uni-Bremen.de

Abstract: Mesoporous ceramic capillary membranes with mean pore sizes of about 20 nm are prepared as model structures to investigate the influence of an altered surface chemistry on the flow behavior of gases. To modify the membrane surface, a wet chemical silanization process with hexadecyltrimethoxysilane (HDTMS) is used to gain an alkyl-functionalized surface. Structural and surface characterizations show that the surface chemistry is altered without affecting the mean pore diameter. For the non-functionalized membrane, single gas permeation measurements at 20 °C reveal ideal permselectivities which are in good agreement with the Knudsen theory. In contrast, the HDTMS-functionalized membrane shows permselectivities regarding carbon dioxide (CO_2) which deviate about 20 % from Knudsen theory. The gas permeation measurements further indicate a relative flow enhancement for CO_2 in comparison to nitrogen (N_2), argon (Ar) and methane (CH_4). Adsorption and desorption isotherms of CO_2 and N_2 at 20 °C show a decreased specific adsorption capacity for both gases, while the adsorption selectivity for CO_2/N_2 is increased. This indicates a weaker interaction of gas molecules and membrane surface due to HDTMS functionalization. This weaker gas-solid interaction along with the increased adsorption selectivity is proposed as reason for the experimentally observed deviation of the permselectivities from Knudsen theory.

4.1. Introduction

In microfluidic systems, biotechnology and separation science, surface modifications of inorganic substrates are an active field of research. Especially in membrane science, this concept is applied to develop new and improved materials, for example to enhance the selectivity of porous, inorganic membranes for gas separation.[1] Mass transport in such mesoporous membranes is mainly governed by Knudsen diffusion, which results only in small separation factors. To increase the separation beyond Knudsen limit, the principle of surface-selective flow, which is attributed to selective adsorption and diffusion, can be utilized. Surface modifications are applied to increase the concentration of a specific adsorbable gas species on the surface to favor surface diffusion.[2]

Processes using silane precursors provide a versatile tool to functionalize and tailor the membrane surface.[3] The surface functionality can be adjusted easily due to a broad spectrum of available silane molecules with different functional groups for example amino-, carboxyl- or alkyl-groups and spacer length, often ranging from $C_3 - C_{18}$.[4–6] In particular, when focusing on CO_2 adsorption, amine-functionalizations show a high potential and are therefore subject in recent investigations.[7,8] For example, Stoltenberg and Seidel-Morgenstern,[2] along with Ostwal et al.[9] and Sakamoto et al.[1] used an amine-modification to increase the CO_2/N_2 selectivity of mesoporous silica membranes. Furthermore, the effect of a membrane functionalization with organosilanes showing different alkyl-chain lengths on the selectivity of especially heavier hydrocarbons[3,10,11] or for purification of aggressive gases such as chlorine[12] has been investigated.

According to Koros and Mahajan,[13] the key requirements for membranes are durability, productivity and separation efficiency. The aimed performance optimum for membranes is therefore a high flux combined with a high selectivity. In general, a bigger pore size and a higher porosity results in a higher flux (permeability). Nevertheless, the contribution of surface diffusion is decreasing with increasing pore sizes, thus limiting an optimization. Therefore, the used membranes in the aforementioned studies possess pore sizes in the lower mesoporous region around 2-10 nm, since high separation factors are aimed. According to the general opinion in the literature, surface diffusion is supposed to be negligible in pores in the upper mesoporous range (10-50 nm) as well as macropores (>50 nm).[12,14,15] In fact, solely Knudsen diffusion is considered as the main governing transport mechanism in the upper mesoporous region >10 nm.[16]

In the supporting material of asymmetric inorganic membranes gas transport usually occurs in pores >10 nm. Until now, adsorption effects such as surface diffusion are neglected in such pores. In this study, deviations from the general rule stated above are observed by investigating the gas diffusion in inorganic membranes with pore sizes in the upper mesoporous region (>10 nm). Here, yttria stabilized zirconia (YSZ) as ceramic material and a well-established extrusion process are used to fabricate capillary membranes serving as model structures for gas permeation measurements. To affect the gas transport, a wet-chemical silanization process is used to immobilize an alkyl silane (hexadecyltrimethoxysilane, HDTMS) onto the surface showing a C_{16}-chain as functional group. Both, the non- and HDTMS-functionalized membranes are characterized by microstructural analysis with focus on pore size, porosity and specific surface area to ensure comparability. Single gas permeation measurements are conducted with argon (Ar) and nitrogen (N_2) as representatives for inert gases, as well as carbon dioxide (CO_2) and methane (CH_4) as gases with a more complex molecule structure and a higher interaction potential. Furthermore, adsorption/desorption measurements using N_2 and CO_2 are performed at 20 °C.

4.2. Experimental

In this section the used materials are briefly presented, followed by an introduction into the processing and functionalization route. Afterwards, the used material characterization methods are described, including structural analysis, characterization of the surface functionalization, as well as gas permeation and adsorption measurements.

4.2.1. Materials

The zirconia powder and reagents were purchased from commercial sources and used without further purification. The yttria (3 mol%) stabilized zirconia powder (YSZ, VP Zirkonoxid 3-YSZ, Lot. 3157061469) was obtained from Evonik Industries, Germany. Furthermore, for slurry preparation, 3-aminopropyltriethoxysilane (APTES, 99 %, prod-

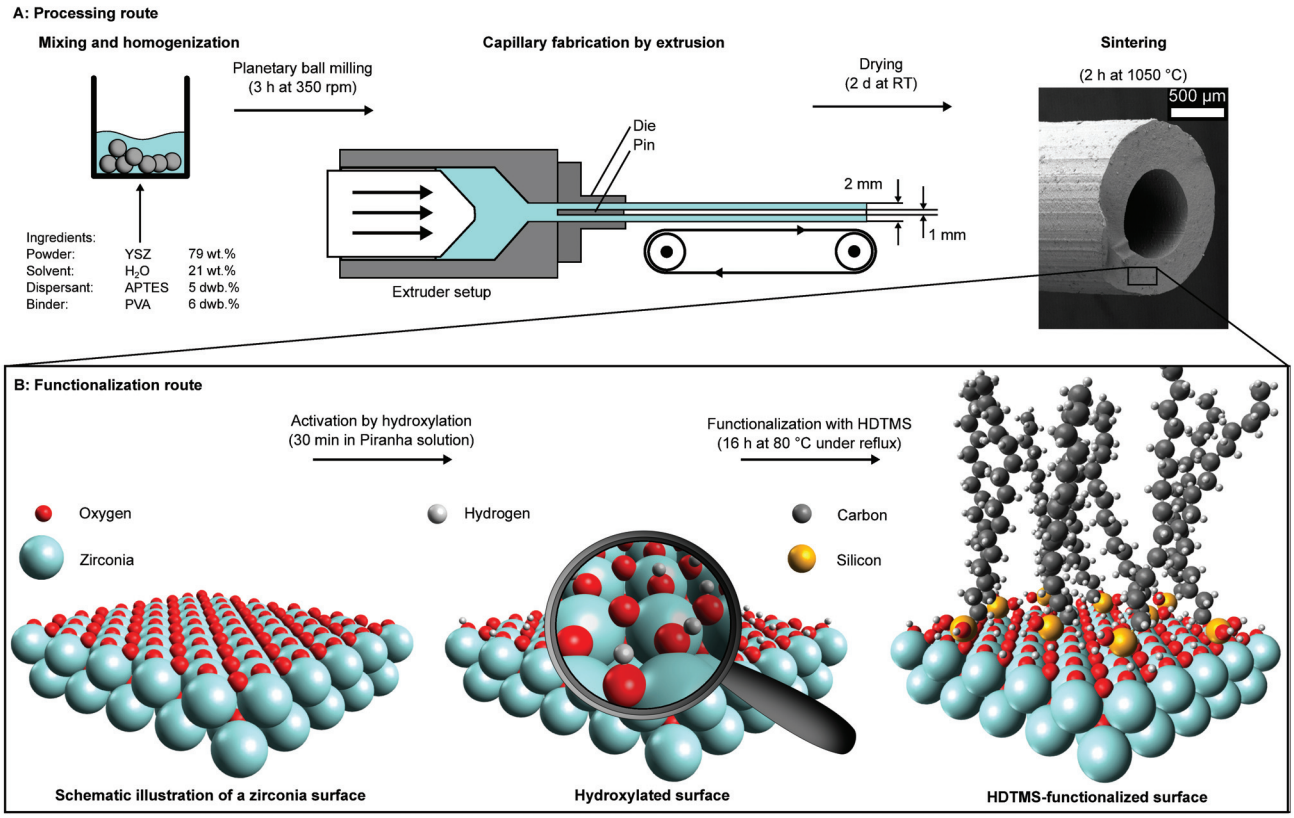

Figure 4.1.: Schematic overview of the slurry preparation, extrusion and sintering process (A), as well as the illustrated membrane functionalization process (B) through activation by hydroxylation and subsequent silanization using hexadecyltrimethoxysilane (HDTMS).

uct number 440140, Lot. SHBC8357V) as dispersant and polyvinyl alcohol (PVA, fully hydrolysed, product number P1763, Lot. SLBC9027V) as binder were obtained from Sigma-Aldrich Chemie GmbH, Germany. Sulfuric acid (H_2SO_4, 95-97 %, product number 30743, Lot SZBD2030V) as well as hydrogen peroxide ((H_2O_2, $\geq$35 %, product number 95299, Lot SZBD2410V) for membrane surface hydroxylation were provided from Sigma-Aldrich Chemie GmbH, Germany. For membrane surface modification acetone ($\geq$99 %, product number 00585, Lot. SZBB0100V) used as organic solvent was purchased from VWR International, Belgium, and hexadecyltrimethoxysilane (HDTMS, 90 %, product number AB111166, Lot. 1010563) was provided by ABCR, Germany. Double deionized water with an electrical resistance of 18 MΩ (Synergy®, Millipore, Germany) was used for all experiments.

4.2.2. Capillary Membrane Preparation

To prepare YSZ capillary membranes an extrusion process is used as described by Werner et al..[17] A schematic overview of the processing route for membrane fabrication is given in Fig. 4.1A. Four ingredients are used for slurry preparation, namely YSZ-nanopowder (79 wt.%, primary particle size 30 nm), double deionized water as solvent (21 wt.%), APTES as dispersant (5 dwb.%) and PVA as binder (6 dwb.%). Here, dwb refers to "dry weight basis" of the YSZ nanopowder. Accordingly, all additives are specified based on the powder content in relation to dwb.%$\equiv m_{\text{additive}}/m_{\text{powder}} \cdot 100$. In contrast to Werner et al.,[17] first, PVA is slowly dissolved in hot water (≈80 °C). Afterwards, YSZ powder, PVA-solution and APTES are mixed in a planetary ball mill (PM400 from Retsch, Germany) for 3 h at 350 rpm changing the rotation direction every 5 min. The obtained homogeneous slurry is then shaped into capillaries using a self-made lab extruder, equipped with an extrusion die of 2 mm diameter and a pin of 1 mm.[18,19] The resulting green bodies are dried at room temperature (RT) for at least two days, followed by final sintering for 2 h at 1050 °C (the detailed sintering program is given in[19]).

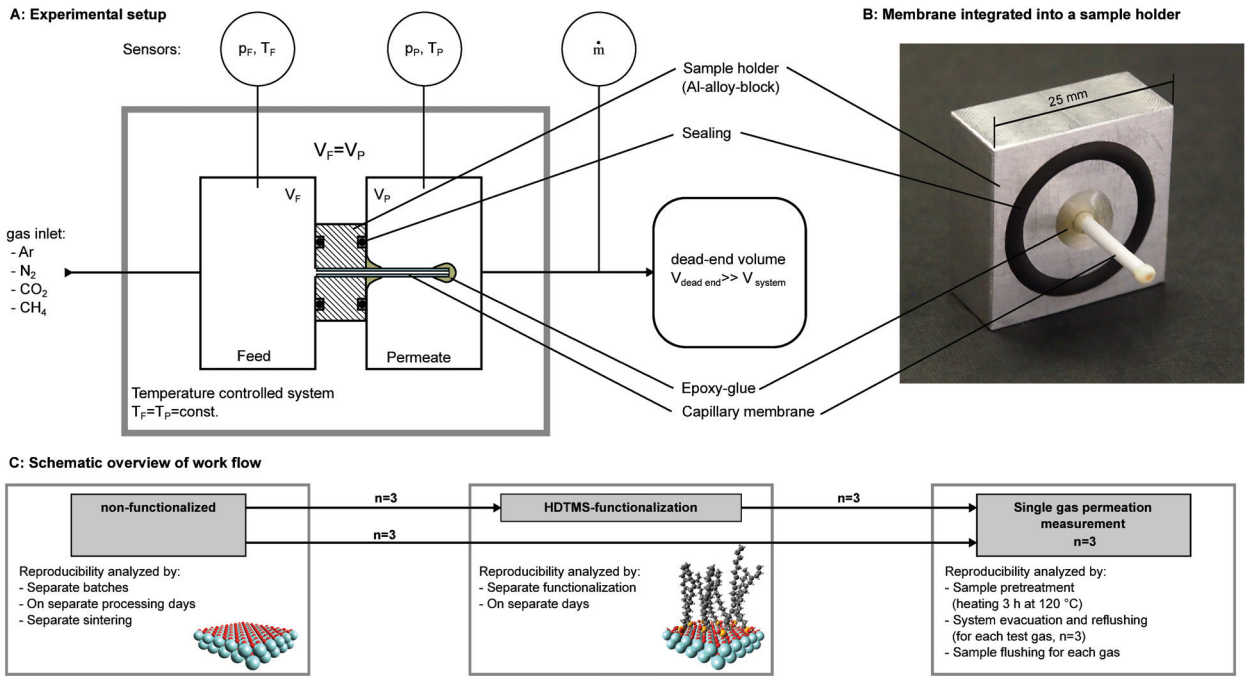

Figure 4.2.: Schematic overview of the experimental setup for single gas permeation measurements operating in dead-end mode (A). Mass flow, temperature and pressure are measured on both sides (feed and permeate) while the pressure difference between feed and permeate ($p_P - p_F$) is controlled. The overall system temperature is controlled and constantly kept at 20 °C. Notation for indices: F: Feed, P: Permeate. Photograph of a capillary membrane integrated into a sample holder (B). Schematic overview of the work flow (C).

4.2.3. Membrane Surface Functionalization

The membrane surface modification is performed by a two-step, wet-chemical process consisting of surface activation by hydroxylation followed by surface functionalization via silanization as schematically shown in Fig. 4.1B. A silane molecule is supposed to condensate and bind covalently onto an existent surface hydroxyl group using a water molecule as reaction partner.[4] To increase the amount of available hydroxyl groups and therefore increase the amount of bonding sites on the membrane surface, the membranes are primarily treated with freshly prepared Piranha solution (95-97 % H_2SO_4:35 % H_2O_2, 3:1, v/v) for 30 min as suggested by Kroll et al..[20] Afterwards, the membranes are washed with double deionized water until neutral pH is reached, subsequently followed by drying at 70 °C for 24 h.
Secondly, the activated membranes are functionalized with HDTMS according to previous works.[21] The modification is carried out using a 0.2 M HDTMS solution where a acetone-water mixture (95:5, v/v) served as solvent. The membranes are incubated for 16 h at 80 °C under reflux. After incubation, the membranes are washed three times with acetone followed by drying for 2 h at 70 °C.

4.2.4. Membrane Characterization

Membrane Structure

To ensure the comparability between the untreated and the HDTMS-functionalized material, detailed structural analyses are carried out. Therefore, the membranes are characterized in terms of pore size distribution, mean pore size (d_{50}), relative pore volume, open porosity and specific surface area. The pore size distribution and the resulting mean pore diameter, along with the relative volume and the open porosity are determined by mercury intrusion porosimetry using a Mercury Porosimeter Pascal 140 and 440 (POROTEC GmbH, Germany). The specific surface area is measured by nitrogen adsorption at -196 °C according to BET method using a BELSORP-mini II (Bel Japan Inc., Japan). Prior to the gas adsorption measurements the membrane samples are degassed for at least 3 h at 120 °C and reduced pressure (≤2 mbar) followed by cooling to RT under argon atmosphere (≥30 min). Furthermore, the membrane microstructures are visualized by scanning electron microscopy (SEM) using a field-emission SEM SUPRA® 40 (Zeiss, Germany).

Membrane Surface Functionalization

The surface functionalization is characterized by thermogravimetry (TGA) and carbon content measurements. Thermogravimetry and differential scanning calorimetry (DSC) experiments are performed with a TGA/DSC1 Star System (Mettler Toledo, Germany). About 70 mg of the membrane samples are placed in an alumina crucible and heated from 30 to 900 °C (heating rate 10 °C/min) while flushing the sample with O_2 (30 mL/min). The amount of total carbon (TC) and inorganic carbon (IC) is measured using a SSM-500A solid sample module (Shimadzu, Japan). For TC measurements, about 50 mg membrane material is placed in a crucible and heated to 900 °C operating in oxygen (O_2) atmosphere. The IC is determined by placing about 100 mg membrane material in a crucible, adding sulfuric acid, and heating the sample to 200 °C. The amount of CO_2 formed during TC and IC experiments, respectively, is determined by an infrared (IR) detector (TOC-V, Shimadzu, Japan) and normalized to the exact sample weight.

Single Gas Permeation Measurements

Single gas dead-end permeation measurements are performed with four different gases, namely argon (Ar), nitrogen (N_2), carbon dioxide (CO_2) and methane (CH_4), as schematically shown in Fig. 4.2A. A detailed description of the used measurement system is given by Veltzke et al..[22,23] The samples are prepared by integrating the membrane capillaries into an alloy-sample holder using a two-component epoxy resin adhesive (UHU Plus endfest 300, UHU GmbH & Co. KG, Germany) as shown in Fig. 4.2B. For each membrane type, three different samples from separate processing batches, including all processing steps as depicted in Fig. 4.1 and indicated in Fig. 4.2C are used. Prior to the gas permeation measurements the membranes are heated to 120 °C for 3 h to desorb moisture. To ensure purity of the applied gas for the measurement, the whole system is evacuated and purged three times with the ongoing test gas. Afterwards, the membrane is flushed with the test gas for 60 s. All measurements are performed at 20 °C and 800 mbar dead-end pressure. As indicted in Fig. 4.2A, temperature and pressure on both sides, as well as the molar flow rate are measured and the data is logged at a frequency of 6 Hz. For each measurement the flow is measured at nine different pressure drops. After adjusting a certain pressure difference and waiting until the system has reached a steady-state condition, the data is averaged over 120 s. In total, each measurement is performed three times to ensure reproducibility. The relation between the pressure difference and the molar flow is used for data evaluation. Particularly, after linear regression of the molar flow onto the pressure difference, the ratio of the slopes from two different gases is used to calculate the ideal permselectivity, as:

$$\alpha_{i,j} = \frac{(\partial \dot{n}/\partial p)_i}{(\partial \dot{n}/\partial p)_j}, \tag{4.1}$$

with $\dot{n}$ as the molar flow rate of gas i or j.

Evaluation of Gas Permeation Measurements

In order to compare the non-functionalized and the HDTMS-functionalized membranes the Knudsen theory is used, which represents the dilute gas flow in mesoporous structures. According to Knudsen,[24] molecular diffusion in porous solids is driven by diffuse reflection of the molecules from the pore walls, predominating when the pore diameter (d) is smaller than the mean free path of the gas molecules (λ). The rarefaction of a gas is quantified by the Knudsen number. Based on the kinetic theory of gases assuming a Maxwell-Boltzmann distribution, the Knudsen number can be defined as:

$$Kn = \frac{\lambda}{d} = \frac{k_B T}{\sqrt{2}\pi\sigma^2 p d}, \tag{4.2}$$

where k_B is the Boltzmann constant, T is the temperature, σ is the collision diameter of the gas molecule and p is the pressure. Furthermore, d is a representative physical length scale, in this case the mean pore diameter of the membrane (d_{50}). According to the Knudsen theory it can be shown that the molar flow of a gas is inversely proportional to the square root of its molar mass, assuming constant temperature and pressure. Therefore, Knudsenselectivities can be calculated for specific gas pairs, knowing their molar mass M, according to:

$$\alpha_{Kn,ij} = \sqrt{\frac{M_j}{M_i}}. \tag{4.3}$$

In the following, the molar mass of the heavier gas is defined as numerator (M_j), resulting in Knudsenselectivities always >1. According to this definition and the definition of indexes in

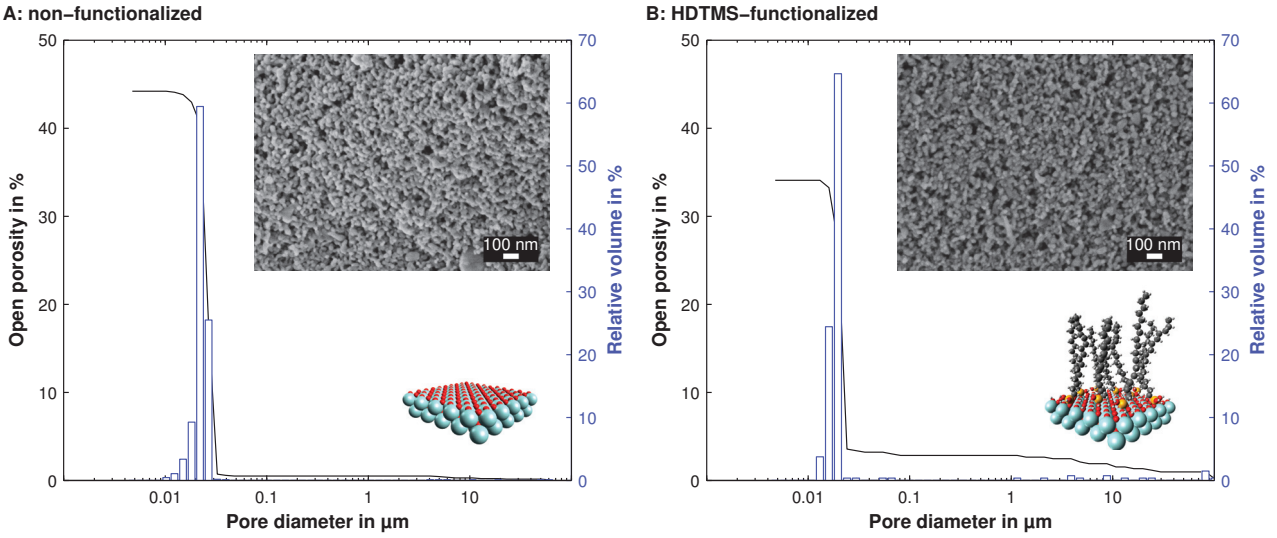

Figure 4.3.: Pore size distributions and open porosities of the non-functionalized (A) and the HDTMS-functionalized membrane (B) obtained from mercury intrusion porosimetry along with SEM micrographs of the corresponding membrane surfaces (inset). The membranes feature a very narrow pore size distribution which is not influenced by the surface functionalization.

equation 4.1 in section 4.2.4, the slope of the heavier gas is therefore defined as the denominator $((\partial\dot{n}/\partial p)_j)$ for the calculation of the permselectivity. To compare the non-functionalized and HDTMS-functionalized membranes, the permselectivity and the Knudsenselectivity are used as key values.

Gas Adsorption and Desorption Measurements

To investigate the interaction between gas and surface under conditions similar to the gas permeation measurements (see section 4.2.4), adsorption/desorption isotherms of N_2 and CO_2 are performed at 20 °C using a Belsorp-Max (Bel Japan Inc., Japan). Additionally, to identify the existent specific surface area, nitrogen adsorption at -196 °C according to BET method are performed with the same measurement device. To analyze the adsorption capacities, the adsorption/desorption isotherms at 20 °C are normalized to the measured specific surface area and recalculated to μmol/m^2. For the above mentioned experiments, about 350 mg membrane material is used and pretreated by degassing for at least 3 h at 120 °C and reduced pressure ($\leq$2 mbar), followed by cooling to RT under argon atmosphere ($\geq$30 min).

4.3. Results and Discussion

4.3.1. Membrane Structure

As given in equation 4.2, the Knudsen number describes the relation between the condition of the gas and the porous structure. Accordingly, the governing transport mechanism is highly dependent on the porous structure represented by the mean pore diameter of the membrane. For this reason, a detailed structural analysis is essential to ensure comparability of the non-functionalized and HDTMS-functionalized membrane structures. In Fig. 4.3, a non-functionalized (part A) and a HDTMS-functionalized (part B) membrane are compared, showing quantitative pore size distributions and open porosities derived from mercury intrusion porosimetry as well as SEM micrographs for qualitatively analysis (insets). Both, the non-functionalized and the HDTMS-functionalized membrane show similar monomodal and narrow pore size distributions in the mesoporous range with a sharp increase in the relative pore volume below 30 nm. This indicates that the basic, overall pore structure of the membrane is not influenced by the applied surface functionalization using HDTMS, which can also be confirmed by the corresponding SEM micrographs of the membrane surfaces as shown in the insets in part A and B of Fig. 4.3. Due to the applied moderate sintering temperature of 1050 °C for 2 h, a relatively high open porosity of the

Table 4.1.: Structural properties of the non-functionalized and HDTMS-functionalized membranes measured by mercury porosimetry and nitrogen adsorption. While the open porosity and the specific surface area are decreased after HDTMS-functionalization, the mean pore diameter is not significantly influenced by the surface functionalization.

Membrane	Pore size range in nm	Mean pore diameter d_{50} in nm	Open porosity in %	Specific surface area in m^2/g
Non-f.	17.0±0.5-29.1±3.2	22.2±1.4	43.7±0.6	20.1±0.5
HDTMS-f.	14.2±0.3-21.3±0.5	18.1±2.0	32.3±2.0	12.3±0.9

non-functionalized membrane of around 44 % is achieved. By functionalization using HDTMS a significant decrease of about one-fourth in open porosity is obtained, as shown in part B of Fig. 4.3. For this particular measurement, a small content of open porosity (3 %) is already detected at bigger pore diameters >0.1 μm, which is attributed to measurement artifacts, since no pores are detected in this region for the untreated membrane material (see Fig. 4.3A). Nevertheless, the characteristic shape of the pore size distribution with a sharp increase in the relative pore volume below 30 nm remains after functionalization.

Table 4.1 summarizes the results derived from mercury porosimetry and BET measurements of non- and HDTMS-functionalized membranes from individual processing batches (n=3) and surface functionalizations (n=3). For specifying the pore size range based on the distribution of relative pore volume, a threshold of 2 % is set to exclude artifacts. The pore size ranges of both membrane types are similar, but slightly shifted to smaller pore sizes after functionalization with HDTMS. This results in a smaller mean pore diameter (d_{50}) of 18.1 nm for the HDTMS-functionalized membrane compared to the non-functionalized membrane (22.2 nm). Based on the molecule length of HDTMS of around 2 nm a decrease of the mean pore diameter of around 4 nm is plausible due to the surface functionalization. In agreement with the open porosity results (Fig. 4.3), the specific surface area of the membrane is decreased by 39 % due to applied HDTMS functionalization. This behavior is also described by Kuraoka et al.[11] for surface functionalizations using organosilanes with long alkyl chains, where a decrease of about 96 % in specific surface area is attributed to a C_{18}-chain functionalization of porous glass membranes with pore sizes of about 4 nm. As a reason for the decrease in specific surface area, pore filling and blocking by immobilization of the long chain molecules is identified by Kuraoka et al. Accordingly, this is also assumed being a reason for the reduction of the porosity and specific surface area due to HDTMS functionalization in this study. Introducing a certain amount of molecules into a limited pore volume inevitable causes a reduction of volume which is represented by the decrease in porosity. Furthermore, small pores and narrow interconnections may be blocked due to steric hindrance of the long HDTMS molecules, resulting in a decrease of specific surface area. The Knudsen number and the ideal selectivity (see equation 4.2 and 4.3) are not influenced by the open porosity or specific surface area. Therefore, the governing transport mechanism for gases is independent of these two membrane properties. In contrast, the mean pore diameter directly influences the Knudsen relation and plays an important role for the analysis of gas transport mechanisms in porous structures. The results show that the mean membrane pore diameter is decreased only slightly due to HDTMS-functionalization and therefore the governing transport mechanisms within both membrane types are considered comparable.

4.3.2. Surface Functionalization

The decrease in porosity and specific surface area indicates a successful HDTMS functionalization and the presence of HDTMS molecules on the membrane surface. For further characterization of the membrane functionalization and for quantification of the silane-molecules attached to the surface, additional analysis are performed including TGA, as well as total- and inorganic carbon content measurements. Fig. 4.4A shows an exemplary TGA/DSC measurement of a non-functionalized and a HDTMS-functionalized membrane from the same processing batch. The non-functionalized membrane only shows little weight loss, mainly below 200 °C, which is related to water desorption. After HDTMS functionalization, the TGA signal shows a significant increase in weight loss above

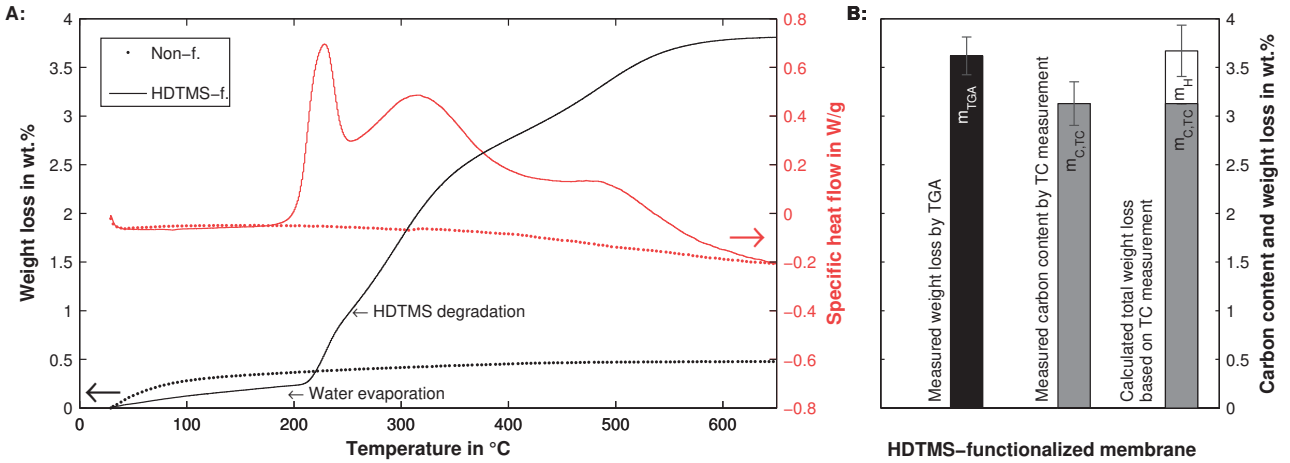

Figure 4.4.: Comparison of the estimated weight loss (resulting from total carbon (TC) content measurements) with the weight loss determined by TGA measurement (A), as well as two exemplary TGA/DSC measurements of a non-functionalized and a HDTMS-functionalized membrane (B). The results from both measurement techniques are in good agreement.

Table 4.2.: Carbon content of the non-functionalized and HDTMS-functionalized membranes derived from total carbon and inorganic carbon measurements as well as the calculated (based on TC measurements) and the measured weight loss from TGA along with the calculated functional groups per membrane surface area.

	Carbon content in wt.%		Weight loss in wt.%		Functional groups[a] in	
Membrane	total	inorganic	calculated[b]	measured[c]	μmol/m^2	groups/nm^2
Non-f.	<0.01	<0.01	0	0.11±0.05	0	0
HDTMS-f.	3.13±0.22	<0.01	3.67±0.26	3.73±0.19	5.20±0.07	3.13±0.04

[a]Calculated amount of functional groups using specific surface area and measured weight loss from TGA
[b]Calculated weight loss due to degradation of HDTMS ($C_{16}H_{33}$) based on the measured total carbon content.
[c]Measured weight loss by TGA measurement (weight loss between 200-600 °C).

200 °C, in particular 3.72 wt.% between 200 °C and 600 °C. Likewise, the associated DSC measurement shows a high heat-uptake above 200 °C. In contrast, the DSC signal obtained from the non-functionalized membrane shows no heat-uptake. In summary, considering the TGA and DSC results for both membrane types, a degradation of the HDTMS molecule above 200 °C is suggested. For additional analysis of the weight loss, carbon content measurements are performed to further detect the degradation of the C_{16}-chains from the HDTMS molecules. Fig. 4.4B compares the results of the TGA and TC measurements. Using the non-functionalized membrane as reference, the specific weight loss due to HDTMS degradation determined by TGA is m_{TGA}=3.62±0.19 wt.%. In contrast, the amount of carbon (TC) measured by the IR detector can be quantified to 3.13±0.22 wt.%. Since the TC measurement only detects carbon, the hydrogen atoms from the desorbing HDTMS molecules ($C_{16}H_{33}$) are not considered by this technique. Therefore, to estimate the total mass loss due to HDTMS desorption, the TC result ($m_{\mathrm{C,TC}}$) is recalculated with respect to the C/H relation (n_{C}=16 and n_{H}=33) according to $m_{\mathrm{HDTMS,TC}} = m_{\mathrm{C,TC}} \cdot (n_{\mathrm{C}} \cdot m_{\mathrm{C}} + n_{\mathrm{H}} \cdot m_{\mathrm{H}})/(n_{\mathrm{C}} \cdot m_{\mathrm{C}})$ using m_{C}=12.011 and m_{H}=1.008 as atomic weights. The resulting calculated total mass loss of $m_{\mathrm{HDTMS,TC}}$=3.67±0.26 wt.% based on the TC detection is in good agreement with the measured weight loss by TGA measurements (m_{TGA}=3.62±0.19 wt.%).

In addition to the TC detection, inorganic carbon content measurements are performed to ensure an organic origin of the detected total carbon. Table 4.2 summarizes the results of the carbon content and weight loss measurements for the non- and HDTMS-functionalized membranes based on three processing batches and HDTMS-functionalizations. For all IC measurements, the signal is below detection limit (<0.01 wt.%), confirming that the measured TC

content is organic carbon. In general, the results from both types of measurements are highly reproducible and show similar results, suggesting that both techniques are suitable for quantification of HDTMS molecule contents. Table 4.2 also presents the calculated amount of functional groups in μmol/m^2 and groups/nm^2. Here, the TGA measurement results are normalized to the specific surface area of the non-functionalized membranes (a) and recalculated according to $c_{\mathrm{HDTMS}} = m_{\mathrm{TGA}} \cdot M_{\mathrm{HDMTS}}/a$ using the molar mass of HDTMS (M_{HDTMS}=346.63 g/mol). Accordingly, the calculated amount of functional HDTMS groups on the surface of the membrane is c_{HDTMS}=3.13±0.04 groups/nm^2.

Due to steric reasons, a condensation reaction of one HDTMS molecule with only one hydroxyl group can be assumed.[4] Therefore, a hydroxyl concentration on the membrane surface of at least 3.13±0.04 groups/nm^2 can be approximated. According to literature data, this is a reasonable value compared with 8-15 hydroxyl groups/nm^2 determined by water adsorption[25–27] on ZrO_2 and 1.2 hydroxyl groups/nm^2 for a porous YSZ membrane, determined by potentiometric titration.[20]

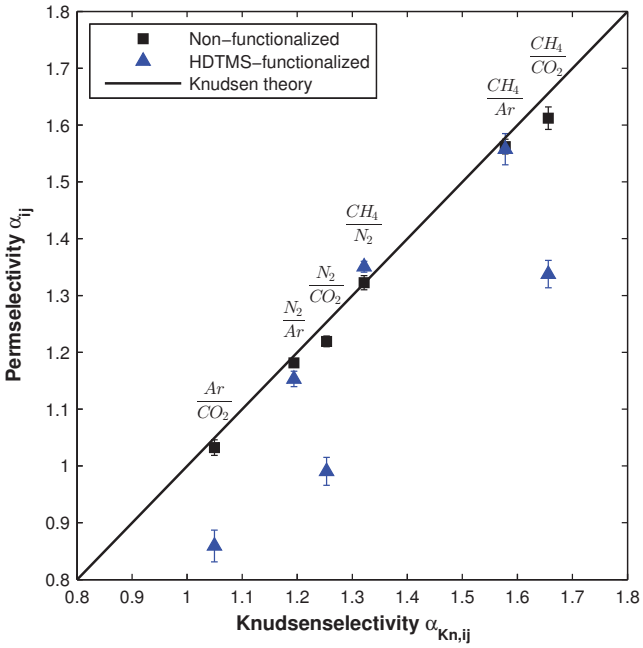

Figure 4.5.: Permselectivity versus Knudsenselectivity of the non-functionalized and HDTMS-functionalized membranes. The black line represents the Knudsen selectivity proposed by the Knudsen theory. The selectivities regarding CO_2 deviate from the theory after functionalization with HDTMS.

4.3.3. Single Gas Permeation Measurements

The membrane structures are evaluated according to their permselectivities α_{ij} and the Knudsenselectivities $\alpha_{Kn,ij}$ as defined in section 4.2.4. As described in section 4.2.4, the gas permeation data is analyzed by linear regression of the molar flow onto the pressure difference. The results show a linear dependency between molar flow and pressure difference, whereas the coefficient of determination for linear regression is R^2 >0.999 for all measurements. This indicates solely Knudsen flow as transport mechanism with no viscous contribution, which would result in a quadratic dependency. Furthermore, multiple measurements with CO_2 as well as N_2 at different dead-end pressures according to the measurement protocol given in section 4.2.4 are performed. The results obtain pressure independence, assuring Knudsen flow as the governing transport mechanism (see Fig. A9). Besides, it should be noticed that a decrease in flow is observed due to HDTMS-functionalization. This behavior is already known from literature as a result for silane functionalizations.[2,3,28]

In Fig. 4.5 the measured permselectivities are plotted against the theoretical Knudsenselectivities. The Knudsen theory is therefore represented by the bisecting line. Accordingly, measurements with membrane structures which feature solely Knudsen diffusion should show results close to the bisecting line. The higher the deviation of the measurement results from the bisecting line, the higher the contribution of an additional transport mechanism that is not described by Knudsen theory.

The non-functionalized membranes show a good agreement with the Knudsen theory and all permselectivities are very close to the bisecting line. Hence, all investigated gases (Ar, N_2, CO_2 and CH_4) propagate through the membrane following the principle of Knudsen diffusion.

After functionalization with HDTMS, not all permselectivities are in agreement with the Knudsen theory (Fig. 4.5). The permselectivities regarding Ar, N_2 and CH_4 meet their theoretical expectations, showing good agreement for $\alpha_{\mathrm{N_2/Ar}}$, $\alpha_{\mathrm{CH_4/N_2}}$ and $\alpha_{\mathrm{CH_4/Ar}}$, respectively. In contrast, the permselectivities regarding CO_2 show lower values as shown for $\alpha_{\mathrm{Ar/CO_2}}$, $\alpha_{\mathrm{N_2/CO_2}}$ and $\alpha_{\mathrm{CH_4/CO_2}}$. Here, all permselectivities of gas pairs containing CO_2 deviate about 20 % from the theoretical values. According to the definitions in section 4.2.4, CO_2 serves as denominator regarding these particular selectivities, since CO_2 is the

heaviest gas investigated. Therefore, these smaller permselectivities in relation to CO_2 represent an enhanced flow of CO_2 compared with Ar, N_2 and CH_4 due to HDTMS-functionalization, since all other permselectivities show a behavior according to the Knudsen theory.

In section 4.3.1 (Fig. 4.3 and Table 4.1) the membrane structures of the non-functionalized and the HDTMS functionalized membranes are discussed. The results show similar pore sizes ($d_{50,\text{non-f.}}$=22.2 nm, $d_{50,\text{HDTMS-f.}}$=18.1 nm), ensuring the comparability of the governing gas transport mechanism in both membrane types. Furthermore, section 4.3.2 examines the presence of HDTMS molecules in the functionalized membranes, which can be estimated to 3.13±0.04 functional groups/nm^2. By summarizing the microstructural and membrane surface analysis, the membrane surface chemistry is altered without changing the important membrane parameter for Knudsen flow. According to the literature, gases propagating through such mesoporous structures with pores >10 nm should follow the laws of Knudsen diffusion.[16] A potential surface diffusion is supposed to affect the gas flow significantly at smaller pores in the lower mesoporous region[12,14,15] and not at pore sizes as big as 20 nm. Nevertheless, an unexpected deviation regarding CO_2 is observed due to the surface functionalization with HDTMS. The decreasing permselecitivities for CO_2 indicate an enhanced gas flow of CO_2 compared to Ar, N_2 and CH_4. Accordingly, there is no influence of the surface functionalization on the gas flow of Ar, N_2 and CH_4. Both, the non-functionalized and the HDTMS-functionalized membrane structures are considered comparable, because the pore size distributions remain similar. Thus, the decrease in selectivity regarding CO_2 represents a specific influence of the surface chemistry on the gas flow of CO_2. This indicates that Knudsen diffusion may be the governing transport mechanism in both membrane types, but for a HDTMS-functionalized membrane it seems not to be the only one. A changed adsorption behavior of the CO_2 molecules with the surface functional groups is proposed as the influencing factor. It is hypothesized that the change in adsorption dynamics due to HDTMS-functionalization affects the gas flow of CO_2. These assumptions are further discussed based on gas adsorption/desorption measurements.

4.3.4. Gas Adsorption and Desorption Measurements

An alternation of the surface functional group composition due to the functionalization with HDTMS changed the flow behavior of CO_2 in comparison to Ar, N_2 and CH_4 (Fig. 4.5). To further investigate the impact of HDTMS functionalization on the interaction between gas molecules and membrane surface, adsorption/desorption measurements are performed. The thermal conditions are kept similar to the gas permeation measurements (20 °C) using CO_2 and N_2 as test gases. Fig. 4.6 shows the adsorbed amount of molecules, given in μmol/m^2, in relation to the equilibrium pressure (in kPa). For both membrane types, a higher adsorption capacity is observed for CO_2 in contrast to N_2. This result is reasonable, since N_2 is an inert gas. Nevertheless, both applied test gases show significantly lower values for the HDTMS-functionalized membranes than for the untreated material. Stoltenberg and Seidel-Morgenstern[2] also detected a decrease in the adsorbed amount of CO_2 per unit volume after an amine functionalization of a mesoporous glass membrane (mean pore diameter of 3.3 nm). The decrease in specific surface area after functionalization is suggested as reason for the decreased amount of adsorbed CO_2. In the present study, the exact amount of surface area of the measured membrane pieces is determined by BET method and used as a reference value. Therefore, the decrease of the specific surface area due to the applied HDTMS-functionalization can be excluded as reason for the decreased amount of adsorbed CO2. In summary, considering a finite surface area fraction, less molecules will adsorb on a surface with HDTMS-functionalization than without functionalization. Besides the decrease of the total amount of adsorbed molecules, the adsorption selectivity of CO_2/N_2 is significantly increased. Comparing the maximum amount of adsorbed molecules for CO_2 and N_2, given in Fig. 4.6, the ratio of CO_2-molecules/N_2-molecules is around four times higher for the HDTMS-functionalized membrane.

The measured decrease of adsorption capacity is assumed to be caused by a weaker interaction between gas molecules and surface due to the functionalization with HDTMS. This can be supported by quantum calculations conducted by Yu et al.,[29] which show a smaller binding energy of CO_2 with alkyl-chains in comparison to functional groups

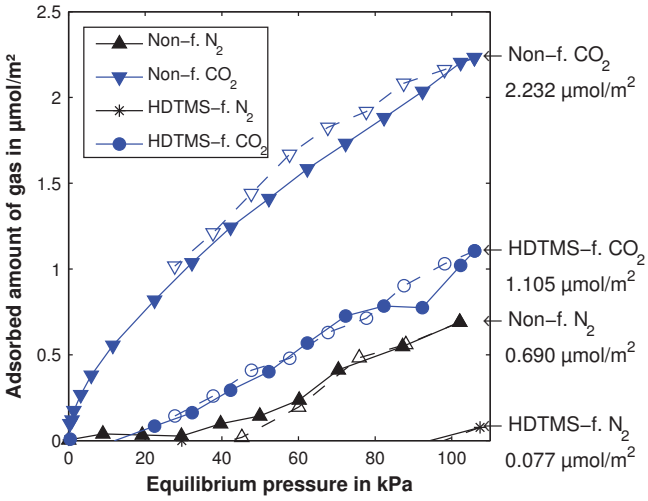

Figure 4.6.: N_2 and CO_2 adsorption-desorption isotherms at 20 °C for non-functionalized and HDTMS-functionalized membranes. Filled symbols are used for adsorption, empty symbols for desorption. The measured adsorbed amount is normalized to the specific surface area of the particular membrane samples and given in μmol/m^2. The adsorption capacity is decreased due to the surface functionalization.

with a higher polarity and therefore a smaller adsorption enthalpy at a given pressure and temperature.

Analyzing the results from both measurement techniques, an influence from the HDTMS-functionalization on gas permeation as well as gas adsorption/desorption behavior is observed. The HDTMS-functionalized membranes show a CO_2 flow which is enhanced disproportionately with respect to Ar, N_2 and CH_4 (Fig. 4.5). This leads to smaller permselectivities deviating from Knudsen theory. Furthermore, these membranes show a lower specific adsorption capacity for CO_2 and N_2 (Fig. 4.6). These altered interactions between gas molecules and surface due to the HDTMS-functionalization are claimed as reason for the change in permselectivity in contrast to the Knudsen theory. One possible explanation for the measured decrease of adsorption capacity is a weaker interaction and a smaller binding energy of CO_2 with the alkyl-functionalized surface[29] and therefore a smaller adsorption enthalpy at a given pressure and temperature. According to the literature, the amount of available adsorption sites, as well as the adsorption enthalpy have a great influence on the mechanism of surface diffusion.[2,30–32] In fact, there is an interplay between adsorption sites, adsorption strength and the amount of molecules which are adsorbed on a surface under certain conditions of pressure and temperature. Under the applied conditions of 20 °C and 800 mbar, a surface functionalization with HDTMS results in a decrease of the adsorbed amount of molecules on the surface, while increasing the selective adsorption of CO_2/N_2, along with a measurable influence on the gas permeation for CO_2. According to the general opinion from the literature adsorption effects and surface diffusion are negligible in pores >10 nm. In this case, surface diffusion may be a possible explanation for the observed deviations in gas permeation, assuming that the altered surface chemistry results in more favorable adsorption conditions for surface diffusion. A definite statement or a prove for surface diffusion cannot be given at this point, therefore this remains as an assumption. Further research is needed to fully understand the gas-solid interactions and diffusion mechanisms at these length scales.

4.4. Conclusion

Mesoporous YSZ capillary membranes with mean pore diameters of around 20 nm are prepared to investigate the influence of a surface functionalization with HDTMS on gaseous flows in mesoporous structures. Before and after functionalization, the membranes feature a similar pore structure with comparable mean pore diameters. Therefore, the crucial membrane property for quantification of gaseous rarefaction, the mean pore diameter, is not affected, ensuring equal flow conditions in both membrane types. Single gas permeation measurements at 20 °C are performed to investigate the influence of the altered surface characteristics on four different gases (Ar, N_2, CO_2 and CH_4). Whereas the non-functionalized membranes show ideal Knudsen diffusion behavior, the HDTMS-functionalized membranes show permselectivities differing about 20 % from the Knudsen theory regarding CO_2. This reveals an enhanced CO_2 flow compared to the other gases due to HDTMS-functionalization. Adsorption/desorption isotherms also measured at 20 °C show a significant reduction of the specific adsorption capacity for CO_2 as well as N_2 after functionalization with HDTMS, suggesting a weaker interaction of the gases with the membrane surface. Furthermore, the adsorption selecitvity of CO_2/N_2 is increased. The detected adsorption effects are proposed as a reason for the deviation of the gas flow from the Knudsen dif-

fusion theory. According to the literature, Knudsen diffusion is supposed to be the driving mechanism for gas flows at the present length scale and that adsorption effects along with surface diffusion are negligible. In contrast, the presented results lead to the conclusion that adsorption effects also play a role in pores of the upper mesoporous region (10-50 nm) and that the contribution of molecule-surface interactions to gas transport in mesoporous structures is not fully understood yet. Surface diffusion may be a possible explanation for the aforementioned deviation from Knudsen theory. Even though, further research is needed to clearly identify all mechanisms affecting the gas flow behavior in this pore size range.

Acknowledgments

This work was supported by German Research Foundation (DFG) within the Research Training Group GRK 1860 "Micro-, meso- and macroporous nonmetallic Materials: Fundamentals and Applications" (MIMENIMA). The support of Petra Witte (University of Bremen, Department of Geosciences) for her work with the SEM is gratefully acknowledged. Furthermore, we thank T. C. Schumacher from the University of Bremen for all the fruitful discussions and the critical feedback which helped to improve this work.

References

[1] Yuzuru Sakamoto et al. "Preparation and CO_2 separation properties of amine-modified mesoporous silica membranes". In: *Microporous Mesoporous Mater.* 101.1-2 (Apr. 2007), pp. 303–311. DOI: 10.1016/j.micromeso.2006.11.007.

[2] Daniel Stoltenberg and Andreas Seidel-Morgenstern. "An attempt to alter the gas separation of mesoporous glass membranes by amine modification". In: *Microporous Mesoporous Mater.* 154 (May 2012), pp. 148–152. DOI: 10.1016/j.micromeso.2011.11.013.

[3] Scott Higgins, William DeSisto, and Douglas Ruthven. "Diffusive transport through mesoporous silica membranes". In: *Microporous Mesoporous Mater.* 117.1-2 (Jan. 2009), pp. 268–277. DOI: 10.1016/j.micromeso.2008.06.030.

[4] Laura Treccani et al. "Functionalized ceramics for biomedical, biotechnological and environmental applications". In: *Acta Biomater.* 9.7 (July 2013), pp. 7115–7150. DOI: 10.1016/j.actbio.2013.03.036.

[5] K. L. Mittal. *Silanes and Other Coupling Agents*. Ed. by K. L. Mittal. Vol. 5. ISBN-10: 9004165916. Koninklijke Brill NV, Leiden, The Netherlands, 2009.

[6] Greg T. Hermanson. "Chapter 13 - Silane Coupling Agents". In: *Bioconjugate Techniques (Third edition)*. Ed. by Greg T. Hermanson. Boston: Academic Press, 2013, pp. 535–548.

[7] Chao Chen, Jun Kim, and Wha-Seung Ahn. "CO_2 capture by amine-functionalized nanoporous materials - A review". In: *Korean J. Chem. Eng.* 31.11 (Oct. 2014), pp. 1919–1934. DOI: 10.1007/s11814-014-0257-2.

[8] Thiam-Leng Chew, Abdul L. Ahmad, and Subhash Bhatia. "Ordered mesoporous silica (OMS) as an adsorbent and membrane for separation of carbon dioxide (CO_2)". In: *Adv. Colloid Interface Sci.* 153.1-2 (Jan. 2010), pp. 43–57. DOI: 10.1016/j.cis.2009.12.001.

[9] Mayur Ostwal et al. "3-Aminopropyltriethoxysilane functionalized inorganic membranes for high temperature CO_2/N_2 separation". In: *J. Membr. Sci.* 369 (Nov. 2011), pp. 139–147. DOI: 10.1016/j.memsci.2010.11.053.

[10] Rajinder P. Singh, J. Douglas Way, and Steven F. Dec. "Silane modified inorganic membranes - Effects of silane surface structure". In: *J. Membr. Sci.* 259.1-2 (Aug. 2005), pp. 34–46. DOI: 10.1016/j.memsci.2005.03.004.

[11] K Kuraoka, Y Chujo, and T Yazawa. "Hydrocarbon separation via porous glass membranes surface-modified using organosilane compounds". In: *J. Membr. Sci.* 182.1-2 (Feb. 2001), pp. 139–149. DOI: 10.1016/S0376-7388(00)00559-7.

[12] Arne Lindbråthen and May-Britt Hägg. "Glass membranes for purification of aggressive gases - Part I. Permeability and stability". In: *J. Membr. Sci.* 259.1–2 (2005),

pp. 145–153. DOI: http://dx.doi.org/10.1016/j.memsci.2005.03.056.

[13] William J Koros and Rajiv Mahajan. "Pushing the limits on possibilities for large scale gas separation - which strategies?" In: *J. Membr. Sci.* 175.2 (Aug. 2000), pp. 181–196. DOI: 10.1016/S0376-7388(00)00418-X.

[14] R. Krishna and J.M. van Baten. "An investigation of the characteristics of Maxwell-Stefan diffusivities of binary mixtures in silica nanopores". In: *Chem. Eng. Sci.* 64.5 (Mar. 2009), pp. 870–882. DOI: 10.1016/j.ces.2008.10.045.

[15] Douglas M. Ruthven, W.J. DeSisto, and S. Higgins. "Diffusion in a mesoporous silica membrane - Validity of the Knudsen diffusion model". In: *Chem. Eng. Sci.* 64.13 (July 2009), pp. 3201–3203. DOI: 10.1016/j.ces.2009.03.049.

[16] A. D. Wiheeb et al. "Identification of Molecular Transport Mechanisms in Micro-Porous Hydrotalcite-Silica Membrane". In: *Transp. Porous Media* 104.1 (May 2014), pp. 133–144. DOI: 10.1007/s11242-014-0324-5.

[17] Julia Werner et al. "Production of ceramic membranes with different pore sizes for virus retention". In: *J. Water Process Eng.* 4 (Dec. 2014), pp. 201–211. DOI: 10.1016/j.jwpe.2014.10.007.

[18] Stephen Kroll et al. "High virus retention mediated by zirconia microtubes with tailored porosity". In: *J. Eur. Ceram. Soc.* 32.16 (Dec. 2012), pp. 4111–4120. DOI: 10.1016/j.jeurceramsoc.2012.07.026.

[19] Stephen Kroll et al. "Development and characterisation of functionalised ceramic microtubes for bacteria filtration". In: *J. Membr. Sci.* 365.1-2 (Dec. 2010), pp. 447–455.

[20] Stephen Kroll et al. "Highly efficient enzyme-functionalized porous zirconia microtubes for bacteria filtration". In: *Environ. Sci. Technol.* 46.16 (July 2012), pp. 8739–8747. DOI: 10.1021/es3006496.

[21] Stephen Kroll et al. "Colored ceramic foams with tailored pore size and surface functionalization used as spawning plates for fish breeding". In: *Ceram. Int.* 40.10 (Dec. 2014), pp. 15763–15773. DOI: 10.1016/j.ceramint.2014.07.100.

[22] Thomas Veltzke, Michael Baune, and Jorg Thöming. "The contribution of diffusion to gas microflow - An experimental study". In: *Phys. Fluids* 24.8 (2012), pages. DOI: 10.1063/1.4745004.

[23] T. Veltzke. "On gaseous microflows under isothermal conditions". Dissertation. University of Bremen, 2013.

[24] Martin Knudsen. "The law of the molecular flow and viscosity of gases moving through tubes". In: *Ann. Phys. (Leipzig)* 28 (1909), pp. 75–130.

[25] J. Randon et al. "Study of ZrO_2 Membrane - Aqueous Solutions Interface". In: *Key Eng. Mater.* 61-62 (1992), pp. 495–498. DOI: 10.4028/www.scientific.net/kem.61-62.495.

[26] J. Nawrocki et al. "Chemistry of zirconia and its use in chromatography". In: *J Chromatogr A* 657.2 (Dec. 1993), pp. 229–282.

[27] J. Nawrocki et al. "A TGA investigation of hydrated monoclinic zirconia". English. In: *Anal. Chim. Acta* 327.3 (July 1996), pp. 261–266. DOI: 10.1016/0003-2670(96)00110-9.

[28] A. Marković et al. "Gas permeation through porous glass membranes - Part I. Mesoporous glasses–Effect of pore diameter and surface properties". In: *J. Membr. Sci.* 336.1–2 (2009), pp. 17–31. DOI: 10.1016/j.memsci.2009.02.031.

[29] Decai Yu et al. "Quantum chemistry calculation and experimental study of CO_2/CH_4 and functional group interactions for the design of solubility selective membrane materials". In: *J. Membr. Sci.* 441 (Aug. 2013), pp. 137–147. DOI: 10.1016/j.memsci.2013.03.052.

[30] A. Marković et al. "Gas permeation through porous glass membranes - Part II. Transition regime between Knudsen and configurational diffusion". In: *J. Membr. Sci.* 336.1–2 (2009), pp. 32–41. DOI: http://dx.doi.org/10.1016/j.memsci.2009.02.030.

[31] Arne Lindbråthen and May-Britt Hägg. "Glass membranes for purification of aggressive gases - Part II. Adsorption measurements and diffusion coefficient estimations". In: *J. Membr. Sci.* 259.1-2 (Aug. 2005), pp. 154–160.

[32] Edwin R. Gilliland et al. "Diffusion on surfaces. I. Effect of concentration on the diffusivity of physically adsorbed gases". In: *Ind. Eng. Chem. Fund.* 13.2 (May 1974), pp. 95–100. DOI: 10.1021/i160050a001.

5. The Influence of Temperature on Gas Flow and Selectivity of C_{16}-Functionalized Mesoporous Structures

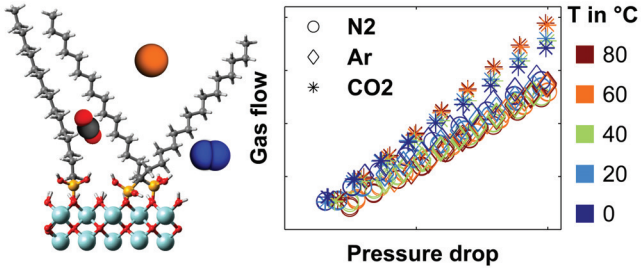

Adapted from:

Applying alkyl-chain surface functionalizations in mesoporous inorganic structures: Their impact on gas flow and selectivity depending on temperature

Published in:

ACS Applied Materials & Interfaces, Received 25.07.2016, Revised 15.09.2016, Accepted 16.09.2016
DOI: 10.1021/acsami.6b09174

Authors:

Benjamin Besser[a], Atiq Ahmed[a], Michael Baune[b], Stephen Kroll[a,c,*], Jorg Thöming[b,c] and Kurosch Rezwan[a,c]

[a] Advanced Ceramics, University of Bremen, Am Biologischen Garten 2, 28359 Bremen, Germany
[b] Center for Environmental Research and Sustainable Technology, University of Bremen, Leobener Strasse 1, 28359 Bremen, Germany
[c] Centre for Materials and Processes (MAPEX), University of Bremen, Bibliothekstraße 1, 28359 Bremen, Germany
[*] Corresponding author. Phone: +49 421 218 64933, E-Mail: Stephen.Kroll@Uni-Bremen.de

Abstract: Porous inorganic capillary membranes are prepared to serve as model structures for the experimental investigation of the gas transport in functionalized mesopores. The porous structures possess a mean pore diameter of 23 nm which is slightly reduced to 20 nm after immobilizing C_{16}-alkyl chains on the surface. Gas permeation measurements are performed at temperatures ranging from 0 to 80 °C using Ar, N_2, and CO_2. Non-functionalized structures feature a gas transport according to Knudsen diffusion with regard to gas flow and selectivity. After C_{16}-functionalization, the gas flow is reduced by a factor of 10, and the ideal selectivities deviate from the Knudsen theory. CO_2 adsorption measurements show a decrease in total amount of adsorbed gas and isosteric heat of adsorption. It is hypothesized that the immobilized C_{16}-chains sterically influence the gas transport behavior without a contribution from adsorption effects. The reduced gas flow derives from an additional surface resistance caused by the C_{16}-chains spacially limiting the adsorption and desorption directions for gas molecules propagating through the structure, resulting in longer diffusion paths. In agreement, the gas flow is found to correlate with the molecular diameter of the gas species (CO_2<Ar<N_2) increasing the resistance for larger molecules. This affects the ideal selectivities with the relation $\frac{N_2}{Ar} < \frac{Ar}{CO_2} < \frac{N_2}{CO_2}$. The influence on selectivity increases with increasing temperature which leads to the conclusion that the temperature induced movement of the C_{16}-chains is responsible for the stronger interaction between gas molecules and surface functional groups.

5.1. Introduction

In many processes and applications, gas molecules interact with a solid surface of a porous material, for example, in catalysis, solid oxide fuel cells, gas chromatography, membrane gas separation, or gas adsorption using solid sorbents.[1–7] While the pore size of the materials can be very different, ranging from several micrometers to nanometers, chemical surface functionalizations are often applied to serve specific purposes. The performance of a process or its characteristics are therefore often defined by gas interactions with functional layers, for example, in gas chromatography columns or at the pore wall of an inorganic membrane. In addition to functional group type, density, and gas species, these interactions strongly depend on temperature.[4,8]

Along with the interaction of the gas molecules with the functional group, various transport mechanisms dominate inside porous structures, depending on the pore size and the Knudsen number (Kn). A very good and well-known example of porous materials where multiple gas transport mechanisms occur simultaneously is asymmetric inorganic membranes. These membranes are usually built up by coating multiple layers of different pore sizes onto a supporting structure. The support structure is usually macroporous (>50 nm, mostly 1-10 μm) and one or two mesoporous intermediate layers (10-50 nm) are coated on top of it before depositing the final micro- or mesoporous top layer with pores < 10 nm.[9,10] The dominating gas transport mechanism within each layer is defined by its structural proportions, resulting in viscous flow in the macroporous support (Kn<1), and Knudsen diffusion in the mesoporous intermediate layers (Kn>1) accompanied by surface diffusion in the top layer (Kn>10).[11–17] The transition between the different transport mechanisms is fluid, but under normal conditions (ambient pressure and room temperature), viscous flow can be neglected in pores smaller than 50 nm and surface diffusion can be neglected in pores larger than 10 nm.

Despite the difference in governing transport mechanism based on the pore size which is in the nanometer range for membranes and in the micrometer range for gas chromatography, the selective properties depend on the surface functionality and the gas-solid interactions on the nanoscale.[18–20] Therefore, the material's surface is often functionalized with numerous types of functional molecules, depending on specific applications.[4,8,21,22] In particular, hydrocarbon functionalizations using reactive silanes are used in both fields of research to tailor the surface chemistry of the solid material. For example, surface functionalizations with alkyl-chains have been successfully applied in chromatographic applications[23] as well as inorganic membrane separation.[24–28] Applying such surface functionalizations, independent of functional group type, often results in a decrease of flux by several orders of magnitude especially determined by membrane separation.[8,21,22,24–27,29–31] This effect is usually explained by the decrease in pore size and porosity due to the functional molecules being immobilized on the pore walls of the membrane although the reduction in pore size and porosity is seldom within the order of magnitude as the decrease in flux. This indicates that the mechanisms between functional group layers and gas molecules which influence the gas flow through the porous material are not fully understood yet.

Especially in membrane science using asymmetric membranes consisting of pore sizes over several length scales, multiple transport mechanisms occur at the same time. Accordingly, asymmetric membranes are not ideally suitable to analyze gas transport phenomena depending on surface functionality as well as pore size, because it is difficult to allocate single gas transport characteristics. For a fundamental understanding about the interaction of gas molecules with functional layers, it is important to study the gas transport mechanisms separately for each length scale.

This study aims to investigate the impact of surface functional layers on the gas diffusion in mesopores where Knudsen diffusion dominates the gas transport (10-50 nm). The focus of this study is solely the experimental determination of the gas transport with high accuracy, without the development of analytical or semiempirical models. For this purpose, mesoporous structures are prepared in form of capillary membranes by an extrusion process using yttria stabilized zirconia (YSZ) nanoparticles. These membranes serve as model structures which are functionalized with an alkyl-silane showing a C_{16}-chain as functional group (hexadecyltrimethoxysilane, HDTMS). Both, the non-functionalized and the C_{16}-functionalized structures are characterized with focus on pore size, porosity and specific surface area. To experimentally analyze the con-

tribution of the immobilized C_{16}-chains on the gas flow, single gas permeation measurements are carried out at temperatures varying from 0 to 80 °C (i.e. 0, 20, 40, 60, 80 °C) using argon (Ar), nitrogen (N_2) and carbon dioxide (CO_2). Additionally, CO_2 adsorption isotherms are measured at the same temperature variations to determine the influence of the surface functionalization on gas adsorption.

5.2. Experimental Section

5.2.1. Materials

All materials were obtained from commercial sources and used as received. Yttria (3 mol%) stabilized zirconia nanopowder (YSZ, VP Zirkonoxid 3-YSZ, Lot. 3157061469) was obtained from Evonik Industries, Germany. For slurry preparation, 3-aminopropyltriethoxysilane (APTES, ≥98 %, product number A3648, Lot. WXBB5181V) as dispersant and poly(vinyl alcohol) (PVA, fully hydrolyzed, product number P1763, Lot. SLBD2875V) as binder were obtained from Sigma-Aldrich Chemie GmbH, Germany. Furthermore, for surface activation with Piranha solution, sulfuric acid (H_2SO_4, 95-97 %, product number 30743, Lot SZBF0330V) and hydrogen peroxide ((H_2O_2, ≥35 %, product number 95299, Lot SZBE2740V) were provided from Sigma-Aldrich Chemie GmbH, Germany. Hexadecyltrimethoxysilane (HDTMS, 90 %, product number AB111166, Lot. 1010563) was purchased from ABCR, Germany, for surface functionalization. Acetone (≥99 %, product number 00585, Lot. STBF6910V) obtained from VWR International, Belgium, and double deionized water with an electrical resistance of 18 MΩ (Synergy®, Millipore, Germany) were used for all experiments.

5.2.2. Processing and Functionalization

Membrane Preparation

Mesoporous structures are prepared using an extrusion process as described in our previous studies.[32,33] In short, four reagents are used for the water-based slurry: Double deionized water (21 wt.%) as solvent, the YSZ nanopowder (79 wt.%, primary particle size 30 nm) as ceramic raw material, APTES as dispersant (5 dwb.%), and PVA as binder (6 dwb.%). The additive contents are given in dwb which refers to "dry weight basis" of the YSZ nanopowder in relation to dwb.%≡ $m_{\text{additive}}/m_{\text{powder}} \cdot 100$. First, PVA is slowly dissolved in hot water (≈80 °C) using a microwave (MD14482 Studio, Medion, Germany). Afterward, all ingredients are mixed in a planetary ball mill (PM400 from Retsch, Germany) for 3 h at 350 rpm changing the rotation direction every 5 min. The homogeneous slurry is then shaped by extrusion into capillaries using a die of 2 mm diameter and a pin of 1 mm.[34] The resulting green bodies are dried at room temperature for at least two days before final sintering for 2 h at 1050 °C (the detailed sintering program is given in[35]).

Surface Functionalization

The material functionalization is performed by a hydrolysis-condensation reaction of HDTMS molecules onto the activated solid surface.[36] First, the surface is activated by acidic hydroxylation with freshly prepared Piranha solution (95-97 % H_2SO_4:35 % H_2O_2, 3:1, v/v, 30 min) followed by washing with double deionized water until neutral pH is reached and drying at 70 °C (30 h). For the drying process, the membranes are placed in an open glass Petri dish which is put into a drying oven. For the functionalization process it is of high importance that the membranes are completely dry before continuing with the surface functionalization. Second, the functionalization is carried out by incubating the activated membranes for 16 h in a boiling 0.2 M HDTMS solution using an acetone-water mixture (95:5, v/v) as solvent, operating under reflux. Finally, the samples are washed with acetone and dried for 2 h at 70 °C.

5.2.3. Membrane Characterization

Structural Characterization

The mesoporous structures are characterized in terms of pore size distribution, open porosity, and specific surface area. The structural analysis is carried out using mercury intrusion porosimetry, as well as nitrogen adsorption. Pore size distribution, mean pore diameter (d_{50}), and open porosity are determined using a Mercury Porosimeter Pascal 140 and 440 (POROTEC GmbH, Germany). Furthermore, pore size distribution, mean pore diameter, total pore volume, open porosity, and specific surface area are additionally determined by nitrogen adsorption at -196 °C using a BELSORP-mini II (Bel Japan Inc., Japan) following the BET-method[37] for the determination of the specific surface area and the BJH-method[38] for mesopore

analysis. The samples are degassed at 120 °C for at least 3 h under reduced pressure (≤2 Pa) followed by cooling to room temperature (RT) under argon atmosphere prior to the measurements.

CO_2 Adsorption Measurements

CO_2 adsorption measurements are performed under isothermal conditions similar to the gas permeation measurements, using temperatures between 0 and 80 °C. The measurements are perfomed with a Belsorp-Max (Bel Japan Inc., Japan) using about 0.6 g of material. Prior to the measurements, the samples are pretreated by degassing for at least 3 h at 120 °C and reduced pressure (≤2 Pa), followed by cooling to RT under argon atmosphere (≥30 min). After CO_2 adsorption measurements, the specific surface area is determined by nitrogen adsorption at -196 °C according to the BET method[37] using the same measurement device. The obtained adsorption capacities are normalized to the measured specific surface area and calculated to μmol/m^2. The measurement data is presented as an isotherm, as well as as isobar. For the latter, the values around 80 kPa are extracted from the measurement data, where all values are within 80.1±0.04 kPa.
To calculate adsorption enthalpies, temperature and pressure relations which yield the same surface coverage (θ) are extracted from the measurement data. This relation is analyzed for different adsorbed amounts to stress the reliability and representatively shown for a coverage of θ=0.5 μmol/m^2. Linear regression in between the two nearest points is used to interpolate the pressure for a constant θ. The isosteric heat of adsorption (ΔH_{ads}) is then calculated by applying the Clausius-Clapeyron equation as stated in equation 5.1.[39]

$$\left(\frac{\partial \ln p}{\partial \frac{1}{T}}\right)_{\theta=const.} = \frac{\Delta H_{ads}}{R} \qquad (5.1)$$

Single Gas Permeation Measurements

Gas permeation measurements are carried out under different isothermal conditions with the temperature varying between 0 and 80 °C. Table 5.1 shows the technical specifications of the used sensors and controllers of the measurements system. Due to the pressure sensors temperature limitations, the system performance is limited to measurements in the range of -20 to 80 °C. The chosen mass flow sensor (F-110C, Bronckhorst) uses a thermal mass flow measuring principle, where the gas is heated at two different points and its temperature is measured at the same time. The mass flow is then directly proportional to the temperature difference at both points. This measurement principle requires that environment, gas stream and sensor possess the same temperature. Consequently, the temperature of the gas needs to be adjusted after leaving the measurement system before entering the mass flow sensor. Therefore, the measurement system is modified compared to our previous study[40] by introducing a heat-exchanger as shown in Fig. 5.1. Prior to integrating the heat exchanger into the measurement setup, measurements are performed on a rectangular microchannel with uniform cross section (20 μm high, 100 μm wide, 30 mm long) at 20 °C using Ar, N_2 and CO_2. Similar measurements are performed after adapting the measurement system with temperatures varying from -20 to 80 °C for validation. All results are analyzed and found to be reproducible and in good agreement with the Navier-Stokes equation

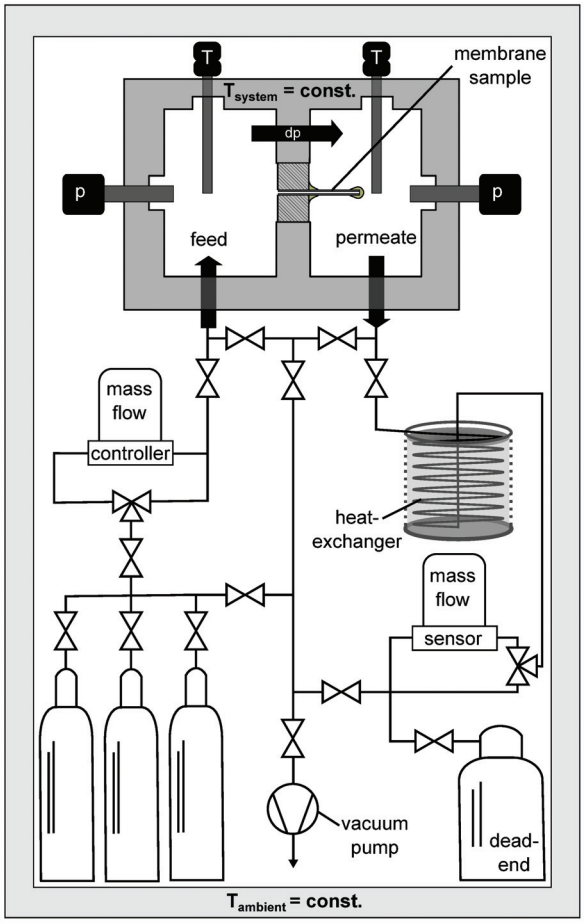

Figure 5.1.: Schematic overview of the experimental setup for single gas permeation measurements operating in dead-end mode.

Table 5.1.: Technical specifications of the measurement equipment used in the gas permeation measurements. All values are manufacturer information.

Device	Name, Manufacturer	Measurement range	Accuracy	Operating temperature
Mass flow controller	F-201CV, Bronckhorst	2.1 - 20.8·10^{-8} kg/s	±0.5 %	-10 - 70 °C
Mass flow sensor	F-110C, Bronckhorst	3.0 - 150.9·10^{-10} kg/s	±0.8 %	-10 - 70 °C
Pressure sensor	PMP4070, GE Sensing	0.1 - 160 kPa	±0.04 %	-20 - 80 °C
Temperature sensor	TF35-PT1000, WIKA	-50 - 300 °C	-	-50 - 300 °C

(data not shown).[41] However, the measurements performed at -20 °C (only) show that the pressure difference slightly oscillates around its set point during the measurements which results in slightly higher standard deviations. The reason for this derives from the automatic mass flow controller which settings are not suitable to operate at conditions where the controlled gas volume is reduced to a great extent within the measurement chamber. Therefore, only measurements from 0 to 80 °C are performed to ensure the highest possible accuracy and precision.

The single gas permeation measurements are performed in dead-end mode with ceramic capillary membranes using three different gases, namely, argon (Ar), nitrogen (N_2), and carbon dioxide (CO_2).[31] The dead-end volume is significantly larger than the total volume of the measurement setup such that nonstationary effects can be considered negligible. For all measurements the steady state flow is measured at nine different pressure drops with a dead-end pressure of 80 kPa. All measurements are performed m=3 times with n=3 individual samples. Prior to measurement, the samples are heated for 3 h at 120 °C to desorb moisture. To ensure purity of the gas during measurement, the whole system is evacuated and purged three times with the ongoing test gas before flushing the membrane for 60 s with a pressure drop of 160 kPa.

The gas permeation measurement results are analyzed on the basis of the law of Knudsen flow, described by equation 5.2.

$$\frac{\dot{n}_i}{A} = \frac{4\epsilon d_{Pore}}{3\kappa\sqrt{2\pi RTM_i}}\frac{\Delta p_i}{\delta}. \tag{5.2}$$

Here, the molar flow $\dot{n}_{i,j}$ is directly proportional to the applied pressure drop Δp_i and depends on material properties represented by porosity (ϵ), pore diameter (d_{Pore}) and the tortuosity factor (κ) as well as the membrane area (A) and thickness (δ). Here, the tortuosity factor κ relates the effective average path length (l_{eff}) of a molecule propagating through the porous medium to the actual length of the porous medium l and should be distinguished from the tortuosity according to $\kappa = \tau^2 = \left(\frac{l_{eff}}{l}\right)^2$.[42] Furthermore, the gas state is described by the universal gas constant (R), temperature (T), and molar mass (M_i). It should be pointed out, that in this study the Knudsen theory is only used for interpretation of the measurement results. The theory serves as an indicator for the mass transport kinetics and it is used to explain effects caused by a C_{16} surface functionalization on the gas flow based on known relations. To analyze the difference in gas transport kinetics caused by the surface functional groups, the gas flow rate and pressure drop are recalculated to dimensionless terms using the Knudsen relation and the maximum applied pressure drop according to equation 5.3.

$$\frac{3\delta\dot{n}_i\sqrt{2\pi RTM_i}}{4A\epsilon d_{Pore}}\frac{1}{p_{i,max}} = \frac{1}{\tau^2}\frac{\Delta p_i}{p_{i,max}}. \tag{5.3}$$

Here, the porosity (ϵ) and pore diameter (d_{Pore}) are obtained from Hg porosimetry and temperature (T), molar flow ($\dot{n}_i$) as well as pressure (p_i) are measured during the gas permeation measurements. The membrane dimensions such as wall thickness and membrane area are determined by optical microscopy. The inner (d_{inner}) and the outer (d_{outer}) diameter are measured using a digital microscope (VHX-600DSO, Keyence, Japan) in eight different directions at the membrane cross section, and the mean thickness ($\delta = \frac{d_{outer}-d_{inner}}{2}$) is calculated using the mean inner and outer diameters. The active membrane area is determined using the mean outer diameter and the average length l of the capillary membranes, according to $A = \pi d_{outer} l$. For this, the membrane length is measured from four sides using a micrometer table (Plμ 2300, Sensofar technology, Spain).

Linear regression of the molar flow rates against the pressure drop is used to calculate ideal selectivities $\alpha_{i,j}$ of gases i and j according to equa-

tion 5.4.

$$\alpha_{i,j} = \frac{(\partial \dot{n}/\partial p)_i}{(\partial \dot{n}/\partial p)_j}. \tag{5.4}$$

With the assumption of constant temperature and pressure as well as similar gas and membrane properties in equation 5.2, theoretical selectivities can be calculated according to equation 5.5. The so called Knudsen selectivities are used as reference.

$$\alpha_{Kn,ij} = \sqrt{\frac{M_j}{M_i}}. \tag{5.5}$$

5.3. Results

5.3.1. Structural Characterization

Ceramic capillary membranes serving as mesoporous model structures are prepared by extrusion. After sintering, the porous material is functionalized with silane molecules possessing a C_{16} alkyl-chain as functional group (HDTMS). Fig. 5.2A exemplary shows two nitrogen adsorption/desorption isotherms obtained before and after functionalization. Both, the non-functionalized and the C_{16}-functionalized structures show similar adsorption/desorption isotherms with a hysteresis loop which can be classified as Type IV according to IUPAC classification.[43] The total pore volume of the membranes is reduced by a factor of 0.42 due to the functionalization with C_{16} alkyl-chains and the adsorption isotherm is not as steep at lower relative pressures, indicating a smaller specific surface area. Part B of Fig. 5.2 shows the incremental pore volume for different pore diameters according to the Barrett–Joyner–Hallenda (BJH) model.[38] Again, both curves possess a similar shape, characterized by a monomodal pore size distribution with a maximum between 20 and 30 nm. The peak of the incremental pore volume is slightly shifted to smaller pore sizes for the C_{16}-functionalized membranes.

Table 5.2 summarizes the results for different structural parameters obtained from three individual nitrogen adsorptions as well as Hg-porosimetry. Both measurement techniques show similar results regarding mean pore diameter and open porosity. As indicated in Fig. 5.2A, the nitrogen adsorption/desorption measurements reveal a significant decrease in specific surface area (factor 0.44) as well as open porosity (factor 0.31) for the C_{16}-functionalized structures. This decrease

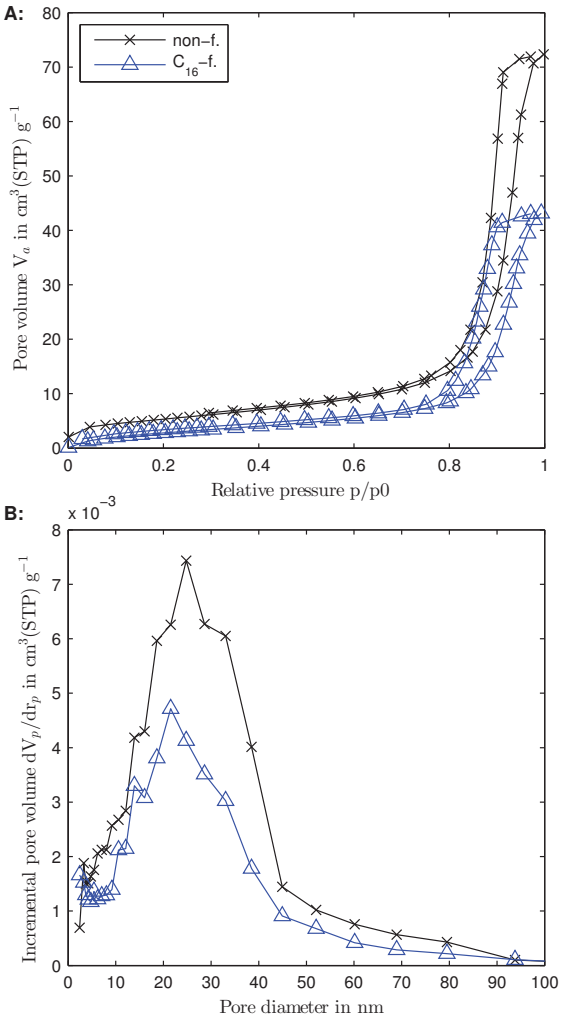

Figure 5.2.: Nitrogen adsorption/desorption isotherms (A) and pore size distribution according to Barrett–Joyner–Hallenda model (B) for a non-functionalized and a C_{16}-functionalized membrane.

is consistent with the decrease in open porosity determined by Hg intrusion porosimetry measurements (factor 0.31). The mean pore diameter (BJH-method) of 25.4 nm decreases only slightly by 3.8 nm to 21.5 nm due to the immobilized C_{16}-chains, which is in good agreement with the results obtained from Hg-porosimetry. Furthermore, the calculated mesopore volume (BJH-method) is nearly identical compared to the obtained total pore volume which reflects a pore structure exclusively consisting of mesopores. This is also consistent with the results derived from Hg-porosimetry measurements showing no incremental volume for larger pores between 35 nm and 120 μm. Furthermore, scanning electron microscopy images from the cross section of the capillaries show a highly homogeneous pore network over the whole wall thickness (data not shown).

Table 5.2.: Structural properties of the non-functionalized and C_{16}-functionalized membranes measured by nitrogen adsorption and Hg-porosimetry.

Nitrogen adsorption	Non-f.	C_{16}-f.	Unit
Specific surface area (BET)	20.0±1.4	11.2±1.2	$m^2\ g^{-1}$
Total pore volume	0.109±0.007	0.063±0.006	$cm^3\ g^{-1}$
Open porosity	38.2±1.4	26.5±2.0	%
Mesopore volume (BJH)	0.106±0.005	0.064±0.006	$cm^3\ g^{-1}$
Mean pore diameter (BJH)	25.37±1.61	21.53±0.01	nm
Hg-porosimetry	Non-f.	C_{16}-f.	Unit
Mean pore diameter	23.2±1.1	19.9±0.1	nm
Open porosity	39.3±2.4	27.0±1.7	%

5.3.2. CO_2 Adsorption Measurements

Part A of Fig. 5.3 shows two exemplary CO_2 adsorption isotherms at 0 and 80 °C for the non- and C_{16}-functionalized structures. In general, the total amount of adsorbed CO_2 per solid surface area is higher for a non-functionalized than for a C_{16}-functionalized membrane in relation to all measured temperatures and pressures. The obtained adsorption isotherms for non-functionalized membranes in between 0 and 80 °C can be described by Freundlich-type isotherms. In contrast, the C_{16}-functionalized structures present adsorption isotherms which only show a non-linear behavior according to Freundlich at low temperatures (0 and 20 °C). At higher temperatures (40 up to 80 °C) the adsorption isotherms show a linear behavior similar to Henry-type isotherms. Part B of Fig. 5.3 presents the adsorbed amount of CO_2 for different temperatures at a constant pressure of 80 kPa, which is equal to the dead-end pressure used in the gas permeation measurements (see section 5.3.3). Here, a reduction of adsorbed molecules with increasing temperature is determined, whereas the adsorbed amount of CO_2 molecules is smaller for the C_{16}-functionalized membranes compared to the non-functionalized samples.

Fig. 5.4 shows the isosteric pressure as a function of temperature. Applying the Clausius-Clapeyron equation according to equation 5.1 leads to the isosteric heat of adsorption of $-\Delta H_{non-f.}$ =28.1 kJ mol^{-1} and $-\Delta H_{C16-f.}$ =9.4 kJ mol^{-1} for non-functionalized and C_{16}-functionalized membranes, respectively. Therefore, a surface functionalization with C_{16}-alkyl chains reduces the isosteric heat of adsorption of CO_2 and the total amount of adsorbed CO_2 molecules per membrane surface area.

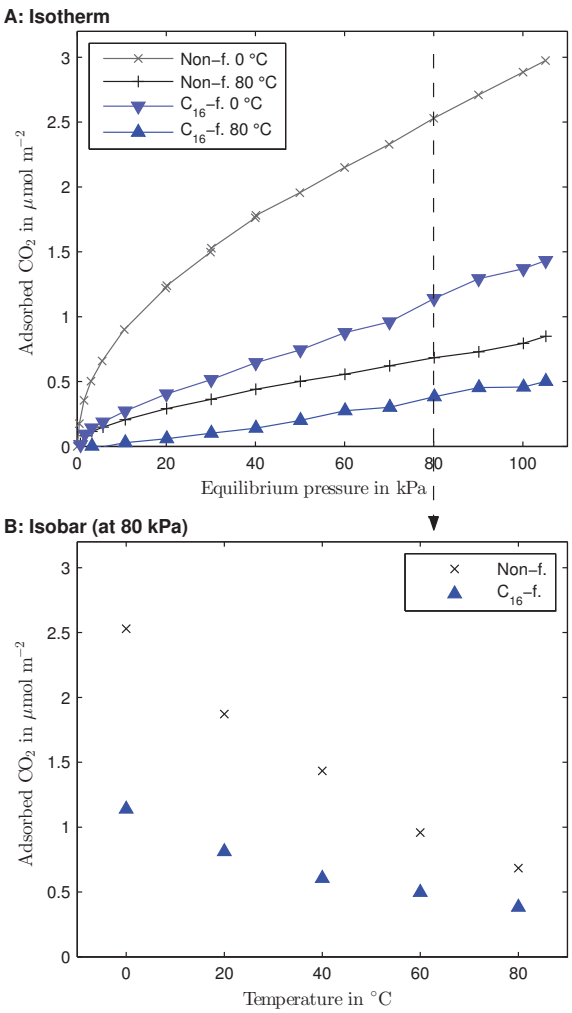

Figure 5.3.: CO_2 adsorption isotherms at 0 and 80 °C for non-functionalized and C_{16}-functionalized membranes (A). Adsorbed amount of CO_2 at 80 kPa for different temperatures (B). The measured adsorbed amount of CO_2 is normalized to the specific surface area of the individual membrane samples and given in μmol/m^2.

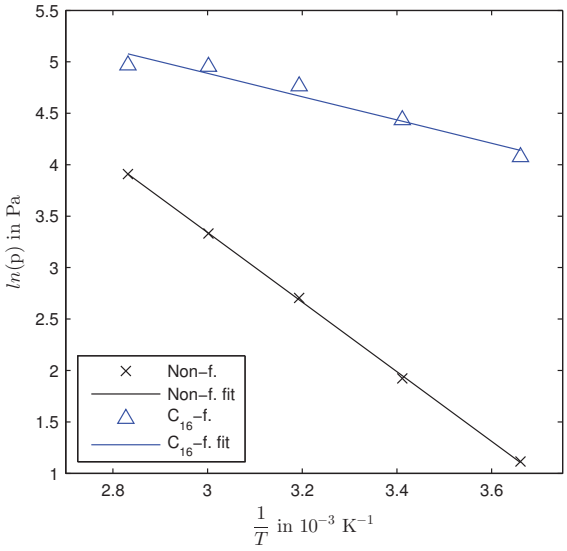

Figure 5.4.: Isosteric pressure of CO_2 as a function of temperature.

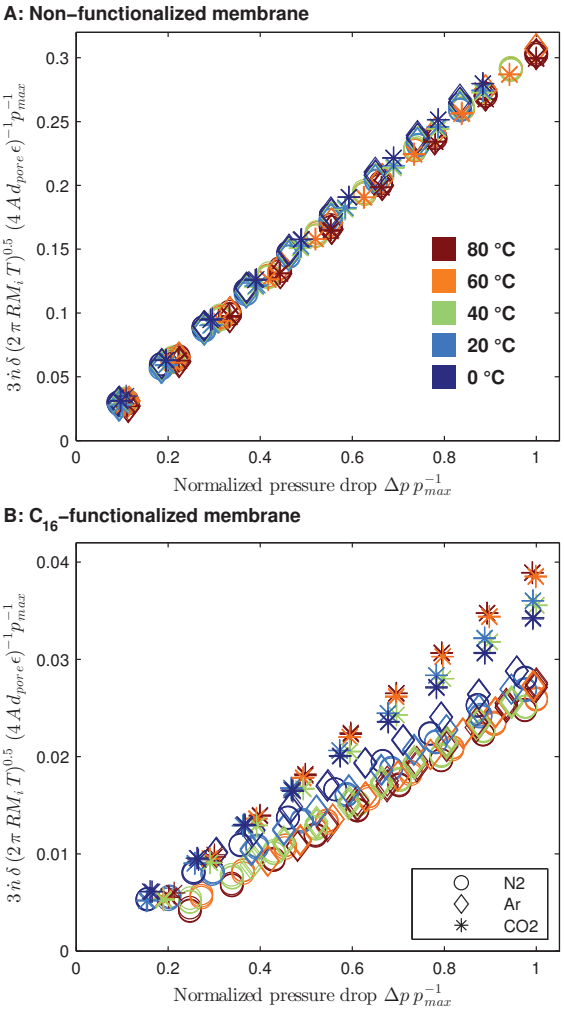

Figure 5.5.: Measured gas flow normalized by membrane and gas parameters versus normalized pressure drop for a non-functionalized (A) and a C_{16}-functionalized membrane (B).

5.3.3. Single Gas Permeation Measurements

Fig. 5.5 shows three consecutive measurements for each gas type (Ar, N_2 and CO_2) and temperature varying between 0 and 80 °C. The measured gas flow through the membranes is normalized according to equation 5.3 and are exemplary shown for a non-functionalized (A) and a C_{16}-functionalized structure (B). Non-functionalized membranes produce a linear flow behavior depending on the pressure drop (part A of Fig. 5.5). After normalizing with gas and structural parameters (except tortuosity) according to Knudsen theory, the gas flow is independent of gas species or temperature. Part B of Fig. 5.5 shows the same gas flow versus pressure relation for a C_{16}-functionalized membrane. Here, the dimensionless gas flow depends on gas species as well as on temperature. In general, the dimensionless gas flow is one order of magnitude lower than for non-functionalized structures. Additionally, CO_2 shows a higher gas flow which is further increased with increasing temperature, whereas the gas flow of Ar and N_2 is decreasing with increasing temperature.
According to equation 5.4, Fig. 5.6 shows the ideal selectivities of three different gas pairs, namely N_2/Ar (part A), Ar/CO_2 (part B) and N_2/CO_2 (part C), for different temperatures ranging from 0 to 80 °C. For each membrane type and temperature, three consecutive measurements for each gas species are performed on three individual samples and the results are given in mean value and standard deviation. It should be mentioned that the presented standard deviations are mostly induced by sample variation due to preparation and functionalization. The relative deviations caused by the measurement system are <0.37 % and <0.72 % for all non-functionalized and C_{16}-functionalized membranes, respectively. The horizontal dashed lines represent the Knudsen selectivities according to $\alpha_{Kn,ij} = \sqrt{\frac{M_j}{M_i}}$. In general, non-functionalized structures show a good agreement with the Knudsen theory, independent of temperature or gas species. C_{16}-functionalized samples present selectivities deviating from Knudsen theory. This deviation depends on gas species as well as on temperature. Part A of Fig. 5.6 presents the ideal selectivities of N_2/Ar. At low temperatures of 0 °C the deviation is

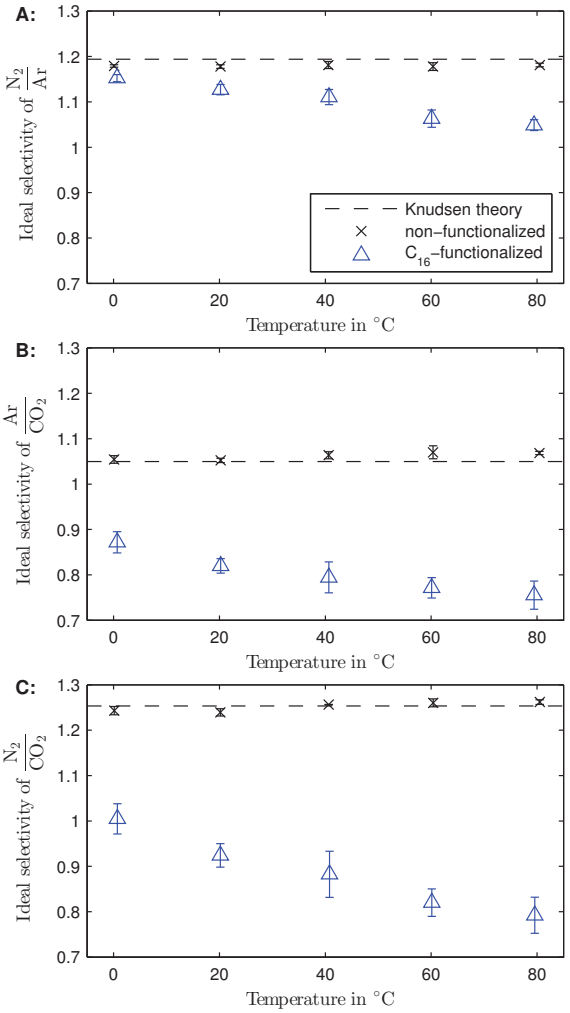

Figure 5.6.: Ideal selectivities of N_2/Ar (A), Ar/CO_2 (B) and N_2/CO_2 (C) for non-functionalized and C_{16}-functionalized membranes. The dashed black line represents the Knudsen selectivity proposed by the Knudsen theory.

small and the selectivity approaches theoretical Knudsen values. For higher temperatures from 20 to 80 °C, the ideal selectivities tend to drop slightly to smaller values following a linear trend. Fig. 5.6B and C show a similar trend for the ideal selectivities of Ar/CO_2 and N_2/CO_2, respectively. In contrast to the selectivities for N_2/Ar, the deviation from Knudsen theory are higher for both gas pairs, where the highest deviation is determined for N_2/CO_2.

5.4. Discussion

5.4.1. Structural Material Properties and CO_2 Adsorption

Before and after functionalization with C_{16}-chains, structural analyses are carried out using nitrogen adsorption and Hg-porosimetry. Both measurement principles reveal similar results with respect to mean pore diameter and open porosity. Both methods show a decrease in pore diameter of 3.3 nm (Hg-porosimetry) and 3.9 nm (BJH-method), respectively. Considering the length of a HDTMS molecule of around 2 nm, this indicates the formation of a homogeneous monolayer of the silane molecules on the pore walls. The decrease in pore diameter determined by Hg-porosimetry is slightly smaller compared to the results from nitrogen adsorption. Here, the functionalized layer is probably compressed due to high applied pressures, resulting in slightly larger pore diameters.
To analyze the impact of the C_{16}-surface functionalization on the gas-solid interaction, CO_2 adsorption measurements are carried out. The results reveal a significantly smaller amount of gas molecules adsorbed on C_{16}-functionalized surfaces than on an untreated oxidic surface combined with a decreased isosteric heat of adsorption. For the physisorption of CO_2, the interaction of the electric quadrupole moment and the electric field gradient often dominates the interactions of CO_2 with the solid surface.[44] An oxidic surface is naturally carrying polar hydroxyl-groups. Due to its high quadrupole moment, CO_2 is more attracted to polar groups, and therefore, the amount as well as the heat of adsorption is smaller on a C_{16}-functionalized, apolar surface.[45]

5.4.2. Gas Transport

To analyze the influence of a C_{16}-functionalized surface on the gas transport kinetics in mesopores, single gas permeation measurements are carried out. The measurements reveal a linear dependency between gas flow and pressure drop which suggests Knudsen diffusion as predominant transport mechanism without the contribution of viscous flow (see Fig. 5.5). For non-functionalized mesoporous structures, applying the Knudsen relation (see equation 5.3) reveals good agreement with the theory especially showing dimensionless values independent of temperature and molar mass of the gas. In contrast, this general relation seems

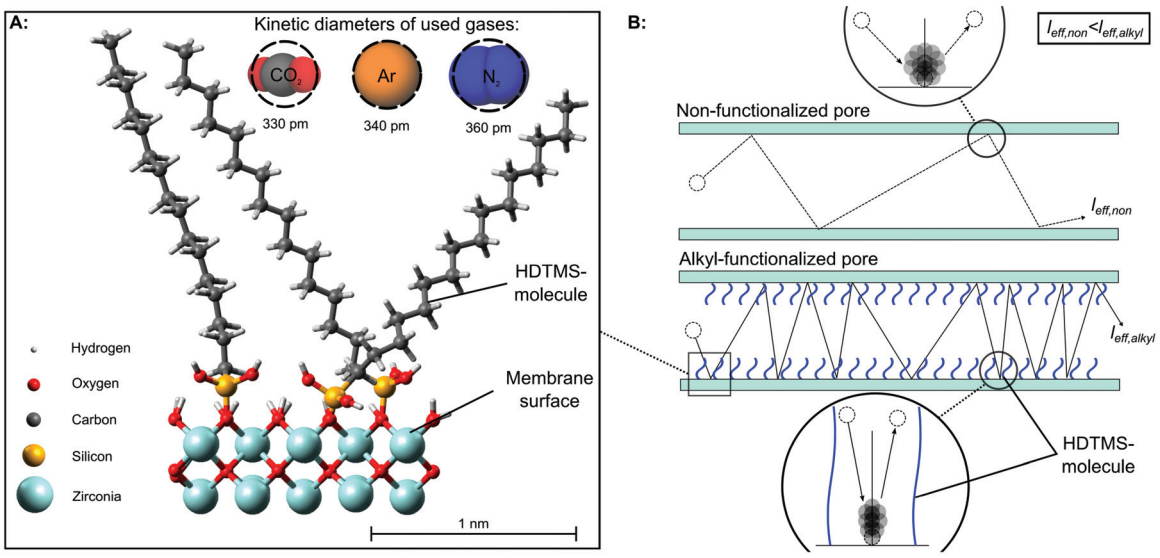

Figure 5.7.: Schematic drawing of the membrane surface functionalized with HDTMS molecules representing a concentration of 3 molecules per nm^2 as determined in[31] (A). In addition, the kinetic diameters of Ar, N_2 and CO_2 obtained from Breck[51] are indicated as dashed circles. Schematic illustration of a gas molecule propagating through pores without and with an C_{16}-chain functionalization (B).

to be rendered inapplicable when C_{16}-chains are immobilized on the material surface. The C_{16}-functionalized membranes show a gas flow behavior which does not follow the Knudsen proportionality of $\sqrt{TM_i}$. Especially noticeable are the different temperature relations depending on gas type, where the flow of CO_2 increases with increasing temperature while the flows of Ar and N_2 decrease. In addition, the gas flow of all gases is decreased by a factor of 10. The decrease in permeability due to surface functionalizations is already known from the literature[8,21,22,24–27,30,46] and is usually explained by the decrease in porosity and pore diameter. As a matter of fact, this cannot be stated as a reason here, because both parameters are used to normalize the flow presented in Fig. 5.5 (see equation 5.3). The Knudsen theory describes the porous structure as a resistance to the gas flow defined by the parameters tortuosity (τ), porosity (ϵ), and pore size (d_{pore}). Being aware of the variety of proposed tortuosity relations[47–50] also dependent on porosity, the measurement results lead to the conclusion that there is an additional resistance linked to the surface functionalization. Apparently, this surface resistance is negligible at "smooth" surfaces without an additional surface functionalization but affects the gas flow when the surface topography is "rough" after immobilizing functional groups (C_{16}-chains) on the surface.

Fig. 5.7A shows a schematic drawing of 1x1 nm^2 membrane surface area with an estimated amount of 3 HDTMS-molecules (C_{16}-chains) as determined in our previous study.[31] In this schematic drawing the kinetic diameters of CO_2, Ar and N_2 are indicated in the same size ratio. Because of the high Knudsen number at pore sizes of around 20 nm (Kn>3) the gas molecules constantly "collide" with the pore walls which can be more accurately described as an adsorption and desorption process which is schematically illustrated in Fig. 5.7B. On a non-functionalized, "smooth" pore surface a molecule desorption will result in a "diffuse" reflection from the pore wall in random directions with the probability proportional to the angle relative to the surface normal vector.[52] Assuming that the gas molecules are able to penetrate into the functionalized silane layer towards the membrane surface until they adsorb, the diffusive desorption direction will be limited by the long C_{16}-chains and therefore the average desorption angle will be smaller. A smaller desorption angle will lead to longer molecule trajectory (higher l_{eff}), because a gas molecule has to collide with the pore walls more often on its way through the pore. This, in turn, will result in a reduced gas flow.

A limited desorption angle is one possible explanation for the determined reduced gas flow. Moreover, the C_{16}-chains cause a reduction in flow for all investigated gases, but affect each of the gas species individually which leads to changes in the selectivities (see Fig. 5.6). The effect of the surface functionalization on the selectivities increases with increasing temperature, always showing the

same relation $\frac{N_2}{Ar} < \frac{Ar}{CO_2} < \frac{N_2}{CO_2}$. In particular the effect on the ideal selectivity of $\frac{N_2}{Ar}$ is counterintuitive, because both gas species are mostly considered to be inert. Accordingly, it is assumed that adsorption effects of Ar and N_2 are negligible. The gases still differ in kinetic diameter as indicated in Fig. 5.7 with N_2 possessing a larger kinetic diameter (360 pm) than Ar (340 pm) and CO_2 (330 pm). In addition, due to the functional group density on the surface, the distance between the C_{16}-chains is within the order of magnitude of the gas molecules. One possible explanation for the effect on the selectivity with the relation $\frac{N_2}{Ar} < \frac{Ar}{CO_2} < \frac{N_2}{CO_2}$ is the different kinetic diameter of the gases being CO_2<Ar<N_2. Assuming that the molecules are able to penetrate into the functional layer, the small distance between the C_{16}-chains may lead to an effect similar to molecular sieving where larger molecules are retained to a greater extent than smaller molecules. This, in turn, will lead to an effect on the gas flows decreasing in the following order N_2<Ar<CO_2 and with the observed selectivity relations (see Fig. 5.5 and Fig. 5.6). Of course, the selectivities of $\frac{N_2}{CO_2}$ and $\frac{Ar}{CO_2}$ (Fig. 5.4B,C) show a much higher deviation from Knudsen theory which does not seem to correlate with the kinetic diameters. Moreover, the decrease with increasing temperature seems to be not as linear as for $\frac{N_2}{Ar}$. A possible explanation for this is the linear shape of the CO_2 molecule. Yu et al.[45] showed that CO_2 will orient with its longitudinal axis parallel to a C_{16}-chain for a minimal energy configuration. This will lead to a significantly smaller effective diameter of CO_2 and can explain the comparably larger deviations. Nevertheless, the dimensionless flow of CO_2 increases with increasing temperature, whereas the flow of Ar and N_2 decrease (see Fig. 5.5B). This suggests that the mechanisms involved affect CO_2 differently from Ar and N_2 or that there is an additional effect on the flow of CO_2. The most obvious transport mechanism, surface diffusion, seems to be most unlikely in this case. Alkyl-functionalizations are known to facilitate surface diffusion of apolar gases such as hydrocarbons with little effect on polar gas species such as CO_2.[25,26,53] Furthermore, the CO_2 adsorption measurements performed in this study show a significant decrease in the adsorbed amount of molecules on C_{16}-functionalized structures. For enhancement of surface diffusion, an increase in adsorbed amount is usually the aim.[8] For these reasons, surface diffusion seems to be unlikely, although, the reduced heat of adsorption (from 28.1 to 9.4 kJ mol^{-1}) indicates an increased mobility of the CO_2 molecules within the C_{16}-chain layer.

Fig. 5.6 shows, that the effect of the surface functionalization on all selectivities increases with increasing temperature. With the assumption that the molecules are able to penetrate into the layer of C_{16}-chains, two explanations are possible. First, the temperature dependency of this effect can derive from the increase in molecular speed of the gas molecules with increasing temperature. With a higher velocity the gas molecules may be able to penetrate deeper into the functionalization layer, consequently increasing the interaction between the functional layer and the gas molecules. Second, the long C_{16}-chains on the membrane surface will constantly be in motion as long as the temperature exceeds the "freezing point" of the C_{16}-chain layer. The C_{16}-chains will not be static as maybe suggested by Fig. 5.6, but under real conditions they will be in motion swinging constantly back and forth. The kinetic energy of the C_{16}-chains will depend on the temperature, thus, defining "frequency" and "amplitude", when expressed as a periodic form of motion. Accordingly, there will not be a constant distance between the C_{16}-chains, but an apparent distance which most likely depends on the kinetic energy and therefore on temperature. The kinetic energy and the apparent distance of the C_{16}-chains will have an effect on the interaction between gas molecules and the functional alkyl-layer which is increased with increasing temperature. While it is possible, that both scenarios occur simultaneously, the temperature induced movement of the functional layer will have a significant impact on the gas transport of molecules trapped between the C_{16}-chains. Nevertheless, both proposed explanations will lead to circumstances, where the C_{16}-chain layer will slow down the movement of the gas molecules depending on their size.

This fundamental study is based on experimental results obtained from single gas permeation measurements, and ideal selectivities are discussed. Therefore, the results can only be partly adapted to mixed gas systems because the diffusion mechanisms are more complex, featuring interactions between the gas molecules of the moving phase in combination with gas molecule-wall interactions. The conclusions drawn here should be used to shed light on the interactions of single gas species

with a chemical functional layer to provide a basis for the understanding of more complex processes. Bearing this in mind, it seems that the "functional molecule of choice" for a specific application does not solely depend on its functional group type but also on its size. For example, with the aim of enhancing the surface selective flow for a gas separation membrane, the functional molecules should be as small as possible whereas a gas chromatography application may benefit from long functional molecules, maximizing the retention effect.

5.5. Conclusion

Mesoporous inorganic membranes are prepared as model structures to investigate the influence of a surface functionalization consisting of C_{16}-chains on the gas flow behavior of Ar, N_2 and CO_2 under different temperatures ranging from 0 to 80 °C. The ceramic capillary membranes made of YSZ possess a monomodal pore size distribution with a mean pore diameter of 23.2 nm which is decreased only slightly to 19.9 nm due to the immobilized C_{16}-chains on the pore walls (Hg-porosimetry). The isosteric heat of adsorption as well as the total amount of adsorbed CO_2 molecules is significantly decreased by the apolar surface functionalization which leads to the conclusion that adsorption effects cannot be responsible for the influence on molecular diffusion. Single gas permeation measurements carried out in dead-end mode at temperatures ranging from 0 to 80 °C suggest that steric effects are responsible for the deviations observed in gas flow and selectivity. All investigated membranes without a surface functionalization show ideal Knudsen diffusion behavior following the laws for Knudsen flow and selectivity. C_{16}-functionalized membranes reveal results which are neither in agreement with the flow relations proposed by the Knudsen theory, nor with the Knudsen selectivity. After all measured and known gas and membrane properties (except the tortuosity) are taken into account, gas flow and pressure show a relation which deviates 1 order of magnitude from the Knudsen theory. It is proposed that the altered surface topography due to the functionalization causes an additional surface resistance. The C_{16}-chains immobilized on the surface limit the adsorption/desorption directions of gas molecules to a certain extent. This leads to longer diffusion paths of the gas molecules which, in turn, result in a reduced gas flow. Furthermore, the ideal selectivities of $\frac{N_2}{Ar}$, $\frac{Ar}{CO_2}$, and $\frac{N_2}{CO_2}$ tend to decrease with increasing temperature. The effect on selectivity ($\frac{N_2}{Ar} < \frac{Ar}{CO_2} < \frac{N_2}{CO_2}$) tends to correlate with the kinetic diameters of the gas species with the relation of CO_2<Ar<N_2. The distance of the C_{16}-chains is within the order of magnitude of the kinetic diameters of the gas molecules. It is proposed that the short distances between the C_{16}-chains cause an effect similar to molecular sieving in which molecules with a larger diameter are retained to a greater extent than smaller molecules. This effect enhances with increasing temperature due to the temperature induced movement of the C_{16}-chains.
In summary, the presented results lead to the conclusion that, besides the purpose of adsorption, gas diffusion can significantly be influenced by surface functionalizations in terms of steric effects. This knowledge can be adapted to other fields of research where the effects can contribute, for example, for the development of inorganic gas separation membranes or gas chromatographic applications.

Acknowledgments

This work was supported by the German Research Foundation (DFG) within the Research Training Group GRK 1860 "Micro-, meso- and macroporous nonmetallic Materials: Fundamentals and Applications" (MIMENIMA). The support of J. Bartels from the University of Bremen for the fruitful discussions and the critical feedback which helped to improve this work is gratefully acknowledged. Furthermore, we thank T. Kühn from the University of Bremen for all the support in the laboratory.

References

[1] Marc-Olivier Coppens. "A nature-inspired approach to reactor and catalysis engineering". In: *Curr. Opin. Chem. Eng.* 1.3 (Aug. 2012), pp. 281–289. DOI: 10.1016/j.coche.2012.03.002.

[2] Weidong He, Weiqiang Lv, and James H. Dickerson. *Gas Transport in Solid Oxide Fuel Cells*. SpringerBriefs in Energy. Springer International Publishing, 2014, pp. 9–17. DOI: 10.1007/978-3-319-09737-4_2.

[3] Jason Baxter et al. "Nanoscale design to enable the revolution in renewable energy". In: *Energy Environ. Sci.* 2 (6 2009), pp. 559–588. DOI: 10.1039/B821698C.

[4] V.G. Berezkin and J. de Zeeuw. *Capillary Gas Adsorption Chromatography*. Hüthig Heidelberg, 1996.

[5] Dennis Y.C. Leung, Giorgio Caramanna, and M. Mercedes Maroto-Valer. "An overview of current status of carbon dioxide capture and storage technologies". In: *Renewable Sustainable Energy Rev.* 39 (Nov. 2014), pp. 426–443. DOI: 10.1016/j.rser.2014.07.093.

[6] Matthew E. Boot-Handford et al. "Carbon capture and storage update". In: *Energy Environ. Sci.* 7 (1 2014), pp. 130–189. DOI: 10.1039/C3EE42350F.

[7] Benjamin Besser et al. "Hierarchical Porous Zeolite Structures for Pressure Swing Adsorption Applications". In: *ACS Appl. Mater. Interfaces* 8.5 (Feb. 2016), pp. 3277–3286. DOI: 10.1021/acsami.5b11120.

[8] Daniel Stoltenberg and Andreas Seidel-Morgenstern. "An attempt to alter the gas separation of mesoporous glass membranes by amine modification". In: *Microporous Mesoporous Mater.* 154 (May 2012), pp. 148–152. DOI: 10.1016/j.micromeso.2011.11.013.

[9] Ahmad F Ismail, Kailash C Khulbe, and Takeshi Matsuura. *Gas Separation Membranes - Polymeric and Inorganic*. Springer International Publishing, 2015. DOI: 10.1007/978-3-319-01095-3.

[10] H. Verweij. "Ceramic membranes - Morphology and transport". In: *J. Mater. Sci.* 38.23 (2003), pp. 4677–4695. DOI: 10.1023/A:1027410616041.

[11] Andreas Seidel-Morgenstern. *Membrane Reactors*. Ed. by Andreas Seidel-Morgenstern. Wiley-VCH, 2010.

[12] Douglas M. Ruthven, W.J. DeSisto, and S. Higgins. "Diffusion in a mesoporous silica membrane - Validity of the Knudsen diffusion model". In: *Chem. Eng. Sci.* 64.13 (July 2009), pp. 3201–3203. DOI: 10.1016/j.ces.2009.03.049.

[13] R. Krishna and J.M. van Baten. "An investigation of the characteristics of Maxwell-Stefan diffusivities of binary mixtures in silica nanopores". In: *Chem. Eng. Sci.* 64.5 (Mar. 2009), pp. 870–882. DOI: 10.1016/j.ces.2008.10.045.

[14] W. V. Chiu et al. "Post-synthesis defect abatement of inorganic membranes for gas separation". In: *J. Membr. Sci.* 377.1-2 (July 2011), pp. 182–190. DOI: 10.1016/j.memsci.2011.04.047.

[15] H.A. Meinema et al. "Ceramic Membranes for Gas Separation - Recent Developments and State of the Art". In: *Interceram* 54 (2005), pp. 86–91.

[16] William J Koros and Rajiv Mahajan. "Pushing the limits on possibilities for large scale gas separation - which strategies?" In: *J. Membr. Sci.* 175.2 (Aug. 2000), pp. 181–196. DOI: 10.1016/S0376-7388(00)00418-X.

[17] A. D. Wiheeb et al. "Identification of Molecular Transport Mechanisms in Micro-Porous Hydrotalcite-Silica Membrane". In: *Transp. Porous Media* 104.1 (May 2014), pp. 133–144. DOI: 10.1007/s11242-014-0324-5.

[18] Yunzhong Zheng, Meiling Qi, and Ruonong Fu. "Graphitic carbon nitride as high-resolution stationary phase for gas chromatographic separations". In: *J. Chromatogr. A* 1454 (July 2016), pp. 107–113.

[19] Yuan Zhang et al. "Current status and development of membranes for CO2/CH4 Separation - A review". In: *Int. J. Greenhouse Gas Control* 12 (Jan. 2013), pp. 84–107. DOI: 10.1016/j.ijggc.2012.10.009.

[20] J.K. Adewole et al. "Current challenges in membrane separation of CO2 from natural gas - A review". In: *Int. J. Greenhouse Gas Control* 17 (Sept. 2013), pp. 46–65. DOI: 10.1016/j.ijggc.2013.04.012.

[21] Shunsuke Suzuki et al. "Development of inorganic-organic hybrid membranes for carbon dioxide/methane separation". In: *J. Membr. Sci.* 471 (Dec. 2014), pp. 402–411.

[22] Christian Leger, Helio De L. Lira, and Russell Paterson. "Preparation and properties of surface modified ceramic membranes. Part III. Gas permeation of 5 nm alumina membranes modified by trichloro-

octadecylsilane". In: *J. Membr. Sci.* 120.2 (Nov. 1996), pp. 187–195.

[23] Dong Wang et al. "Highly Stable Surface Functionalization of Microgas Chromatography Columns Using Layer-by-Layer Self-Assembly of Silica Nanoparticles". In: *Anal. Chem.* 85.17 (Sept. 2013), pp. 8135–8141. DOI: 10.1021/ac401080u.

[24] Asad Javaid et al. "Solubility-based gas separation with oligomer-modified inorganic membranes". In: *J. Membr. Sci.* 187.1-2 (June 2001), pp. 141–150.

[25] Rajinder P. Singh, J. Douglas Way, and Steven F. Dec. "Silane modified inorganic membranes - Effects of silane surface structure". In: *J. Membr. Sci.* 259.1-2 (Aug. 2005), pp. 34–46. DOI: 10.1016/j.memsci.2005.03.004.

[26] K Kuraoka, Y Chujo, and T Yazawa. "Hydrocarbon separation via porous glass membranes surface-modified using organosilane compounds". In: *J. Membr. Sci.* 182.1-2 (Feb. 2001), pp. 139–149. DOI: 10.1016/S0376-7388(00)00559-7.

[27] Arne Lindbråthen and May-Britt Hägg. "Glass membranes for purification of aggressive gases - Part II. Adsorption measurements and diffusion coefficient estimations". In: *J. Membr. Sci.* 259.1-2 (Aug. 2005), pp. 154–160.

[28] Arne Lindbråthen and May-Britt Hägg. "Membrane separation of chlorine gas". In: *Chem. Eng. Process.* 48.1 (Jan. 2009), pp. 1–16.

[29] Arne Lindbråthen and May-Britt Hägg. "Glass membranes for purification of aggressive gases - Part I. Permeability and stability". In: *J. Membr. Sci.* 259.1–2 (2005), pp. 145–153. DOI: http://dx.doi.org/10.1016/j.memsci.2005.03.056.

[30] Yuzuru Sakamoto et al. "Preparation and CO_2 separation properties of amine-modified mesoporous silica membranes". In: *Microporous Mesoporous Mater.* 101.1-2 (Apr. 2007), pp. 303–311. DOI: 10.1016/j.micromeso.2006.11.007.

[31] Benjamin Besser et al. "A comparative experimental study on the deviation of the ideal selectivity in HDTMS-functionalized and untreated ceramic structures with pores in the upper mesoporous range". In: *Microporous Mesoporous Mater.* 217 (Nov. 2015), pp. 253–261.

[32] Julia Werner et al. "Production of ceramic membranes with different pore sizes for virus retention". In: *J. Water Process Eng.* 4 (Dec. 2014), pp. 201–211. DOI: 10.1016/j.jwpe.2014.10.007.

[33] Julia Bartels et al. "Amino-functionalized ceramic capillary membranes for controlled virus retention". In: *Environ. Sci. Technol.* 50.4 (Jan. 2016), pp. 1973–1981. DOI: 10.1021/acs.est.5b05124.

[34] Stephen Kroll et al. "High virus retention mediated by zirconia microtubes with tailored porosity". In: *J. Eur. Ceram. Soc.* 32.16 (Dec. 2012), pp. 4111–4120. DOI: 10.1016/j.jeurceramsoc.2012.07.026.

[35] Stephen Kroll et al. "Development and characterisation of functionalised ceramic microtubes for bacteria filtration". In: *J. Membr. Sci.* 365.1-2 (Dec. 2010), pp. 447–455.

[36] Stephen Kroll et al. "Highly efficient enzyme-functionalized porous zirconia microtubes for bacteria filtration". In: *Environ. Sci. Technol.* 46.16 (July 2012), pp. 8739–8747. DOI: 10.1021/es3006496.

[37] Stephen Brunauer, P. H. Emmett, and Edward Teller. "Adsorption of Gases in Multimolecular Layers". In: *J. Am. Chem. Soc.* 60.2 (Feb. 1938), pp. 309–319. DOI: 10.1021/ja01269a023.

[38] Elliott P. Barrett, Leslie G. Joyner, and Paul P. Halenda. "The Determination of Pore Volume and Area Distributions in Porous Substances. I. Computations from Nitrogen Isotherms". In: *J. Am. Chem. Soc.* 73.1 (Jan. 1951), pp. 373–380. DOI: 10.1021/ja01145a126.

[39] Oliver L. I. Brown. "The Clausius-Clapeyron equation". In: *J. Chem. Educ.* 28.8 (Aug. 1951), p. 428. DOI: 10.1021/ed028p428.

[40] Thomas Veltzke, Michael Baune, and Jorg Thöming. "The contribution of diffusion to gas microflow - An experimental study". In: *Phys. Fluids* 24.8 (2012), pages. DOI: 10.1063/1.4745004.

[41] R.B. Bird, W.E. Stewart, and E.N. Lightfoot. *Transport Phenomena*. Wiley International edition. Wiley, 2007.

[42] N. Epstein. "On tortuosity and the toruosity factor in flow and diffusion through porous media". In: *Chem. Eng. Sci.* 44.3 (1989), pp. 777–779.

[43] S. W. Sing K. "Reporting physisorption data for gas/solid systems with special reference to the determination of surface area and porosity". In: *Pure Appl Chem* 54.11 (1982), pp. 2201–2218. DOI: doi:10.1351/pac198254112201.

[44] Niklas Hedin et al. "Adsorbents for the post-combustion capture of CO2 using rapid temperature swing or vacuum swing adsorption". In: *Appl. Energy* 104 (Apr. 2013), pp. 418–433.

[45] Decai Yu et al. "Quantum chemistry calculation and experimental study of CO_2/CH_4 and functional group interactions for the design of solubility selective membrane materials". In: *J. Membr. Sci.* 441 (Aug. 2013), pp. 137–147. DOI: 10.1016/j.memsci.2013.03.052.

[46] Souha Belhaj Messaoud et al. "Alkylamine–silica hybrid membranes for carbon dioxide/methane separation". In: *J. Membr. Sci.* 477 (2015), pp. 161–171. DOI: http://dx.doi.org/10.1016/j.memsci.2014.12.022.

[47] Xuechao Gao, João C. Diniz da Costa, and Suresh K. Bhatia. "Understanding the diffusional tortuosity of porous materials - An effective medium theory perspective". In: *Chem. Eng. Sci.* 110 (May 2014), pp. 55–71. DOI: 10.1016/j.ces.2013.09.050.

[48] Lihua Shen and Zhangxin Chen. "Critical review of the impact of tortuosity on diffusion". In: *Chem. Eng. Sci.* 62.14 (July 2007), pp. 3748–3755.

[49] Suresh K. Bhatia and David Nicholson. "Comments on "Diffusion in a mesoporous silica membrane - validity of the knudsen diffusion model", by ruthven, d.m., et al., chem. eng. sci. 64 (2009) 3201-3203". In: *Chem. Eng. Sci.* 65.15 (Aug. 2010), pp. 4519–4520.

[50] Suresh K. Bhatia and David Nicholson. "Some pitfalls in the use of the Knudsen equation in modelling diffusion in nanoporous materials". In: *Chem. Eng. Sci.* 66.3 (2011), pp. 284–293.

[51] D.W. Breck. "Crystalline Molecular Sieves". In: *J. Chem. Educ.* (1964), pp. 678–689.

[52] Jichang Liu and James Wei. "Knudsen diffusion in channels and networks". In: *Chem. Eng. Sci.* 111 (May 2014), pp. 1–14.

[53] Scott Higgins, William DeSisto, and Douglas Ruthven. "Diffusive transport through mesoporous silica membranes". In: *Microporous Mesoporous Mater.* 117.1-2 (Jan. 2009), pp. 268–277. DOI: 10.1016/j.micromeso.2008.06.030.

6. The Influence of the C_{16}-Chain Density on Gas Flow and Selectivity of Mesoporous Structures

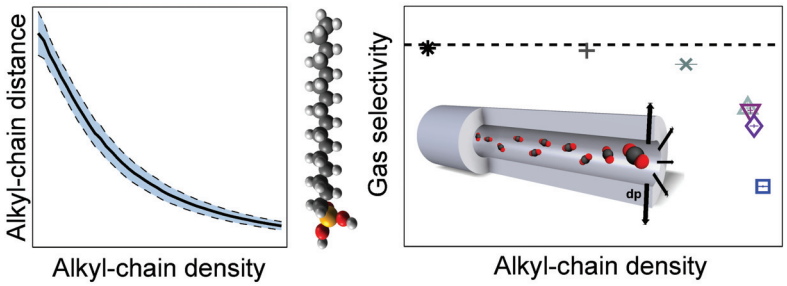

Adapted from:

The influence of the functional group density on gas flow and selectivity: Nanoscale interactions in alkyl-functionalized mesoporous membranes

Published in:

Microporous and Mesoporous Materials, Received 29.07.2016, Revised 02.09.2016, Accepted 14.09.2016
DOI: 10.1016/j.micromeso.2016.09.026

Authors:

Benjamin Besser[a], Saad Malik[a], Michael Baune[b], Stephen Kroll[a,c,*], Jorg Thöming[b,c] and Kurosch Rezwan[a,c]

[a] Advanced Ceramics, University of Bremen, Am Biologischen Garten 2, 28359 Bremen, Germany
[b] Center for Environmental Research and Sustainable Technology, University of Bremen, Leobener Strasse 1, 28359 Bremen, Germany
[c] Centre for Materials and Processes (MAPEX), University of Bremen, Bibliothekstraße 1, 28359 Bremen, Germany
[*] Corresponding author. Phone: +49 421 218 64933, E-Mail: Stephen.Kroll@Uni-Bremen.de

Abstract: Mesoporous inorganic structures with mean pore diameters of 26 nm are prepared by extrusion based on a yttria stabilized zirconia nanopowder. The sintered capillary membranes serve as model structures to investigate the influence of an alkyl-chain (C_{16}) surface functionalization on the gas diffusion kinetics of argon (Ar), nitrogen (N_2) and carbon dioxide (CO_2) in mesopores. The density of the C_{16} alkyl-chains immobilized on the membrane surface has an effect on both, gas flow as well as gas selectivity. For low functional group densities ($<4\,\text{groups}\,\text{nm}^{-2}$), the gas flow is reduced without having an effect on the selectivity. In contrast, for high alkyl-chain densities ($>4\,\text{groups}\,\text{nm}^{-2}$) the mean distance between the C_{16}-chains is reduced to the order of magnitude of the gas molecules leading to a reduction in gas flow and a significant change of the gas selectivity. The selectivity is found to be influenced depending on the molecular diameter of the gas species, being more evident for CO_2 compared to Ar and N_2, suggesting a separation mechanism more comparable to molecular sieving than to surface diffusion.

6.1. Introduction

Gas-solid interactions within porous materials are important for many processes and applications such as solid oxide fuel cells, catalysis, gas chromatography, gas separation or gas adsorption on solid sorbents.[1–7] The pore size of the material can be very different ranging from several micrometers to nanometers. Nevertheless, the performance of a process and its characteristics are often defined or driven by nanoscale interactions of gas molecules with the solid material surface, for example in the capillary of a gas chromatography column or at the pore walls of an inorganic membrane.

Depending on the pore size and the Knudsen number (Kn), various transport mechanisms dominate inside the porous structures. Asymmetric inorganic membranes are a very good and well known example of porous materials where different transport mechanisms can occur simultaneously. They usually consist of a macroporous support structure (>50 nm, usually 1-10 μm), one or two mesoporous intermediate layers (10-50 nm) and a micro- or mesoporous top layer with pores < 10 nm.[8,9] Determined by the structural proportions, the gas transport is dominated by viscous flow in the macropores of the support structure (Kn<1), Knudsen diffusion in mesoporous intermediate layers (Kn>1), and surface diffusion or molecular sieving in the top layer (Kn>10).[10–16] The transitions between the transport mechanisms are fluid, but under ambient pressure and room temperature (RT) viscous flow can be neglected in pores <50 nm and surface diffusion is negligible in pores >10 nm.

In particular in gas chromatography as well as in membrane separation based on surface selective flow, the gas-wall interactions define the properties of the material.[17–19] Despite the difference in pore dimensions which are in the micrometer range for chromatography columns and in the nanometer range for membranes, in both cases the selective properties depend on the surface functionality. Therefore, different surface functionalization strategies with numerous functional groups are used to alter the surface chemistry and influence the gas-solid interactions.[4,20–22] For example, alkyl-functionalizations have been successfully applied in both, chromatographic applications[23] as well as membrane separation.[24–28]

Especially in membrane separation, it is often observed that the membrane flux is reduced by several orders of magnitude as a result of the surface functionalization, independent of functional group type.[20–22,24–30] Usually this is explained by the reduction in pore size and porosity due to the functional groups immobilized on the pore walls. Surprisingly, the decrease in pore size and porosity is seldom in the order of magnitude of the decrease in flux. This indicates that the full impact of surface functionalizations on the gas flow through a porous material has not been completely understood yet.

Asymmetric membranes are often used for the investigation of surface functionalizations and their impact on gas flow properties. But, the total gas flow of the membrane will be a superposition of multiple transport phenomena, because they consist of multiple layers with pore sizes over several length scales. For this reason, asymmetric membranes are not the most favorable structures for the analysis of transport phenomena depending on surface functionality as well as pore size. To achieve fundamental understanding about nanoscale interactions of gas molecules with functional layers and their relations to pore size and porosity, the gas transport mechanisms need to be studied separately for each length scale.

This study aims to experimentally investigate the impact of the surface functional group density on the gas diffusion dynamics in mesopores between 10 and 50 nm, where Knudsen diffusion is dominating. The study is focused on the experimental determination of the gas transport with high accuracy, without the development of analytical or semi-empirical gas transport models. For this purpose, mesoporous ceramic capillary membranes are prepared by an extrusion process using yttria stabilized zirconia nanopowder. These membranes serve as model structures which are functionalized in a second step with varying amounts of an alkyl-silane showing a C_{16}-chain as functional group (hexadecyltrimethoxysilane, HDTMS). All membranes are characterized concerning their pore size, open porosity, specific surface area and alkyl-chain density on the surface. Single gas permeation measurements using argon (Ar), nitrogen (N_2) and carbon dioxide (CO_2) are performed to investigate the impact of the functional group density on the gas diffusion kinetics within the mesoporous structures.

6.2. Experimental

6.2.1. Materials

The mesoporous ceramic structures are fabricated using a yttria (3 mol%) stabilized zirconia nanopowder (YSZ, primary particle size 30 nm, VP Zirkonoxid 3-YSZ, Lot. 3157061469) purchased from Evonik Industries, Germany. 3-aminopropyltriethoxysilane (APTES, ≥98 %, A3648, Lot. WXBB5181V) and polyvinyl alcohol (PVA, fully hydrolyzed, P1763, Lot. SLBD2875V), used as additives, are obtained from Sigma-Aldrich Chemie GmbH, Germany. For the surface functionalization, sulfuric acid (H_2SO_4, 95-97 %, 30743, Lot SZBF0330V) as well as hydrogen peroxide (H_2O_2, ≥35 %, 95299, Lot SZBE2740V) are provided from Sigma-Aldrich Chemie GmbH, Germany, whereas acetone (≥99 %, 20063.365, Lot. 16E041994) is obtained from VWR International, Belgium, and hexadecyltrimethoxysilane (HDTMS, 90 %, AB111166, Lot. 1270013) is purchased from ABCR, Germany. For all experiments, double deionized water with an electrical resistance of 18 MΩ (Synergy®, Millipore, Germany) is used. All materials are used as received and without further purification.

6.2.2. Processing and Functionalization

Membrane Preparation

Mesoporous membrane model structures are prepared based on an established extrusion process.[31,32] In short, using water as solvent (21 wt.%), the YSZ nanopowder (79 wt.%) is mixed with APTES (5 dwb.%) serving as dispersant as well as sintering additive and PVA (6 dwb.%) serving as temporary binder. All ingredients are mixed and homogenized using a planetary ball mill (PM400 from Retsch, Germany). Prior to milling, the PVA is dissolved in hot water (≈80 °C) using a microwave (MD14482 Studio, Medion, Germany) to ensure a homogeneous slurry and avoid membrane defects due to PVA granules. The preparation process is schematically shown in Fig. 6.1A. After mixing, the homogeneous slurry is shaped into capillaries using a self-made lab extruder with a 2 mm die and a 1 mm pin.[33] After drying the green bodies for 2 days at room temperature, the membranes are finally sintered for 2 h at 1050 °C (the sintering program is given in[34]).

Surface Functionalization

To alter the surface chemistry of the membrane, the surface is functionalized with HDTMS (C_{16}-chain) molecules based on a wet chemical functionalization process.[35] The process consists of the surface activation by acidic hydroxylation followed by a chemical functionalization using the silane HDTMS as indicated in Fig 6.1B. The surface activation is carried out by immersing the membranes into freshly prepared Piranha solution (95-97 % H_2SO_4:35 % H_2O_2, 3:1, v/v). After 30 min of incubation the membranes are washed with double deionized water until reaching neutral pH and subsequently dried at 70 °C for 30 h. For the drying process, the membranes are placed in an open glass petri dish which is finally put into a drying oven. It should be pointed out at this point, that it is of high importance for the functionalization process that all membranes are completely dry before continuing with the surface silanization. After successful drying of the membranes, the membranes are immersed into a HDTMS solution with an acetone-water mixture (95:5, v/v) as solvent. The surface functionalization is carried out by boiling under reflux for 16 h aiming at monolayer formation of HDTMS molecules. In this study, the HDTMS concentration of the solution is varied from 0.01 to 0.2 M to adjust the loading capacitiy of immobilized alkl-chains on the surface. Finally, the membranes are washed with acetone and dried for 2 h at 70 °C. The samples are named according to the HDTMS concentration of the stock solution used as subscript, namely $M_{0.01}$, $M_{0.05}$, $M_{0.1}$, $M_{0.125}$, $M_{0.15}$ and $M_{0.2}$, samples without a surface functionalization are named $M_{non-f.}$.

6.2.3. Membrane Characterization

Structural Characterization

Nitrogen adsorption/desorption measurements as well as thermogravimetric analysis (TGA) are carried out to obtain information about the porous membrane structure (i.e. pore size distribution, pore volume and porosity) and the functional group density of immobilized alkyl-chains per membrane surface area as schematically shown in Fig. 6.1C. Nitrogen adsorption measurements are performed at -196 °C using a BELSORP-mini II (Bel Japan Inc., Japan). Prior to the measurement, the samples are degassed at 120 °C for at least 3 h under reduced pressure (≤2 Pa) followed

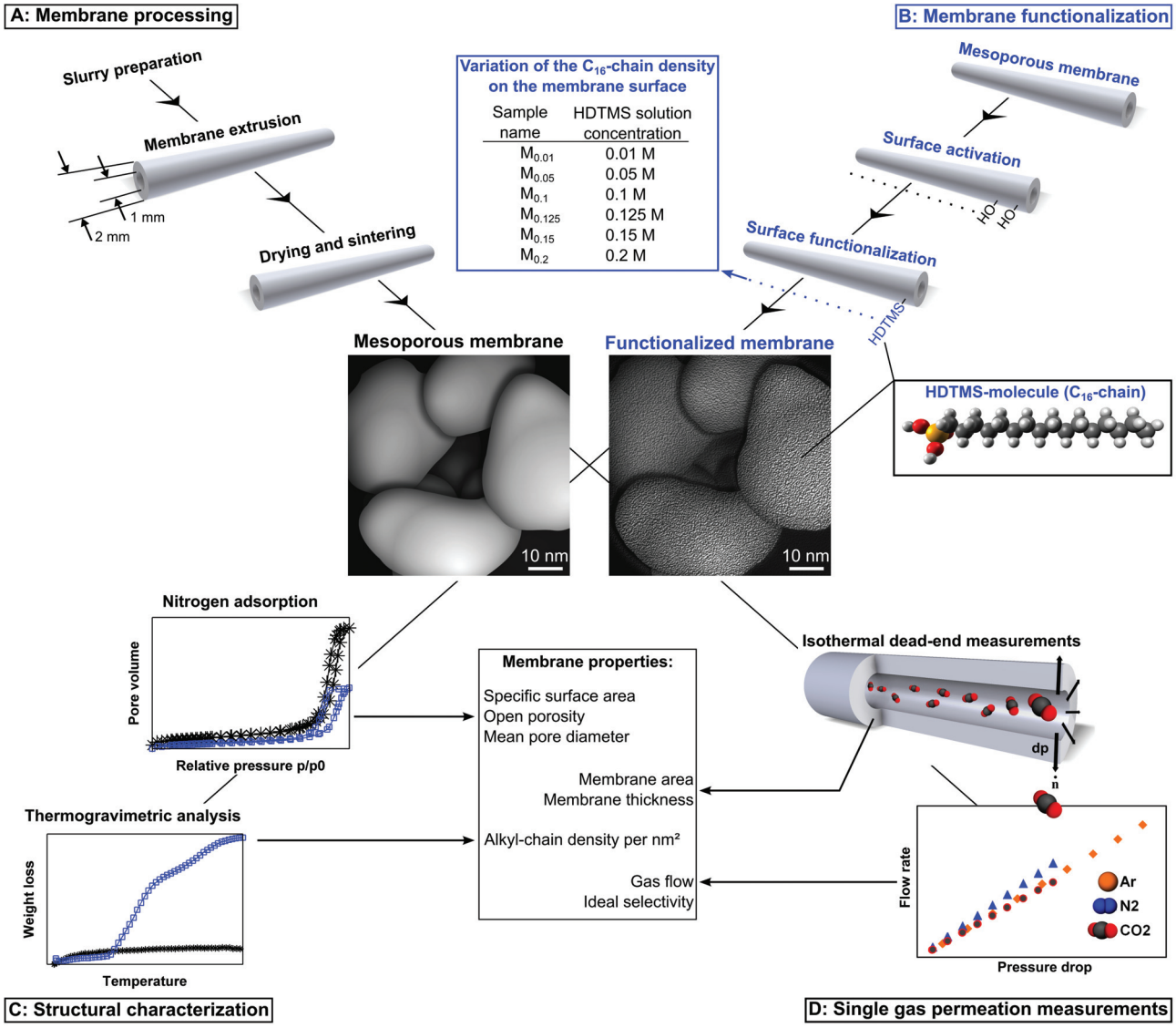

Figure 6.1.: Schematical overview over membrane preparation (A), membrane functionalization (B), structural characterization (C) and gas permeation measurements (D). The pictures of the membrane structures are modeled based on transmission electron microscopy images of the YSZ powder.

by cooling to RT under argon atmosphere. Based on the adsorption isotherms, the mesopore size distribution and mean pore diameter are determined according to the BJH-method.[36] Furthermore, the specific surface area is calculated according to BET-method[37] and the open porosity is obtained based on the true density determined by helium pycnometry (Pycnomatic ATC, Porotec, Germany). All measurements are performed three times to ensure reproducibility.

The amount of alkyl-chains on the surface is characterized by TGA as well as differential thermal analysis (DTA) using a STA503 (Bähr-Thermoanalyse GmbH, Germany). Between 70 and 100 mg of membrane sample is placed in a crucible and heated from 20 to 900 °C with a heating rate of 10 °C min^{-1} operating in air with a constant air flow rate of 10 L min^{-1}. All measurements are performed three times to ensure reproducibility. The quantitative analysis of the measurement data is performed similar to our previous study.[30] In short, it is assumed that the weight loss below 200 °C is predominantly caused by water desorption and the weight loss above 600 °C is not caused by organic decomposition. Therefore, the weight loss between 200 and 600 °C is taken into account to calculate the amount of immobilized alkyl-chains. For reference, the average weight loss of non-functionalized membranes between 200 and 600 °C is used. Furthermore, the final results are correlated with the specific surface area determined by nitrogen adsorption and the molecular mass of the organic compounds of an HDTMS molecule (ideally) covalently bound

to the surface ($229.5\,\mathrm{g\,mol^{-1}}$). The resulting values given in the number of alkyl-chains per membrane surface area are presented in groups $\mathrm{nm^{-2}}$ and further referred to as functional group density or alkyl(C_{16})-chain density.

Single Gas Permeation Measurements

Gas permeation measurements are performed to investigate the influence of the functional group density on the gas transport of the mesoporous structures analyzed in terms of gas flow and selectivity as indicated in Fig. 6.1D. Single gases, namely argon (Ar), nitrogen (N_2) and carbon dioxide (CO_2) are used with the system operating in dead-end mode.[30,38] The temperature is kept constant at 20 °C and the applied dead-end pressure is 80 kPa. In general, the dead-end pressure remains constant over the measurement time and non-stationary effects are considered negligible due to the very large dead-end volume compared to the total volume of the measurement system. Before integrating the membranes into the measurement system, they are heated for 3 h at 120 °C to desorb moisture. To ensure a high purity of the gas phase within the measurement system, the whole system is washed three times with the ongoing gas species by reducing the pressure to around 0.3 kPa and refilling to 160 kPa. Prior to measurement, the membrane sample is flushed with the used test gas for 1 min with a pressure difference of around 160 kPa. The measurements are performed by measuring the gas flow rate over nine different pressure drops applied over the membrane. After reaching steady state conditions, gas flow, pressure and temperature are averaged over 120 s. Each measurement is performed three times to ensure reproducibility.

The results of the gas permeation measurements are analyzed in terms of ideal selectivity and gas flow in comparison to the Knudsen theory. Ideal selectivities $\alpha_{i,j}$ of gas i and j are obtained by linear regression of the flow rates against the pressure drop according to equation 6.1.

$$\alpha_{i,j} = \frac{(\partial \dot{n}/\partial p)_i}{(\partial \dot{n}/\partial p)_j}. \tag{6.1}$$

According to the Knudsen theory, the molar flow $\dot{n}_{i,j}$ through a porous media with porosity ϵ, pore diameter d_{Pore} and tortuosity τ is directly proportional to the pressure drop Δp_i of a gas i possessing the molar mass M_i at a given temperature T (see equation 6.2).

$$\frac{\dot{n}_i}{A} = \frac{4\epsilon d_{Pore}}{3\tau^2\sqrt{2\pi RTM_i}}\frac{\Delta p_i}{\delta}. \tag{6.2}$$

Here, R is the universal gas constant and A and δ represent membrane area and thickness, respectively. Following this equation and assuming constant temperature and pressure as well as similar gas and membrane properties, theoretical selectivities can be calculated as shown in equation 6.3. These so called Knudsen selectivities are used as reference.

$$\alpha_{Kn,ij} = \sqrt{\frac{M_j}{M_i}}. \tag{6.3}$$

To analyze the gas flow of membranes possessing different densities of alkyl-chains, gas flow rate and pressure drop are recalculated to dimensionless terms using the relation for the Knudsen flow and the maximum applied pressure as given in equation 6.4.

$$\frac{3\delta\dot{n}_i\sqrt{2\pi RTM_i}}{4A\epsilon d_{Pore}}\frac{1}{p_{i,max}} = \frac{1}{\tau^2}\frac{\Delta p_i}{p_{i,max}}. \tag{6.4}$$

Here, the porosity (ϵ) and pore diameter (d_{Pore}) are obtained from nitrogen adsorption measurements and temperature (T), molar flow ($\dot{n}_i$) as well as pressure (p_i) are determined during the gas permeation measurements. The membrane wall thickness is determined by measuring the inner (d_{inner}) and the outer diameter (d_{outer}) in eight different directions at the membrane cross section using a digital microscope (VHX-600DSO, Keyence, Japan). The mean thickness is defined as $\delta = \frac{d_{outer}-d_{inner}}{2}$ using the mean inner and outer diameters. The membrane surface area is calculated using the mean outer diameter and the average length l of the capillary membrane measured from four sides using a micrometer table (Plμ 2300, Sensofar technology, Spain), where the mean membrane area is defined as $A = \pi d_{outer} l$.

Modeling of Alkyl-Chain Distance

To theoretically analyze the functional group density, a simple modeling approach is used to calculate the mean distance between C_{16}-chains immobilized on the membrane surface as schematically shown in Fig. 6.2. For each iteration step, uniform and non-overlapping circles, each representing a single alkyl-chain, are distributed randomly over a circular region with the chosen radius of 10 nm representing an ideal fraction of the membrane surface area (see Fig. 6.2A). The number of circles depends on the desired C_{16}-chain density per membrane surface area. The diameter of the circles is chosen according to the kinetic diameter of methane to 380 pm,[39] assuming a similar kinetic diameter along the C_{16}-chain. To exclude boundary effects, only the circles within a radius of 5 nm are used for further analysis. For each circle within this radius all nearest neighbors which are directly facing are determined and the distances are calculated (see Fig. 6.2B). This procedure, randomly distribution and determining all neighbor distances for all circles within 5 nm, is repeated 100 times for each chosen C_{16}-chain density to ensure a sufficient amount of data for a statistical distribution (see Fig. 6.2C). The results are presented in mean value and standard deviation using the distances from all considered circles in 100 iterations. Based on the experimental determination of the alkyl-chain density by TGA, functional group densities ranging from 0.1 to 4.4 groups per nm^2 with a step size of 0.1 are used for calculation.

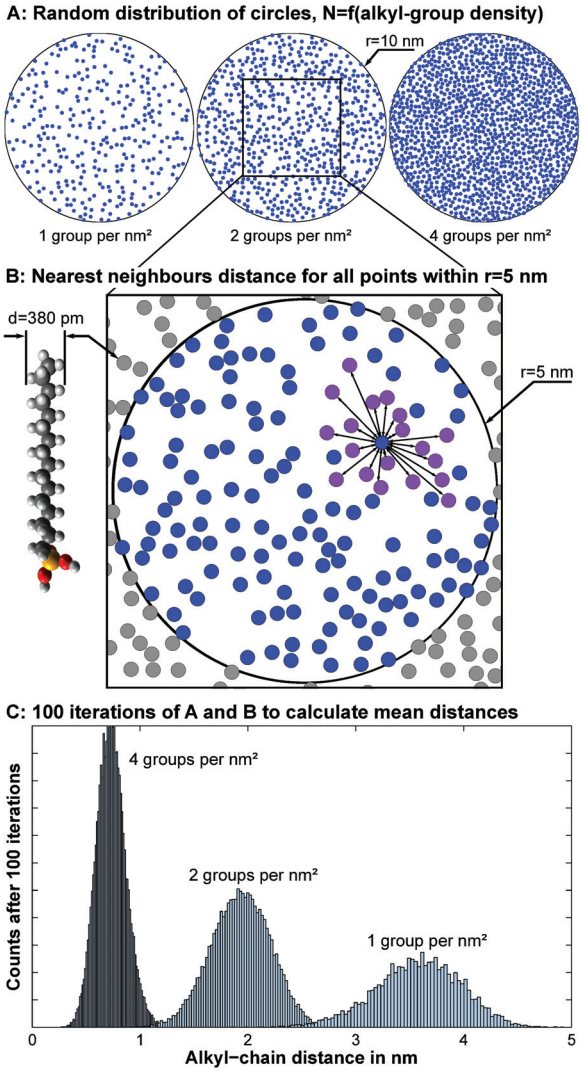

Figure 6.2.: Schematical overview of the model used to calculate the mean distance between C_{16}-chains. Nonoverlapping circles are randomly distributed within a radius r=10 nm (A). For all circles within a r=5 nm the distances to their nearest neighbors are calculated (B). After repeating the process for 100 iterations the data is statistically analyzed (C).

6.3. Results

6.3.1. Structural Characterization

Porous capillary membranes made of YSZ with a mono-modal pore size distribution are prepared by extrusion to serve as mesoporous model structures. To verify the pore structure, nitrogen adsorption/desorption measurments are performed. Fig. 6.3A shows exemplary nitrogen adsorption/desorption isotherms for membranes functionalized with varying C_{16}-chain concentrations (subscripts according to HDTMS concentration 0.01-0.2 M). All adsorption/desorption isotherms feature a hysteresis loop which can be classified as type IV according to IUPAC classification.[40] With increasing HDTMS concentration of the applied stock solution the total pore volume of the functionalized membranes decreases from 69.9 ± 4.8 ($M_{non-f.}$) to $42.1 \pm 1.1\,cm^3\,(STP)\,g^{-1}$ ($M_{0.2}$). Following the Barrett–Joyner–Hallenda (BJH) model,[36] Fig. 6.3B shows the corresponding incremental pore volume distributions depending on the pore diameter. All membranes show a similar, mono-modal pore size distribution with the maximum of incremental pore volume between 20 and 30 nm. The total mesopore volume (data not shown) is nearly identical with the total pore volume which indicates a pore structure solely consisting of mesopores. In addition, scanning electron microscopy images of the cross section

Table 6.1.: Structural properties of the non-functionalized and C_{16}-functionalized membranes measured by nitrogen adsorption/desorption. Sample name subscripts according to the HDTMS concentration (M) used for functionalization.

Sample name	Specific surface area in $m^2\ g^{-1}$ (BET)	Open porosity in %	Mean pore diameter in nm (BJH)
$M_{non-f.}$	21.17±0.40	37.86±2.21	26.07±2.23
$M_{0.01}$	16.83±0.26	34.69±0.13	21.23±0.00
$M_{0.05}$	15.10±1.04	32.21±0.80	21.23±0.00
$M_{0.1}$	12.21±1.28	30.16±0.47	21.23±0.00
$M_{0.125}$	10.95±0.19	28.75±0.03	19.80±2.02
$M_{0.15}$	10.95±0.88	27.91±1.03	21.23±0.00
$M_{0.2}$	11.22±0.63	26.73±0.47	22.40±1.78

of the membrane show a highly homogeneous pore network throughout the whole membrane thickness (data not shown).

In table 6.1 the results for the structural analysis derived from nitrogen adsorption/desorption measurements are summarized. Following the trend indicated by the isotherms in Fig. 6.3A, both, the specific surface area as well as the open porosity decrease with increasing HDTMS concentration of the stock solution. Here, the decrease in specific surface area of 47 % is higher than the reduction in open porosity, which decreases by 29 % comparing $M_{non-f.}$ and $M_{0.2}$. Furthermore, the mean pore diameter determined by the BJH-method is reduced due to the C_{16}-functionalization from 26 nm to around 21 nm. It is especially noticeable, that the decrease in mean pore diameter is similar for all functionalized membranes ($M_{0.01}$ to $M_{0.2}$) and therefore independent from the HDTMS concentration in the stock solution as well as the correlating decrease in open porosity and specific surface area.

To analyze and quantify the amount of C_{16}-chains immobilized on the membrane surface depending on the HDTMS concentration of the applied stock solution, TGA/DTA measurements are carried out. Fig. 6.4 shows the TGA curves of exemplary measurements for the functionalized membranes with varying HDTMS concentrations ($M_{0.01}$ to $M_{0.2}$) in comparison to a non-functionalized membrane ($M_{non-f.}$) for a temperature ranging from room temperature (20 °C) to 650 °C. $M_{non-f.}$ shows only a small weight loss (∼0.5 %), mostly below 200 °C (∼0.4 %). In turn, all C_{16}-functionalized membranes show little amount of weight loss up to 200 °C (∼0.2 %), which significantly increases when the temperature exceeds 200 °C (>2 %). At small concentrations ($M_{0.01-0.1}$), an increase of the HDTMS molecules

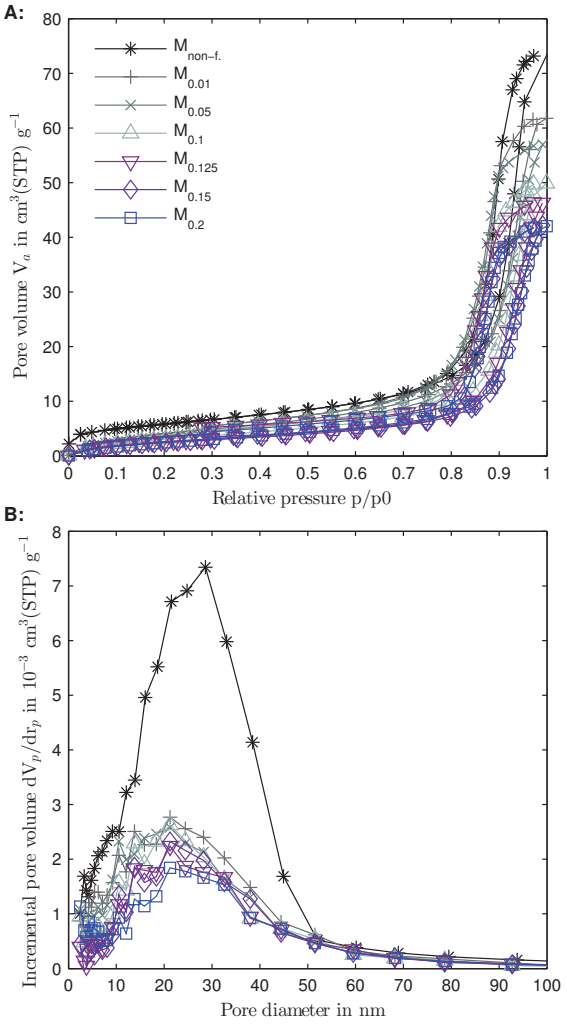

Figure 6.3.: Exemplary nitrogen adsorption/desorption isotherms (A) and pore size distributions according to Barrett–Joyner–Hallenda model (B) for a non-functionalized and functionalized membranes treated with varying HDTMS concentrations. Sample name subscripts according to the HDTMS concentration (M) used for functionalization.

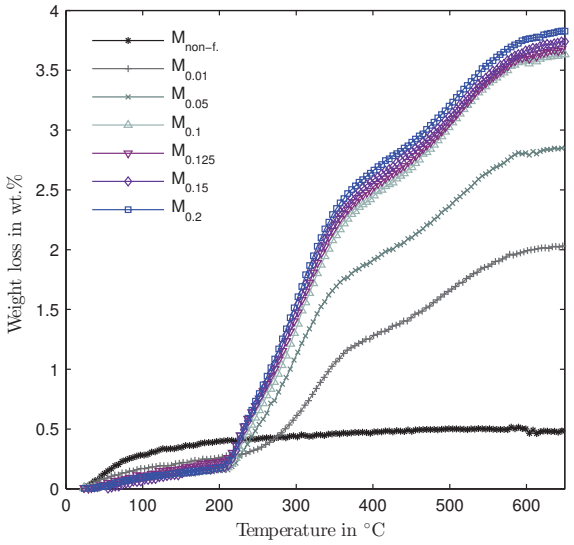

Figure 6.4.: Exemplary measurements of weight loss determined by TGA of functionalized membranes with varying HDTMS concentration (M) in the stock solution indicated by the subscripts in the sample names.

in the solution leads to a significant increase in weight loss. However, this dependency stagnates at higher HDTMS concentrations ($M_{0.1-0.2}$). While the total amount of weight loss differs depending on the HDTMS concentration, all curves possess a similar shape. All corresponding DTA signals are very similar (data not shown), showing exothermal reactions for all functionalized membranes when the temperature exceeds 200 °C. In general, the results are in good agreement with measurements performed on non-functionalized and 0.2 M C_{16}-functionalized membranes using TGA and differential scanning calorimetry method as well as total organic and inorganic carbon content tests presented in our previous study.[30]

The measured weight loss between 200 and 600 °C obtained from three individual measurements is given in table 6.2. Furthermore, the weight loss is recalculated to a functional group density per surface area using the amount of organic compound of the HDTMS molecules (229.5 g mol^{-1}) and the specific surface area determined by nitrogen adsorption/desorption. As already indicated by Fig. 6.4, the weight loss increases rapidly within relatively low applied HDTMS concentrations ($M_{0.01-0.1}$) and stagnates at higher concentrations ($M_{0.1-0.2}$). Based on the weight loss determined by TGA, the calculated C_{16}-chain density on the membrane surface varies between 2 and 4 groups per nm^2.

Table 6.2.: Alkyl-chain density obtained from TGA for samples functionalized with different HDTMS concentrations. Sample name subscripts according to the HDTMS concentration (M) used for functionalization.

Sample name	Weight loss in wt.%	Alkyl-chain density in mmol m^{-2}	groups nm^{-2}
$M_{non-f.}$	0.13±0.03	-	-
$M_{0.01}$	1.58±0.03	3.25±0.01	1.96±0.01
$M_{0.05}$	2.64±0.16	5.44±0.23	3.28±0.14
$M_{0.1}$	3.28±0.08	6.74±0.04	4.06±0.02
$M_{0.125}$	3.3±0.04	6.8±0.04	4.1±0.03
$M_{0.15}$	3.34±0.02	6.88±0.09	4.14±0.05
$M_{0.2}$	3.43±0.01	7.07±0.11	4.25±0.06

6.3.2. Single Gas Permeation Measurements

To investigate the influence of the alkyl-chain density on the membrane surface on the gas transport, gas permeation measurements are carried out under isothermal conditions using Ar, N_2 and CO_2. Fig. 6.5 shows the results for permeation measurements performed at 20 °C and 80 kPa dead-end pressure. In Fig. 6.5A the dimensionless molar flow rate is plotted against the dimensionless pressure difference according to equation 6.4. For each membrane type indicated by different colors, three consecutive measurements for Ar (◇), N_2 (△) and CO_2 (○) are shown. The standard deviations include the errors for temperature, membrane thickness, membrane area, pore diameter and porosity based on the propagation of uncertainty. Especially noticable for the non-functionalized structures, the most significant impact on the standard deviation are caused by pore size, porosity and membrane surface area and thickness. The deviations deriving from the gas permeation measurements are comparably small. All membrane types show a linear behavior of the gas flow depending on the pressure drop. However, the higher the C_{16}-chain density on the membrane surface, the smaller the slope becomes. After considering the molar mass of the gases, non-functionalized membranes and membranes with a small alkyl-chain density show a gas flow which is independent of gas species.

Fig. 6.5B shows the slopes obtained by linear regression of the data presented in Fig. 6.5A depending on the C_{16}-chain density on the membrane surface determined by TGA (see table 6.2). The standard deviations presented here include

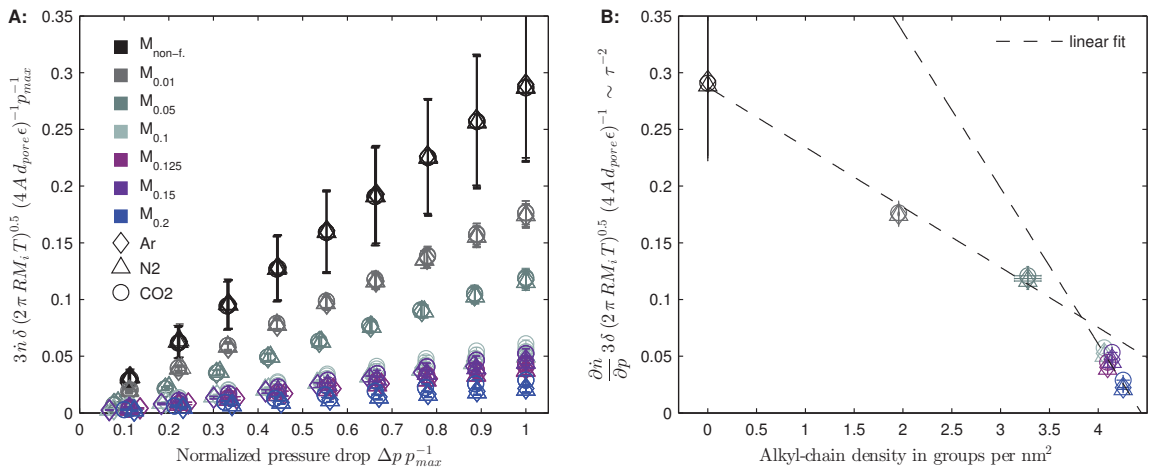

Figure 6.5.: Dimensionless gas flow versus dimensionless pressure drop (A). Part B shows the slope of linear regression of the data presented in (A) depending on the alkyl-chain density determined by TGA. The slope represents τ^{-2} according to the Knudsen theory. Results are obtained from single gas permeation measurements at 20 °C and 80 kPa dead-end pressure.

further the deviations from linear regression. Following the Knudsen theory, the slope represents τ^{-2}. It should be pointed out, that in this study the parameter τ^{-2} is not analyzed by means of the conventional definition of tortuosity. This value is used here for interpretation of the measurement results and only serves as an indicator for the mass transport kinetics. It is used to explain effects caused by a C_{16} surface functionalization on the gas flow after considering all membrane parameters such as the change in pore structure according to known relations. As already indicated in Fig. 6.5A, the slope of linear regression decreases with increasing C_{16}-chain density. Here, a non-linear behavior of τ^{-2} depending on the alkyl-chain density is observed. This is indicated by two linear fits through the data points of the particular region. At very high densities of the surface functionalization ($M_{0.1-0.2}$), the decrease in τ^{-2} is steeper. Furthermore, comparing the slopes of the normalized gas flow for all gas species, CO_2 shows slightly higher values at very high C_{16}-chain densities than Ar and N_2.

To analyze the relation between the different gas species, the ideal selectivities for all three gas pair combinations are calculated according to equation 6.1. Fig. 6.6 shows the resulting selectivities, namely N_2/Ar (A), Ar/CO_2 (B) and N_2/CO_2 (C) again depending on the C_{16}-chain density per surface area (see table 6.2). The non-functionalized membranes show ideal selectivities in agreement to the Knudsen theory (see equation 6.3) represented by the dashed lines for all gas pairs. Similar results are obtained for membranes possessing low alkyl-chain densities ($M_{0.01-0.05}$). However, increasing the number of C_{16}-chains on the surface of the membranes towards high values of around 4 groups per nm^2 leads to a deviation of the ideal selectivities from the Knudsen relation ($M_{0.1-0.2}$). Especially noticeable is the effect on the selectivity of both inert gases N_2/Ar which decreases at high C_{16}-chain densities. Nevertheless, the ideal selectivities regarding CO_2 are affected to a greater extent, where the highest deviations are obtained for N_2/CO_2.

6.3.3. Modeling of the Alkyl-Chain Distance

To analyze and understand the influence of the C_{16}-chain density on the gas flow characteristics, the distances between alkyl-chains depending on their density is theoretically calculated by a random distribution approach. Fig. 6.7 shows the mean distance between the C_{16}-chains on the membrane surface depending on the C_{16}-chain density as a result from theoretical calculations. For low densities (<2 groups nm^{-}2), the mean distance between the functional molecules on the surface is several nanometers large. In turn, for high densities (>4 groups nm^{-}2), the mean distance drops into the sub nanometer range, specifically, for a density of 4 groups per nm^2 the mean distance is calculated to be 0.73±0.14 nm.

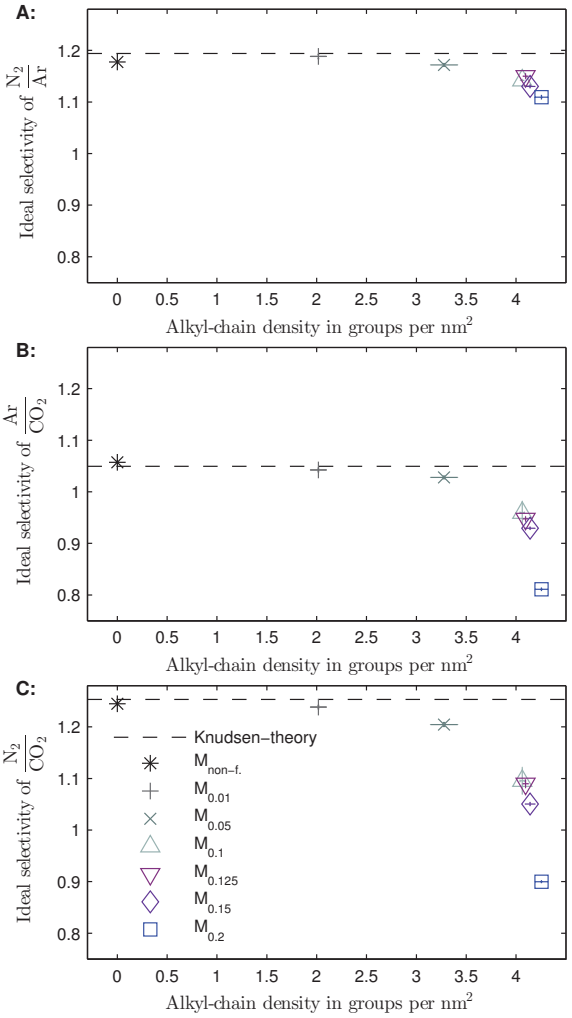

Figure 6.6.: Ideal selectivities of the non-functionalized and C_{16}-functionalized membranes depending on the alkyl-chain density determined by TGA. The dashed black line represents the Knudsen selectivity proposed by the Knudsen theory. Results are obtained from single gas permeation measurements at 20 °C and 80 kPa dead-end pressure.

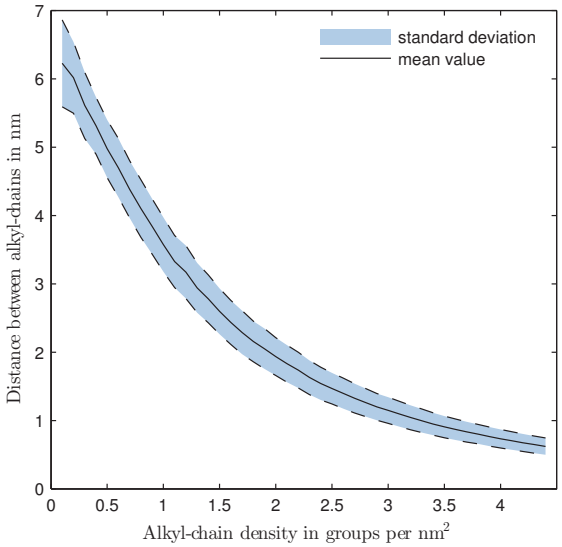

Figure 6.7.: Distance between the C_{16}-chains in nm depending on the alkyl-chain density on the membrane surface as a result of the theoretical model.

6.4. Discussion

6.4.1. Structural Properties and Surface Functionalization

To ensure comparability of the porous structures before and after functionalization with HDTMS, nitrogen adsorption/desorption isotherms are carried out. The results show a decrease in porosity and mean pore diameter when functionalized with alkyl-chains. While the open porosity decreases with an increase in HDTMS concentration, the mean pore diameter is similar for all functionalized membranes $M_{0.01}$ to $M_{0.2}$. Fig. 6.8 illustrates the capillary condensation of nitrogen in pore structures with different alkyl-chain densities aiming to explain the decrease in pore diameter. A homogeneous distribution of the C_{16}-chains on the pore walls of the membrane surface as well as mono-layer formation with straight oriented alkyl-chains is assumed. Accordingly, a relatively small amount of molecules will already lead to a decrease in pore radius by the length of the C_{16}-chains ($M_{0.01}$). Additional alkyl-chains at higher densities($M_{0.05-0.2}$) will fill up the free space between the existing chains on the membrane surface. This leads to a decrease in the amount of nitrogen molecules which can be introduced into the porous structure, i.e. resulting in a decrease in open porosity while the pore radius will remain the same. The measurements show that the mean pore radius is decreased by around 2.4 nm due to the C_{16}-functionalization which indicates a mono-layer formation given by the size of the C_{16}-chains of around 2.3 nm assuming straight orientation of the alkyl chains from the pore wall surface.

Fig. 6.9 combines the decrease in open porosity determined by nitrogen adsorption/desorption and the alkyl-chain density obtained by TGA. Depending on the HDTMS concentration of the stock solution, the open porosity decreases and the C_{16}-chain density increases. For high concentrations ($M_{0.125-0.2}$), the open porosity decreases by a high content, whereas the increase in C_{16}-chain density is rather small. Following the illustrative condensation model presented in Fig. 6.8, introducing C_{16}-chains with a low density ($M_{0.01-0.1}$) will lead to a decrease in open porosity. Incre-

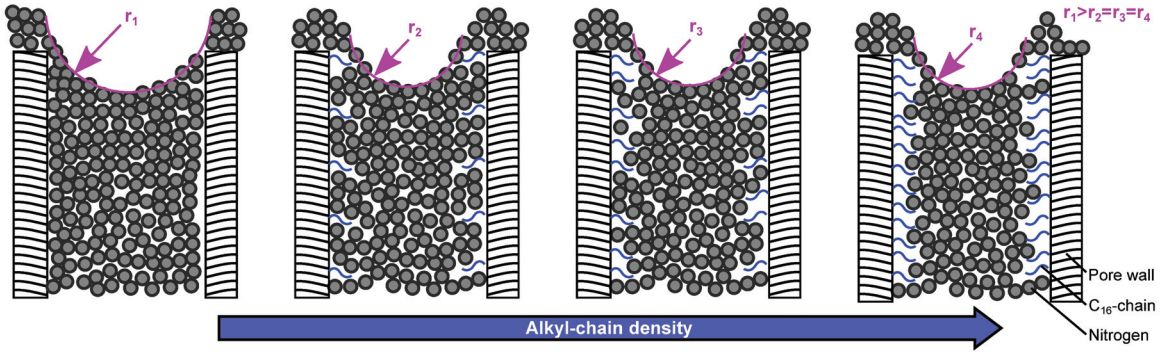

Figure 6.8.: Schematical illustration of the capillary condensation during nitrogen adsorption/desorption on membranes with different alkyl-chain densities.

mentally added alkyl-chains ($M_{0.125-0.2}$) will fill and eventually close the gaps between the already immobilized C_{16}-chains. Closing the gaps will result in a high decrease in open porosity caused by a comparably small amount of additional alkyl-chains, which can be observed in Fig. 6.9. For some polar surface functionalizations, for example silanes showing amino-groups, it is assumed that they are able to form multi-layers when the functional groups react with each other or the silane-hydroxyl group, which eventually results in pore blocking.[41] Of course, pore blocking as well as multi-layer formation can be another explanation for the decrease in open porosity. In contrast, the HDTMS molecules in hydrolyzed state present a structure similar to amphiphilic fatty acids with a hydrophobic tail and a hydrophilic head, which interacts with a hydrophilic membrane surface obtained by acicid hydroxylation (activation). Accordingly, a mono-layer formation similar to a self assembly of lipids on an oil-water interface is more likely than a multi-layer formation or extensive pore blocking. An additional random test with a membrane functionalized using a 0.3 M HDTMS solution showed no further decrease of open porosity or pore diameter nor an increase in weight loss which supports this assumption (data not shown). Therefore, it is assumed that $M_{0.2}$ possesses a functional group density close to the maximum possible surface coverage. This is supported by the alkyl-chain density values obtained from TGA of around 4.3 groups per nm^2 (see table 6.2). In comparison, literature values obtained from water adsorption show a hydroxyl group density of 8-15 groups nm^{-2} on ZrO_2.[42–44] Taking into account the size of a HDTMS molecule compared to water, 4.3 groups nm^{-2} is considered rather high and close to the maximum possible packing density due to steric reasons, assuming

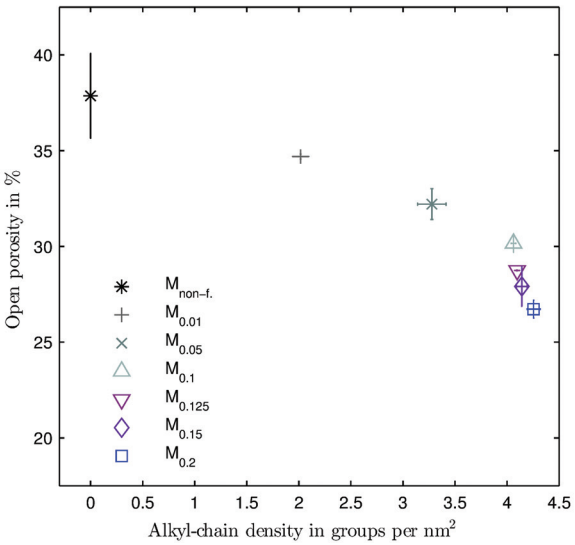

Figure 6.9.: Open porosity determined by nitrogen adsorption/desorption versus C_{16}-chain density obtained from TGA.

that one HDTMS molecule can covalently bond to one hydroxyl group.

6.4.2. Gas Transport Through Alkyl-Functionalized Structures

Gas permeation measurements are carried out to investigate the influence of the C_{16}-chain density on the gas flow behavior. The measurements reveal a linear dependency between gas flow and pressure drop which indicates that the predominant gas transport mechanism is Knudsen diffusion without any influence of viscous flow (see Fig. 6.5A). Applying the Knudsen relation, especially regarding temperature and molar mass of the gas reveals good agreement with the Knudsen theory because the normalized flow is independent of gas species. Nevertheless, linear regression of the permeation data shows a decreasing slope (τ^{-2}) with

increasing C_{16}-chain density (see Fig. 6.5B). τ^{-2} first linearly decreases with increasing alkyl-chain density ($M_{non.-f-0.05}$) until $\sim$ 4 groups nm^{-2} after which, the decrease seems to follow a different trend ($M_{0.1-0.2}$). In summary, for high C_{16}-chain densities ($M_{0.2}$) the normalized flow is about one order of magnitude lower which is consistent with literature data.[20–22,24–27,29,45] The decrease in gas flow is usually explained by the decrease in porosity and pore size. Clearly, this cannot be suggested as a reason in this case, because the decrease in porosity and pore diameter has already been accounted for by normalizing the gas flow according to equation 6.4. This equation describes the porous structure as a resistance to the gas flow depending on porosity, pore diameter and tortuosity. Being aware of the variety of proposed tortuosity relations[46–49] also dependent on porosity, the measurement results lead to the conclusion that the resistance is not solely defined by the pore morphology but also linked to the functional group density. This suggests that the resistance to the gas flow is a combination of a pore resistance characterized by structural proportions and an additional surface resistance, induced by functional molecules immobilized on the surface. This surface resistance seems to be negligible for non-functionalized "smooth surfaces" but affects the gas flow if the surface is "rough" as in the case of a surface functionalization. Furthermore, its impact seems to depend on the functional group density with strong effects present at high functional group densities ($M_{0.1-0.2}$). One possible explanation is related to the altered surface topography caused by the long alkyl-chains. The observed relation between the C_{16}-chain density and the reduction of gas flow supports this hypothesis. The Knudsen relation assumes smooth surfaces and a diffuse desorption in random directions where the probability is proportional to the angle relative to the surface normal vector.[50] Grafting long alkyl-chains onto the surface renders these assumptions inapplicable. In principle, instead of facing a surface similar to a desert, the gas molecules face an environment similar to a savanna ($M_{0.01-0.05}$). The "free" Knudsen diffusion is still possible, because the distance between the "trees" is rather large. Still, the desorption angle is limited in certain directions. Accordingly, the gas flow is reduced due to longer diffusion paths for the gas molecules through the porous structures. With increasing the C_{16}-chain density ($M_{0.1-0.2}$), the savanna turns into a dense forest, where the distances between the "trees" are eventually within the order of magnitude of the gas molecules (see Fig. 6.7). At this point, a "free" Knudsen diffusion is prohibited in almost all directions which reduces the diffusion to a great extent and may even force the molecules to diffuse through the forest without desorption into the free pore volume.

Analyzing the ideal selectivities in Fig. 6.6 reveals a similar behavior and supports this hypothesis. Here, the ideal selectivities follow the Knudsen selectivity for low C_{16}-chain densities ($M_{non-f.-0.05}$), suggesting that the governing transport mechanism is dominated by Knudsen diffusion. Nevertheless, for high alkyl-chain densities of >4 groups nm^{-2} ($M_{0.1-0.2}$), the ideal selectivities begin to deviate from the Knudsen selectivity. One hypothesis aiming to explain the change in selectivity for high functionalization densities is related to the different kinetic diameter of the gas molecules. Fig. 6.7 theoretically shows that for very high densities of functional molecules (>4 groups nm^{-2}), the mean distance between the alkyl-chains gets within the order of magnitude of the molecular diameter of the gases. In this case, different molecular sizes will have an impact on the gas diffusion within the functionalization layer. Following this assumption, larger gas molecules will face a higher resistance due to a reduced mobility than smaller ones which will result in an effect comparable to molecular sieving. The three investigated gases possess kinetic diameters of d_{N_2}=360 pm, d_{Ar}=340 pm and d_{CO_2}=330 pm.[39] Accordingly, N_2 will face a higher resistance than Ar due to the larger molecular diameter, in turn the selectivity N_2/Ar will decrease when the distance between the alkyl-chains gets very small (i.e. high functional group density, see Fig. 6.6). The same selectivity decrease is observed for the selectivities regarding CO_2 which can be explained in the same way. The higher deviations for Ar/CO_2 and N_2/CO_2 may be due to the linear shape of the CO_2 molecule where the diameter perpendicular to the longitudinal axis is significantly smaller than the length. Based on simulations, Yu et al. showed that the CO_2 molecule orients with its longitudinal axis parallel to an alkyl-chain for a minimal energy configuration.[51] Assuming this orientation, the effective molecular diameter of CO_2 will be significantly smaller than 330 pm which will lead to a smaller resistance and a higher deviation from the Knudsen selectivities when compared to

the flow of other, more spherical gas species such as Ar or N_2.
Usually, surface diffusion and viscous flow are the most obvious transport mechanisms causing a deviation from the Knudsen theory. Viscous flow can be excluded due to the linear flow rate as well as the relation of the dynamic viscosity of the gas species (CO_2<N_2<Ar) which will cause a different effect on the selectivities. Surface diffusion seems to be unlikely in this case as well. In general, surface diffusion is understood as a transport mechanism, which results from a selective adsorption and diffusion, increasing the flow of a specific gas species. Here, the diffusion resistance is significantly increased for all gas species, where slight differences are observed depending on the molecular size of the gas. Furthermore, alkyl-functionalizations are known to facilitate surface diffusion of apolar gas species such as hydrocarbons with little affect on polar gases such as CO_2.[25,26,52] A more appropriate description of the mechanism will be analogue to the molecular sieving effect.

6.5. Conclusion

Model mesoporous structures are prepared using a yttria-stabilized zirconia nanopowder to investigate the impact of the surface functionalization density of alkyl-chains (C_{16}-chains) on the gas diffusion in mesopores. The inorganic non-functionalized membrane structures feature a mono-modal pore size distribution with a mean pore diameter of 26 nm. Solutions containing different concentrations of the surface functionalization molecules (HDTMS) are used to achieve mesoporous membranes with different alkyl-group densities on the surface. After functionalization, the pore diameter is reduced to around 21 nm due to the C_{16}-chains immobilized on the membrane surface. While the reduction in pore size is found to be independent from functional group density, the open porosity decreases with increasing C_{16}-chain density. Assuming that the HDTMS molecules are distributed homogeneously on the membrane surface, an increase in the alkyl-group density will result in filling the space between the immobilized chains. Therefore, results obtained from nitrogen adsorption/desorption measurements show a decrease in open porosity with increasing functional group density whereas the determined pore diameter remains constant.

To determine the effect of the functional group density on the gas diffusion behavior, single gas permeation measurements are performed using Ar, N_2 and CO_2. Gas diffusion in mesopores usually occurs according to the laws of Knudsen diffusion which is confirmed for mesoporous structures without surface functionalization. In contrast, membranes with a alkyl-chain functionalization show gas diffusion kinetics where the gas flow decreases with increasing chain density on the membrane surface. It is proposed, that relatively long C_{16}-chains ($\sim$2.3 nm) attached to the surface lead to an increased resistance for the Knudsen diffusion because the diffuse desorption of the gas molecules is limited to a certain extent by the chains acting as steric barriers. For high functional group densities (>4 groups nm^{-2}) where the mean distance of the chains is in the order of magnitude of the size of the gas molecules, the gas flow is reduced disproportional. At the same time the ideal selectivities of the functionalized membranes begin to deviate from Knudsen selectivity. The observed deviations in selectivity are not considered to be related to surface diffusion, which is defined by selective adsorption and diffusion increasing the flow of a specific gas species. Here, the selective mechanism is caused by retention of the gas molecules depending on their size which is better described by an effect similar to molecular sieving. It is proposed, that the different molecular sizes of the gases gain importance when the mean distance between the surface functional groups is in the range of the gas molecular diameters. This leads to a size dependent separation effect within the functional alkyl-layer with a higher retention for large molecules compared to smaller gas species. Furthermore, the results can lead to the conclusion, that the size of the surface functional molecules play a significant role for the gas transport properties. Following this assumption, the "molecule of choice" for a specific application does not solely depend on its functional group type, but also on its size. Accordingly, molecules for a gas separation membrane aiming at enhancing the surface selective flow should be as small as possible whereas a gas chromatography application may benefit from long functional molecules, maximizing the retention effect.

Acknowledgments

This work was supported by the German Research Foundation (DFG) within the Research Training Group GRK 1860 "Micro-, meso- and macroporous nonmetallic Materials: Fundamentals and Applications" (MIMENIMA). The support of M. Hoog Antink from the University of Bremen for the fruitful discussions and the critical feedback which helped to improve this work is gratefully acknowledged. Furthermore, we thank T. Kühn from the University of Bremen for all the support in the laboratory.

References

[1] Weidong He, Weiqiang Lv, and James H. Dickerson. *Gas Transport in Solid Oxide Fuel Cells*. SpringerBriefs in Energy. Springer International Publishing, 2014, pp. 9–17. DOI: 10.1007/978-3-319-09737-4_2.

[2] Marc-Olivier Coppens. "A nature-inspired approach to reactor and catalysis engineering". In: *Curr. Opin. Chem. Eng.* 1.3 (Aug. 2012), pp. 281–289. DOI: 10.1016/j.coche.2012.03.002.

[3] Jason Baxter et al. "Nanoscale design to enable the revolution in renewable energy". In: *Energy Environ. Sci.* 2 (6 2009), pp. 559–588. DOI: 10.1039/B821698C.

[4] V.G. Berezkin and J. de Zeeuw. *Capillary Gas Adsorption Chromatography*. Hüthig Heidelberg, 1996.

[5] Dennis Y.C. Leung, Giorgio Caramanna, and M. Mercedes Maroto-Valer. "An overview of current status of carbon dioxide capture and storage technologies". In: *Renewable Sustainable Energy Rev.* 39 (Nov. 2014), pp. 426–443. DOI: 10.1016/j.rser.2014.07.093.

[6] Matthew E. Boot-Handford et al. "Carbon capture and storage update". In: *Energy Environ. Sci.* 7 (1 2014), pp. 130–189. DOI: 10.1039/C3EE42350F.

[7] Benjamin Besser et al. "Hierarchical Porous Zeolite Structures for Pressure Swing Adsorption Applications". In: *ACS Appl. Mater. Interfaces* 8.5 (Feb. 2016), pp. 3277–3286. DOI: 10.1021/acsami.5b11120.

[8] Ahmad F Ismail, Kailash C Khulbe, and Takeshi Matsuura. *Gas Separation Membranes - Polymeric and Inorganic*. Springer International Publishing, 2015. DOI: 10.1007/978-3-319-01095-3.

[9] H. Verweij. "Ceramic membranes - Morphology and transport". In: *J. Mater. Sci.* 38.23 (2003), pp. 4677–4695. DOI: 10.1023/A:1027410616041.

[10] Andreas Seidel-Morgenstern. *Membrane Reactors*. Ed. by Andreas Seidel-Morgenstern. Wiley-VCH, 2010.

[11] Douglas M. Ruthven, W.J. DeSisto, and S. Higgins. "Diffusion in a mesoporous silica membrane - Validity of the Knudsen diffusion model". In: *Chem. Eng. Sci.* 64.13 (July 2009), pp. 3201–3203. DOI: 10.1016/j.ces.2009.03.049.

[12] R. Krishna and J.M. van Baten. "An investigation of the characteristics of Maxwell-Stefan diffusivities of binary mixtures in silica nanopores". In: *Chem. Eng. Sci.* 64.5 (Mar. 2009), pp. 870–882. DOI: 10.1016/j.ces.2008.10.045.

[13] W. V. Chiu et al. "Post-synthesis defect abatement of inorganic membranes for gas separation". In: *J. Membr. Sci.* 377.1-2 (July 2011), pp. 182–190. DOI: 10.1016/j.memsci.2011.04.047.

[14] H.A. Meinema et al. "Ceramic Membranes for Gas Separation - Recent Developments and State of the Art". In: *Interceram* 54 (2005), pp. 86–91.

[15] William J Koros and Rajiv Mahajan. "Pushing the limits on possibilities for large scale gas separation - which strategies?" In: *J. Membr. Sci.* 175.2 (Aug. 2000), pp. 181–196. DOI: 10.1016/S0376-7388(00)00418-X.

[16] A. D. Wiheeb et al. "Identification of Molecular Transport Mechanisms in Micro-Porous Hydrotalcite-Silica Membrane". In: *Transp. Porous Media* 104.1 (May 2014), pp. 133–144. DOI: 10.1007/s11242-014-0324-5.

[17] Yunzhong Zheng, Meiling Qi, and Ruonong Fu. "Graphitic carbon nitride as high-resolution stationary phase for gas chromatographic separations". In: *J. Chromatogr. A* 1454 (July 2016), pp. 107–113.

[18] Yuan Zhang et al. "Current status and development of membranes for CO2/CH4 Separation - A review". In: *Int. J. Greenhouse Gas Control* 12 (Jan. 2013), pp. 84–107. DOI: 10.1016/j.ijggc.2012.10.009.

[19] J.K. Adewole et al. "Current challenges in membrane separation of CO2 from natural gas - A review". In: *Int. J. Greenhouse Gas Control* 17 (Sept. 2013), pp. 46–65. DOI: 10.1016/j.ijggc.2013.04.012.

[20] Christian Leger, Helio De L. Lira, and Russell Paterson. "Preparation and properties of surface modified ceramic membranes. Part III. Gas permeation of 5 nm alumina membranes modified by trichlorooctadecylsilane". In: *J. Membr. Sci.* 120.2 (Nov. 1996), pp. 187–195.

[21] Daniel Stoltenberg and Andreas Seidel-Morgenstern. "An attempt to alter the gas separation of mesoporous glass membranes by amine modification". In: *Microporous Mesoporous Mater.* 154 (May 2012), pp. 148–152. DOI: 10.1016/j.micromeso.2011.11.013.

[22] Shunsuke Suzuki et al. "Development of inorganic-organic hybrid membranes for carbon dioxide/methane separation". In: *J. Membr. Sci.* 471 (Dec. 2014), pp. 402–411.

[23] Dong Wang et al. "Highly Stable Surface Functionalization of Microgas Chromatography Columns Using Layer-by-Layer Self-Assembly of Silica Nanoparticles". In: *Anal. Chem.* 85.17 (Sept. 2013), pp. 8135–8141. DOI: 10.1021/ac401080u.

[24] Asad Javaid et al. "Solubility-based gas separation with oligomer-modified inorganic membranes". In: *J. Membr. Sci.* 187.1-2 (June 2001), pp. 141–150.

[25] Rajinder P. Singh, J. Douglas Way, and Steven F. Dec. "Silane modified inorganic membranes - Effects of silane surface structure". In: *J. Membr. Sci.* 259.1-2 (Aug. 2005), pp. 34–46. DOI: 10.1016/j.memsci.2005.03.004.

[26] K Kuraoka, Y Chujo, and T Yazawa. "Hydrocarbon separation via porous glass membranes surface-modified using organosilane compounds". In: *J. Membr. Sci.* 182.1-2 (Feb. 2001), pp. 139–149. DOI: 10.1016/S0376-7388(00)00559-7.

[27] Arne Lindbråthen and May-Britt Hägg. "Glass membranes for purification of aggressive gases - Part II. Adsorption measurements and diffusion coefficient estimations". In: *J. Membr. Sci.* 259.1-2 (Aug. 2005), pp. 154–160.

[28] Arne Lindbråthen and May-Britt Hägg. "Glass membranes for purification of aggressive gases - Part I. Permeability and stability". In: *J. Membr. Sci.* 259.1–2 (2005), pp. 145–153. DOI: http://dx.doi.org/10.1016/j.memsci.2005.03.056.

[29] Yuzuru Sakamoto et al. "Preparation and CO_2 separation properties of amine-modified mesoporous silica membranes". In: *Microporous Mesoporous Mater.* 101.1-2 (Apr. 2007), pp. 303–311. DOI: 10.1016/j.micromeso.2006.11.007.

[30] Benjamin Besser et al. "A comparative experimental study on the deviation of the ideal selectivity in HDTMS-functionalized and untreated ceramic structures with pores in the upper mesoporous range". In: *Microporous Mesoporous Mater.* 217 (Nov. 2015), pp. 253–261.

[31] Julia Werner et al. "Production of ceramic membranes with different pore sizes for virus retention". In: *J. Water Process Eng.* 4 (Dec. 2014), pp. 201–211. DOI: 10.1016/j.jwpe.2014.10.007.

[32] Julia Bartels et al. "Amino-functionalized ceramic capillary membranes for controlled virus retention". In: *Environ. Sci. Technol.* 50.4 (Jan. 2016), pp. 1973–1981. DOI: 10.1021/acs.est.5b05124.

[33] Stephen Kroll et al. "High virus retention mediated by zirconia microtubes with tailored porosity". In: *J. Eur. Ceram. Soc.* 32.16 (Dec. 2012), pp. 4111–4120. DOI: 10.1016/j.jeurceramsoc.2012.07.026.

[34] Stephen Kroll et al. "Development and characterisation of functionalised ceramic microtubes for bacteria filtration". In: *J. Membr. Sci.* 365.1-2 (Dec. 2010), pp. 447–455.

[35] Stephen Kroll et al. "Highly efficient enzyme-functionalized porous zirconia microtubes for bacteria filtration". In: *Environ. Sci. Technol.* 46.16 (July 2012), pp. 8739–8747. DOI: 10.1021/es3006496.

[36] Elliott P. Barrett, Leslie G. Joyner, and Paul P. Halenda. "The Determination of Pore Volume and Area Distributions in Porous Substances. I. Computations from Nitrogen Isotherms". In: *J. Am. Chem. Soc.* 73.1 (Jan. 1951), pp. 373–380. DOI: 10.1021/ja01145a126.

[37] Stephen Brunauer, P. H. Emmett, and Edward Teller. "Adsorption of Gases in Multimolecular Layers". In: *J. Am. Chem. Soc.* 60.2 (Feb. 1938), pp. 309–319. DOI: 10.1021/ja01269a023.

[38] Thomas Veltzke, Michael Baune, and Jorg Thöming. "The contribution of diffusion to gas microflow - An experimental study". In: *Phys. Fluids* 24.8 (2012), pages. DOI: 10.1063/1.4745004.

[39] D.W. Breck. "Crystalline Molecular Sieves". In: *J. Chem. Educ.* (1964), pp. 678–689.

[40] S. W. Sing K. "Reporting physisorption data for gas/solid systems with special reference to the determination of surface area and porosity". In: *Pure Appl Chem* 54.11 (1982), pp. 2201–2218. DOI: doi:10.1351/pac198254112201.

[41] Mojun Zhu, Maria Z. Lerum, and Wei Chen. "How To Prepare Reproducible, Homogeneous, and Hydrolytically Stable Aminosilane-Derived Layers on Silica". In: *Langmuir* 28.1 (Jan. 2012), pp. 416–423. DOI: 10.1021/la203638g.

[42] J. Randon et al. "Study of ZrO_2 Membrane - Aqueous Solutions Interface". In: *Key Eng. Mater.* 61-62 (1992), pp. 495–498. DOI: 10.4028/www.scientific.net/kem.61-62.495.

[43] J. Nawrocki et al. "Chemistry of zirconia and its use in chromatography". In: *J Chromatogr A* 657.2 (Dec. 1993), pp. 229–282.

[44] J. Nawrocki et al. "A TGA investigation of hydrated monoclinic zirconia". English. In: *Anal. Chim. Acta* 327.3 (July 1996), pp. 261–266. DOI: 10.1016/0003-2670(96)00110-9.

[45] Souha Belhaj Messaoud et al. "Alkylamine–silica hybrid membranes for carbon dioxide/methane separation". In: *J. Membr. Sci.* 477 (2015), pp. 161–171. DOI: http://dx.doi.org/10.1016/j.memsci.2014.12.022.

[46] Xuechao Gao, João C. Diniz da Costa, and Suresh K. Bhatia. "Understanding the diffusional tortuosity of porous materials - An effective medium theory perspective". In: *Chem. Eng. Sci.* 110 (May 2014), pp. 55–71. DOI: 10.1016/j.ces.2013.09.050.

[47] Lihua Shen and Zhangxin Chen. "Critical review of the impact of tortuosity on diffusion". In: *Chem. Eng. Sci.* 62.14 (July 2007), pp. 3748–3755.

[48] Suresh K. Bhatia and David Nicholson. "Comments on "Diffusion in a mesoporous silica membrane - validity of the knudsen diffusion model", by ruthven, d.m., et al., chem. eng. sci. 64 (2009) 3201-3203". In: *Chem. Eng. Sci.* 65.15 (Aug. 2010), pp. 4519–4520.

[49] Suresh K. Bhatia and David Nicholson. "Some pitfalls in the use of the Knudsen equation in modelling diffusion in nanoporous materials". In: *Chem. Eng. Sci.* 66.3 (2011), pp. 284–293.

[50] Jichang Liu and James Wei. "Knudsen diffusion in channels and networks". In: *Chem. Eng. Sci.* 111 (May 2014), pp. 1–14.

[51] Decai Yu et al. "Quantum chemistry calculation and experimental study of CO_2/CH_4 and functional group interactions for the design of solubility selective membrane materials". In: *J. Membr. Sci.* 441 (Aug. 2013), pp. 137–147. DOI: 10.1016/j.memsci.2013.03.052.

[52] Scott Higgins, William DeSisto, and Douglas Ruthven. "Diffusive transport through mesoporous silica membranes". In: *Microporous Mesoporous Mater.* 117.1-2 (Jan. 2009), pp. 268–277. DOI: 10.1016/j.micromeso.2008.06.030.

7. Conclusions

The aim of this work is to contribute to a more comprehensive understanding on how surface functionalizations affect the gas transport in mesoporous structures by investigating the gas transport in non-functionalized and C_{16}-functionalized membranes with uniform pores of around 20 nm in diameter. To achieve this, capillary membranes are prepared using an extrusion process based on a yttria stabilized zirconia nanopowder. Due to the optimization and the precise control of the slurry preparation and the processing route, highly homogeneous membranes with a uniform microstructure are prepared. The membranes feature a narrow pore size distribution with a mean pore diameter between 23 and 26 nm. In general, the preparation process proved to be highly reproducible. In particular, the tubular shape of the membranes is advantageous, because of the high surface-to-volume-ratio and that the active membrane surface area can easily be controlled by the capillary length, for example, in gas permeation measurements.

To immobilize C_{16}-chains on the membrane surface, a wet-chemical functionalization process using hexadecyltrimethoxysilane (HDTMS) is presented. By applying this functionalization, the HDTMS molecules are covalently bound onto the membrane surface, which can be concluded from the temperature stability up to 200 °C, clearly exceeding the boiling (155 °C) and flash point (165 °C) of HDTMS. In general, TGA is identified as an easy method for the quantification of the amount of functional groups present on the membrane surface.

The C_{16}-functionalized membranes show a pore size distribution similar to the non-functionalized membranes with slightly smaller mean pore diameters of around 20 nm. In total, the pore radius decreases about 2 nm and considering the length of a hydrolyzed HDTMS molecule of around 2.3 nm, this leads to the conclusion that the immobilization of the functional molecules results in a monolayer formation. Nevertheless, the crucial membrane property for the gas transport, the mean pore diameter, is only reduced slightly and the governing gas transport mechanisms can be assumed to be comparable in both membrane types. To analyze the gas transport properties of non-functionalized and C_{16}-functionalized membranes, single gas permeation measurements are carried out in dead-end mode using Ar, N_2, CO_2 and CH_4. The measurement setup was redesigned and optimized to perform measurements at temperatures between 0 and 80 °C and a testing procedure is developed. All linear regressions show coefficients of determination of R^2 >0.9992, leading to the conclusion that the gas permeation measurements are highly reproducible. The measurements performed on both membrane types, non-functionalized and C_{16}-functionalized, lead to the following four conclusions based on the given experimental conditions:

Non-functionalized membranes show ideal Knudsen diffusion behavior.

The non-functionalized membranes show gas transport properties following the laws of Knudsen diffusion for the gas flow, as well as the ideal selectivities. This leads to the conclusion that Knudsen diffusion is the dominating transport mechanism within these mesoporous structures. Furthermore, the high degree of linearity between pressure drop and gas flow shows no evidence of a viscous contribution to the gas flow.

Immobilized C_{16}-chains are responsible for increased diffusion resistance.

The gas flow through the mesoporous membranes is significantly decreased by the C_{16}-alkyl chain functionalization and the higher the functional group density is, the higher is the decrease in flux. It is hypothesized that the functional groups attached to the membrane surface act as steric barriers, limiting the desorption directions of adsorbed molecules. Consequently, the gas molecules are forced to longer molecule trajectories, which results in a decrease in flow, and therefore, can be described as an additional resistance for the Knudsen diffusion. This leads to the general conclusion that surface functionalizations also affect the gas flow in large mesopores due to steric

reasons. Accordingly, besides the functional group type, the length of the immobilized molecules will have a significant impact on the gas transport properties.

C_{16}-chain functionalization causes molecular sieving effect.

For high functional group densities, the ideal selectivities deviate from the Knudsen selectivities. The effect on selectivity follows the relation $\frac{N_2}{Ar} < \frac{Ar}{CO_2} < \frac{N_2}{CO_2}$, where selectivities regarding CO_2 show the highest deviations. The impact seems to correlate with the kinetic diameter of the gas species N_2>Ar>CO_2 (360>340>330 pm). Theoretical modeling shows that the average distance between the C_{16}-chains for high functional group densities is within the order of magnitude of the kinetic diameter of the gas molecules. These configurational conditions lead to the conclusion that the effect on selectivity is caused by a size dependent retention of the gas molecules within the functional layer. Furthermore, the disproportional effect on CO_2 derives from its linear shape, which reduces the effective kinetic diameter of the gas molecule, when it is oriented parallel to the alkyl-chains of the functional layer.

Molecular interactions are intensified at higher temperatures leading to stronger effects.

The effect of the C_{16}-chain functionalization on the ideal selectivities increases with increasing temperature. It is hypothesized, that the increased temperature movement of the C_{16}-chains and the increased molecular velocity of the gas molecules result in increased interactions between functional group layer and gas molecules. In conclusion, this leads to an increase in size dependent retention of the gas molecules, causing stronger effects on the ideal selectivities.

In summary, the presented experimental observations show that a C_{16}-functionalization significantly influences the gas transport properties in mesopores of around 20 nm. It is concluded that the observed effects are based on steric interactions between the surface functional groups and the gas molecules resulting in an additional resistance for the Knudsen diffusion. This causes a significant decrease in gas flow and a selective characteristic which depends on the molecular diameter of the gas species. In general, the presented results lead to the conclusion, that surface functionalizations of porous structures significantly contribute to the gas transport properties, also in mesopores larger than 10 nm. This should be considered when working with hierarchical structures, such as asymmetric membranes. Here, effects caused by surface functionalizations within the supporting structure are usually neglected. This study shows that this assumption is not always correct and that further research is needed to understand the complex interactions between surface functional groups and gas molecules. Nevertheless, the selective effects caused by the C_{16}-functionalization may also be transferred to other fields of research, such as gas-solid chromatography.

Furthermore, based on the obtained results, it can be concluded that uniform structures with homogeneous pore networks are well-suited model structures for the fundamental investigation of gas transport phenomena. Especially uniform structures with pores in the upper mesoporous region (10-50 nm) present a suitable platform for the investigation of surface functionalizations. The transport mechanisms are dominated by Knudsen diffusion which provides a linear correlation between pressure drop and gas flow, being simple to analyze. Furthermore, the mean pore diameter is not reduced significantly by immobilizing functional groups on the surface, which means that the governing transport mechanism is not affected. This may also be the case when investigating surface functionalizations in small mesopores, where the ratio between the pore size and the length of the functional molecules is small.

8. Outlook

"How does a surface functionalization influences the gas transport in large mesopores?"
This work addresses to the above stated general question, by focusing on a C_{16}-alkyl chain functionalization in mesopores of about 20 nm in diameter. To understand the interactions and effects observed within this study in more detail, nuclear magnetic resonance spectroscopy may be used to study the self-diffusion of CO_2 and CH_4 within these structures. The results may lead to a more comprehensive understanding of the interaction between the functional layer and the gas molecules.
Furthermore, measurements performed with other noble gases, such as neon or helium, may support the hypothesis of a molecular sieving effect within the functional layer. A very interesting study would also be the investigation of the gas transport at temperatures $<0\,°C$: The temperature dependency of the results lead to the conclusion that the movement of the functional chains has great influence on the ideal selectivities. Hence, another question to be asked may be: "What happens when the functional layer is "frozen", and therefore, the C_{16}-alkyl chains are not moving?" Apart from that, gas permeation measurements with gaseous hydrocarbons of higher chain length than methane, such as ethane, propane or butane, may reveal additional information that could be applied for possible gas-solid chromatography applications.
Based on the answers given in this work regarding C_{16}-chain functionalizations, additional questions arise, for example: "How does the alkyl-chain length influences the gas flow and the ideal selectivity?" Following the conclusions of this work, that the observed effects are caused by sterical interactions between functional groups and gas molecules, the length of the alkyl-chains would have a significant influence. Another interesting question could be: "What role does the functional group type have?" In this work only alkyl-groups are investigated. In practice, surface functionalizations with different types of functional groups, such as amino-, carboxyl-, sulfonate- or phenyl-groups are applied. Each of these functional groups has different electron configurations and will interact with the gas species in an unique way. Another possibility to tune the properties of functionalized structures may be a bi-functionalization using a suitable combination of two different functional group types. Nevertheless, when using functional groups with different bonding strengths, analyzing the gas diffusion at different temperatures would be of great interest.
Besides using different functional molecules, varying the pore size would be interesting. A different pore size means a different Knudsen number, which gradually decreases with increasing pore size. Therefore, the contribution of the gas molecule-wall interactions will gradually decrease in larger pores, until it eventually vanishes, when the gas transport is dominated by viscous flow for very small Knudsen numbers. The interplay and dependences between the pore size and the effects caused by surface functional groups would be of great value for the fundamental understanding of the gas transport in porous structures.

A. Appendix

A.1. Additional Information for Chapter 2: Scientific Background

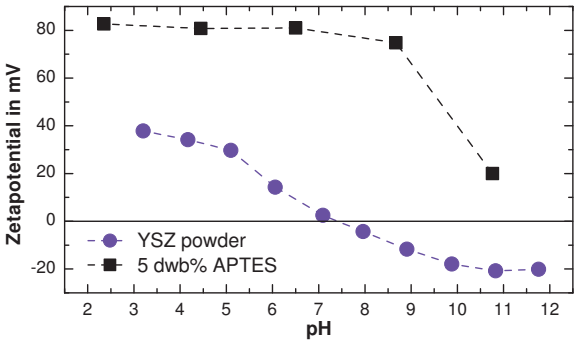

Figure A1.: Zeta-potential measurements of the YSZ nanopowder without and with 5 dwb% APTES as dispersant.

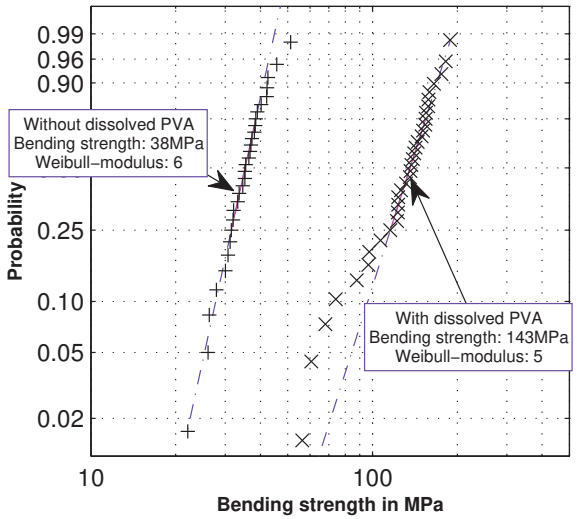

Figure A2.: Weibull distribution obtained from three point bending tests of sintered capillaries prepared without and with dissolved PVA. 30 samples were tested for each type according to DIN EN 843-1 using a Proline table-top testing machine (Zwick/Roel, Z005, Germany).

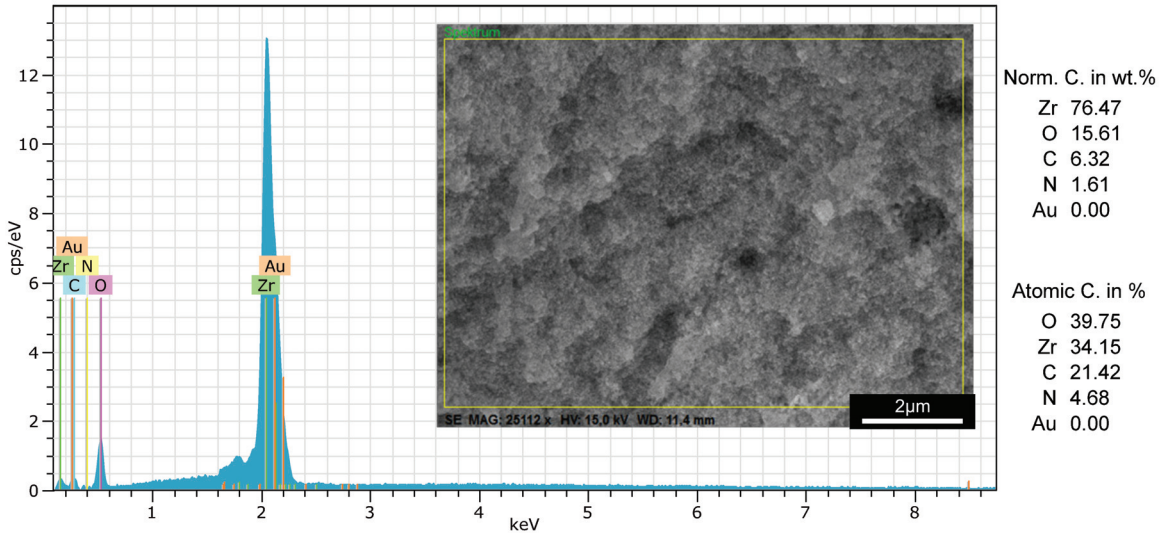

Figure A3.: Energy dispersive X-ray measurements (HV:15.0 kV, ImpD:4.35 kcps, SEM SUPRA® 40, Zeiss, Germany) of the sintered YSZ capillary microstructure.

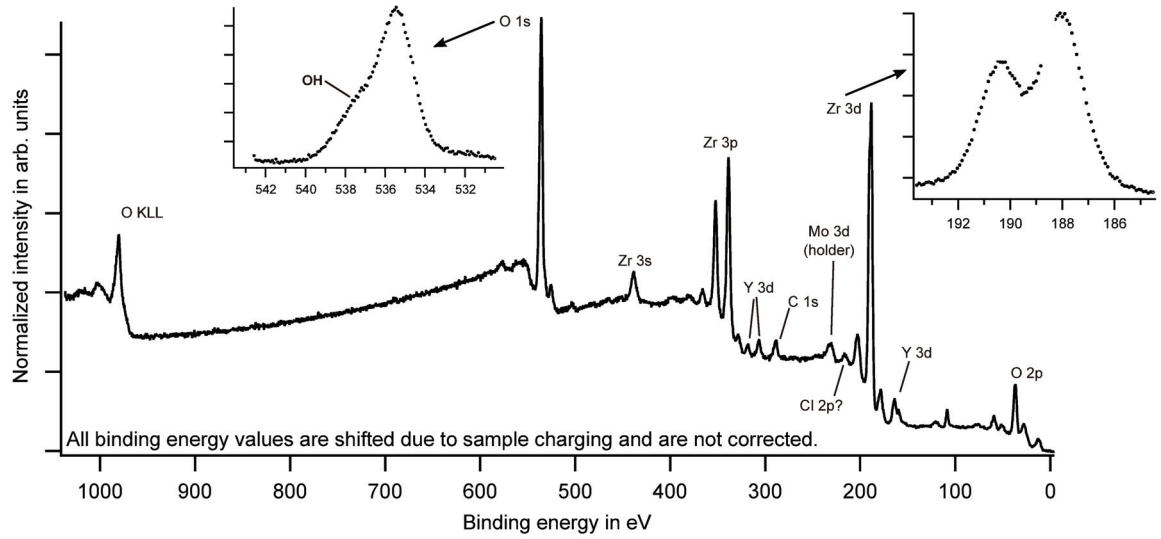

Figure A4.: X-ray photoelectron spectroscopy measurements of a sintered YSZ capillary surface.

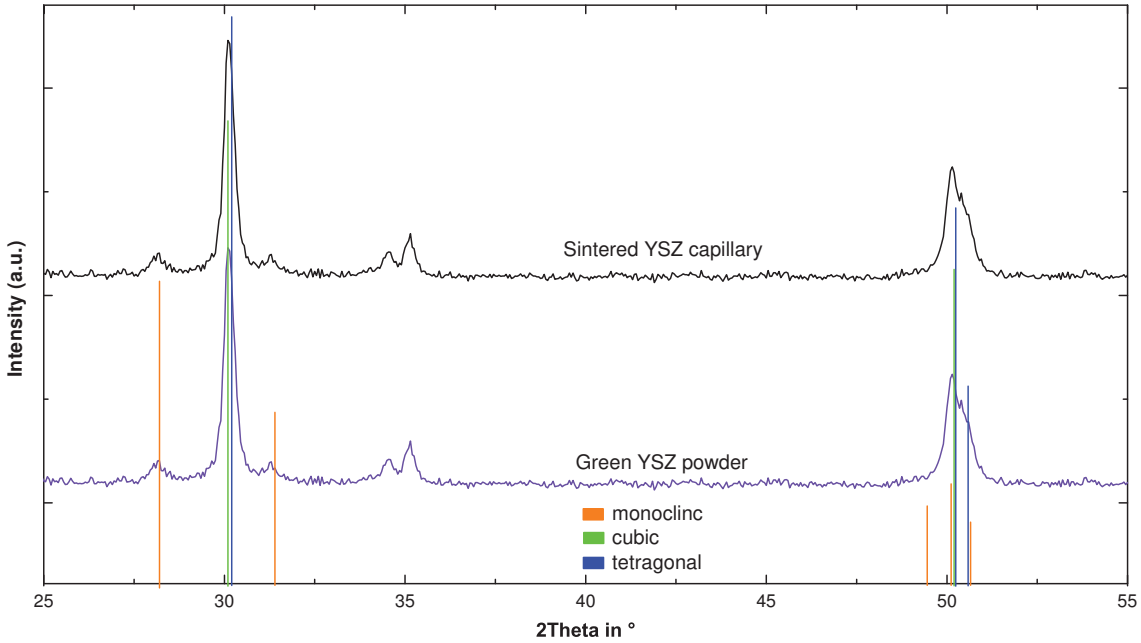

Figure A5.: X-ray diffraction measurements of the as received YSZ powder and the finally sintered YSZ capillaries.

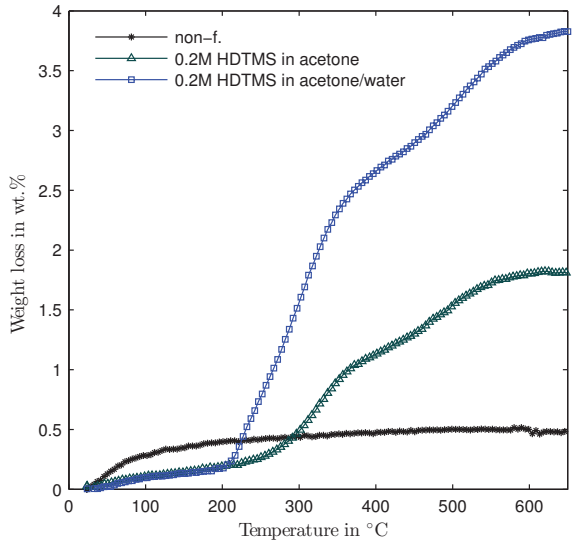

Figure A6.: Weight loss determined by TGA of HDTMS functionalized membranes using acetone without and with water as solvent.

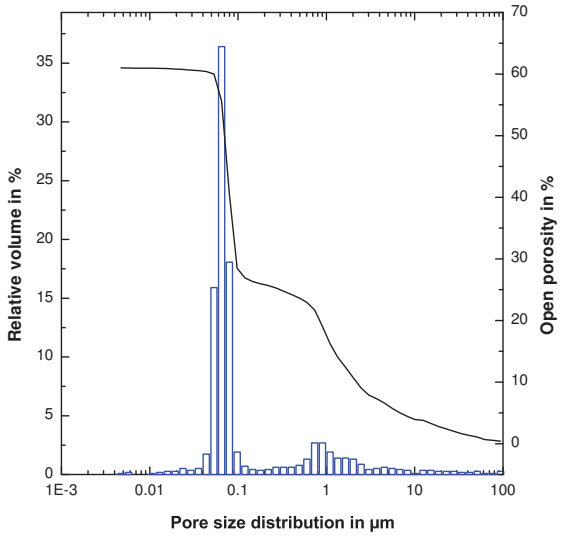

Figure A7.: Mercury intrusion porosimetry of a flat sheet membrane prepared by uniaxial pressing of the YSZ nanopowder and PVA as binder.

A.2. Additional Information for Chapter 3: Characterization Methods

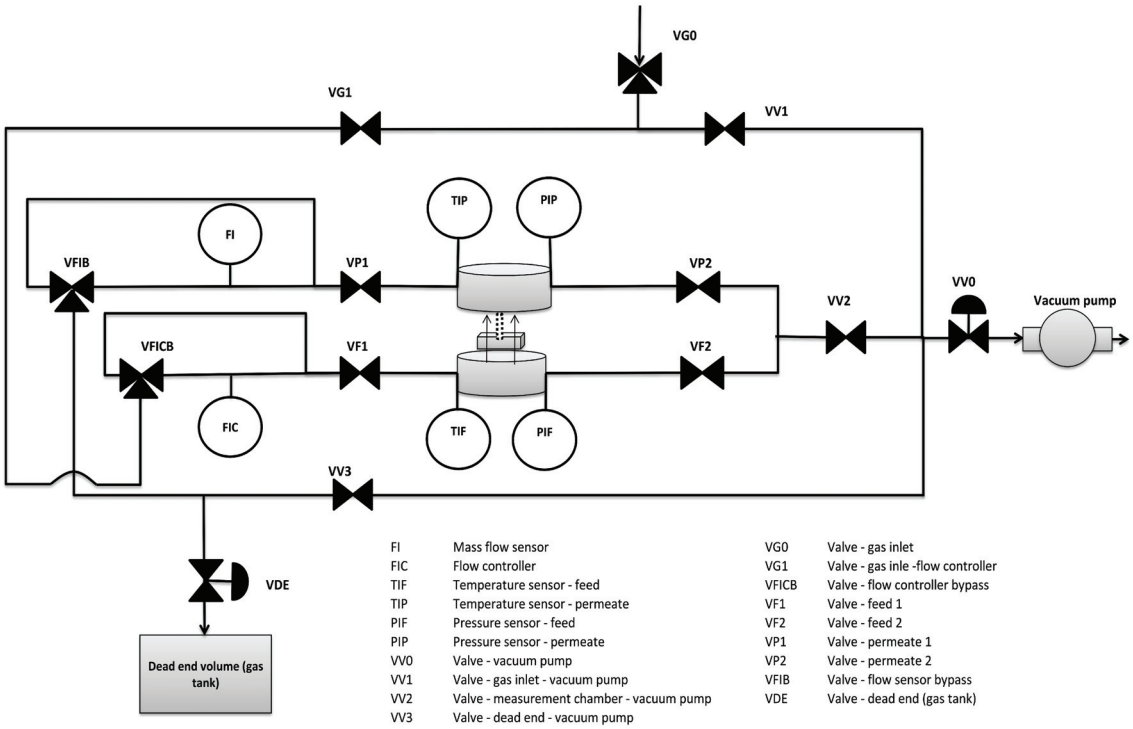

Figure A8.: Schematic representation of the measurement system.

A.3. Supporting Information for Chapter 4: The Deviation of the Ideal Selectivities in C_{16}-Functionalized Mesoporous Structures

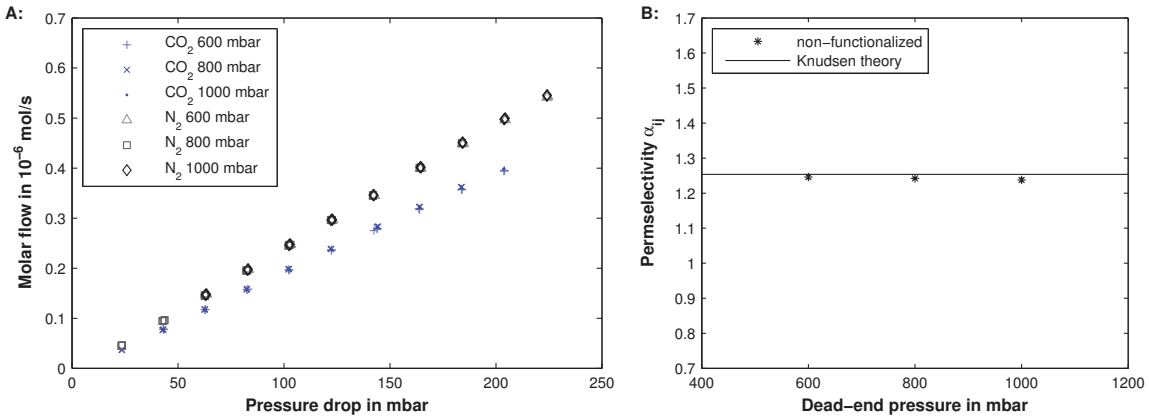

Figure A9.: Results for CO_2 and N_2 from multiple gas permeation measurements at different dead-end pressures for a non-functionalized membrane (A), as well as the corresponding permselectivities (B).

Curriculum Vitae

PERSONAL INFORMATION	
Name	**Benjamin Besser** (m)
Email	dissertation@besser-ing.de

EDUCATION	
04/2010 – 05/2012	**M.Sc.** in Production Engineering at the University of Bremen
10/2006 – 03/2010	**B.Sc.** in Production Engineering at the University of Bremen
05/2005	High school diploma at "Schulzentrum Carl von Ossietzky ", Germany

RESEARCH EXPERIENCE	
09/2012 - current	**Ph.D. student**, University of Bremen, Department of Production Engineering, Keramische Werkstoffe und Bauteile (Advanced Ceramics), Head: Prof. Dr.-Ing. Kurosch Rezwan, Bremen, Germany
10/2013 - 09/2016	**Member of the research training group** "Micro-, meso- and macroporous nonmetallic Materials: Fundamentals and Applications (MIMENIMA)", University of Bremen, Germany
10/2011 - 05/2012	**Master thesis**: "Development of a Matlab-Tool for the numeric calculation of the velocity- and pressure distributions of simple airfoil geometries with OpenFOAM", Center of Applied Space Technology and Microgravity (ZARM), University of Bremen, Germany, Supervisor: Prof. Dr.-Ing. Hans J. Rath and Dipl.-Ing. Holger W. Oelze
10/2011 - 05/2012	**Student research assistant** at the Center of Applied Space Technology and Microgravity (ZARM), Department Hyper-G-Centrifuge, Bremen, Germany
04/2011 - 09/2011	**Master Project**: "Development of a chemical process in production scale (solar hydrogen production)", Center for Environmental Research and Sustainable Technology (UFT), University of Bremen, Germany, Supervisor: Prof. Dr.-Ing. Jorg Thöming and Dr. rer. nat. Michael Baune
05/2010 - 09/2011	**Student research assistant** of Bremen Institute for Metrology, Automation and Quality Science (BIMAQ), Bremen, Germany
01/2010 - 04/2010	**Bachelor thesis**: "generation of material accumulated linked parts by laser melting", Bremen Institute of applied Laser Technology (BIAS), University of Bremen, Germany, Supervisor: Prof. Dr.-Ing. T. Vollertsen and Dipl.-Phys. A. Stephen
01/2008 - 08/2009	**Student research assistant** at the Bremen Institute of applied Laser Technology (BIAS)

INTERNSHIPS	
09/2009 - 12/2010	Internship at "Norddeutsche Seekabelwerke GmbH" (NSW), Nordenham, Germany

List of Publications (peer-reviewed)

Benjamin Besser, Saad Malik, Michael Baune, Stephen Kroll, Jorg Thöming and Kurosch Rezwan, "The influence of the functional group density on gas flow and selectivity: Nanoscale interactions in alkyl-functionalized mesoporous membranes". In: Microporous and Mesoporous Materials (2016), accepted 14.09.2016, DOI: 10.1016/j.micromeso.2016.09.026.

Benjamin Besser, Atiq Ahmed, Michael Baune, Stephen Kroll, Jorg Thöming and Kurosch Rezwan, "Applying alkyl-chain surface functionalizations in mesoporous inorganic structures: Their impact on gas flow and selectivity depending on temperature". In: ACS Applied Materials & Interfaces (2016), accepted 16.09.2016, DOI: 10.1021/acsami.6b09174.

Benjamin Besser, Henrique Akira Tajiri, Gerd Mikolajczyk, Jens Möllmer, Thomas C. Schumacher, Stefan Odenbach, Roger Gläser, Stephen Kroll and Kurosch Rezwan, "Hierarchical Porous Zeolite Structures for Pressure Swing Adsorption Applications". In: ACS Applied Materials & Interfaces 8.5 (2016), pp. 3277-3286, DOI: 10.1021/acsami.5b11120.

Benjamin Besser, Thomas Veltzke, Jochen A.H. Dreyer, Julia Bartels, Michael Baune, Stephen Kroll, Jorg Thöming and Kurosch Rezwan, "A comparative experimental study on the deviation of the ideal selectivity in HDTMS- functionalized and untreated ceramic structures with pores in the upper mesoporous range". In: Microporous and Mesoporous Materials 217.15 (2015), pp. 253–261. DOI: 10.1016/j.micromeso.2015.06.042.

Julia Werner, *Benjamin Besser*, Christoph Brandes, Stephen Kroll, Jorg Thöming and Kurosch Rezwan "Production of ceramic membranes with different pore sizes for virus retention". In: Journal of Water Process Engineering 4 (2014), pp. 201-211. DOI: 10.1016/j.jwpe.2014.10.007.

Author Contributions for the Publications presented in this Work

Publication presented in chapter 4:

Benjamin Besser, Thomas Veltzke, Jochen A.H. Dreyer, Julia Bartels, Michael Baune, Stephen Kroll, Jorg Thöming and Kurosch Rezwan "A comparative experimental study on the deviation of the ideal selectivity in HDTMS- functionalized and untreated ceramic structures with pores in the upper mesoporous range". In: Microporous and Mesoporous Materials 217.15 (2015), pp. 253–261. DOI: 10.1016/j.micromeso.2015.06.042.

Author	Contributions
Benjamin Besser	Concept and planning of work, fabrication of samples, preparation of samples, adsorption/desorption measurements, scanning electron microscopy, gas permeation measurements, data analysis and interpretation, manuscript preparation (design, editing, writing)
Thomas Veltzke	Gas permeation measurements, data analysis, gave conceptual advices, discussed data, edited manuscript
Jochen A.H. Dreyer	TGA and TOC measurements and analysis, discussed data, writing manuscript
Julia Bartels	Fabrication of samples, gave conceptual advices, discussed data, edited manuscript
Michael Baune	Gave conceptual advices, discussed data, edited manuscript
Stephen Kroll	Gave conceptual advices, discussed data, edited manuscript
Jorg Thöming	Gave conceptual advices, discussed data, edited manuscript
Kurosch Rezwan	Gave conceptual advices, discussed data, edited manuscript

Publication presented in chapter 5:

Benjamin Besser, Atiq Ahmed, Michael Baune, Stephen Kroll, Jorg Thöming and Kurosch Rezwan "Applying alkyl-chain surface functionalizations in mesoporous inorganic structures: Their impact on gas flow and selectivity depending on temperature". In: ACS Applied Materials & Interfaces (2016), accepted 16.09.2016, DOI: 10.1021/acsami.5b11120.

Author	Contributions
Benjamin Besser	Concept and planning of work, fabrication of samples, preparation of samples, adsorption/desorption measurements, gas permeation measurements, sample geometry measurements, data analysis and interpretation, manuscript preparation (design, editing, writing)
Atiq Ahmed	Preparation of samples, gas permeation measurements
Michael Baune	Gave conceptual advices, discussed data, edited manuscript
Stephen Kroll	Gave conceptual advices, discussed data, edited manuscript
Jorg Thöming	Gave conceptual advices, discussed data, edited manuscript
Kurosch Rezwan	Gave conceptual advices, discussed data, edited manuscript

Publication presented in chapter 6:

Benjamin Besser, Saad Malik, Michael Baune, Stephen Kroll, Jorg Thöming and Kurosch Rezwan "The influence of the functional group density on gas flow and selectivity: Nanoscale interactions in alkyl-functionalized mesoporous membranes". In: Microporous and Mesoporous Materials (2016), accepted 14.09.2016, DOI: 10.1016/j.micromeso.2016.09.026.

Author	Contributions
Benjamin Besser	Concept and planning of work, fabrication of samples, preparation of samples, adsorption/desorption measurements, helium pycnometry measurements, thermo gravimetric analysis, gas permeation measurements, sample geometry measurements, data analysis and interpretation, modeling, manuscript preparation (design, editing, writing)
Saad Malik	Preparation of samples, gas permeation measurements
Michael Baune	Gave conceptual advices, discussed data, edited manuscript
Stephen Kroll	Gave conceptual advices, discussed data, edited manuscript
Jorg Thöming	Gave conceptual advices, discussed data, edited manuscript
Kurosch Rezwan	Gave conceptual advices, discussed data, edited manuscript

List of Oral and Poster Presentations

Benjamin Besser, Atiq Ahmed, Michael Baune, Stephen Kroll, Jorg Thöming and Kurosch Rezwan "The deviation of ideal selectivities from Knudsen theory of alkyl-functionalized, mesoporous membranes". Invited talk, EMN Meeting on Mesoporous Materials 2016, Prague, Czech Republic.

Benjamin Besser, Henrique Akira Tajiri, Gerd Mikolajczyk, Jens Möllmer, Stefan Odenbach, Stephen Kroll and Kurosch Rezwan "Hierarchical porous zeolite monoliths for swing adsorption applications". Poster, conference organization and session chair, MIMENIMA Symposium "Porous Structures - Where Science meets Application" 2015, Grömitz, Germany.

Benjamin Besser, Thomas Veltzke, Jochen A.H. Dreyer, Julia Bartels, Michael Baune, Stephen Kroll, Jorg Thöming and Kurosch Rezwan "A comparative experimental study on the deviation of the ideal selectivity in HDTMS- functionalized and untreated ceramic structures with pores in the upper mesoporous range". Poster, Euromembrane 2015, Aachen, Germany.

Benjamin Besser, Thomas Veltzke, Jochen A.H. Dreyer, Julia Bartels, Michael Baune, Stephen Kroll, Jorg Thöming and Kurosch Rezwan "A comparative experimental study on the deviation of the ideal selectivity in HDTMS- functionalized and untreated ceramic structures with pores in the upper mesoporous range". Oral presentation, 11^{th} International Conference on Diffusion in Solids and Liquids 2015, Munich, Germany.

List of Student Projects

Raik Dräger, Luca Häuser, Marcel Hesselman, Aygul Khabipova, Mielad Khil	Keramische Membranen für die Gastrennung, Students project 2016

If you can't explain it to a six year old, you don't understand it yourself.*

*Albert Einstein